MODELLING OF CASCADING HAZARDS IN NATURALLY-DAMMED LAKES

ANISH RATNA SHAKYA

June, 2020

SUPERVISORS:

Prof. Dr, C. V., Westen

Ir, G. N., Parodi

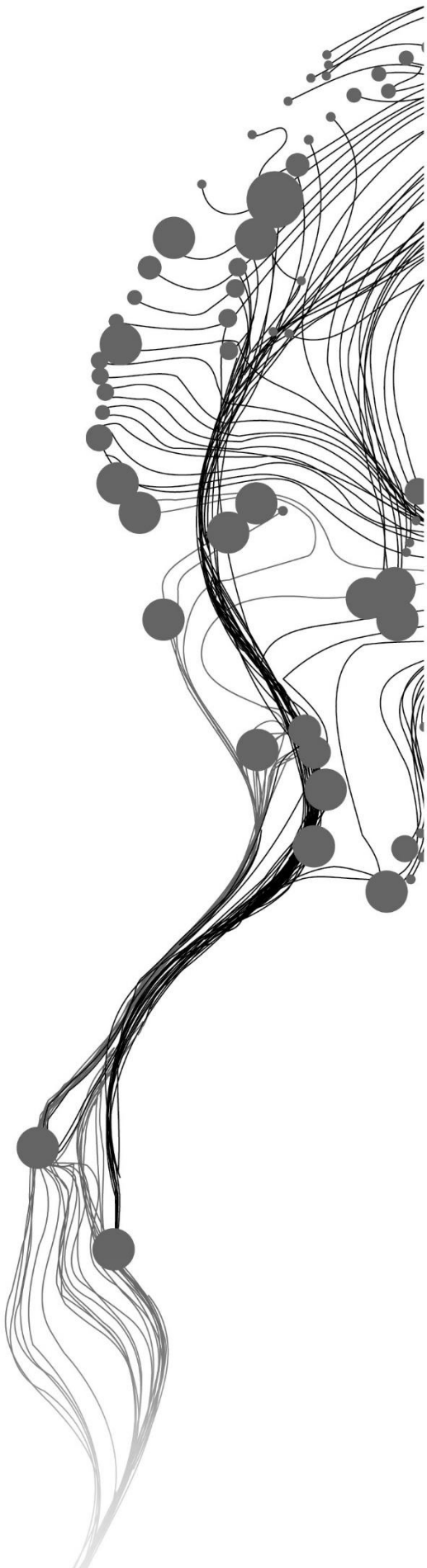

MODELLING OF CASCADING HAZARDS IN NATURALLY-DAMMED LAKES

ANISH RATNA SHAKYA

Enschede, The Netherlands, June, 2020

Thesis submitted to the Faculty of Geo-Information Science and Earth Observation of the University of Twente in partial fulfilment of the requirements for the degree of Master of Science in Geo-information Science and Earth Observation.

Specialization: Natural Hazards and Disaster Risk Reduction

SUPERVISORS:

Prof. Dr, C. V., Westen

Ir, G. N., Parodi

THESIS ASSESSMENT BOARD:

Prof. Dr, N., Kerle (Chair)

Dr, M., Mergili (External Examiner, BOKU University, Austria)

DISCLAIMER

ABSTRACT

Naturally-dammed lake outburst floods are sudden, catastrophic events releasing high volume of water and sediments with high peak discharges in the mountainous region. The lake outburst results from the interaction of the underlying series of natural events affecting one upon another, also known as cascading hazards. Insights of the cascading hazards can be understood by modelling them in an integrative way. Among several processes involved in the lake outburst flood, this study focusses on integrated modelling of three major cascading processes: slope stability, impulse wave and flood.

The main objective of this research is to evaluate the outburst flood hazard modelling of naturally-dammed lakes by integrated process chain modelling under different scenarios which aim to support the disaster risk mitigation planning. For this, Lake Sarez and Lake Rivakkul were chosen as two case study areas from the mountainous region of Tajikistan. Three scenarios were designed for Lake Sarez and two scenarios were designed for Lake Rivakkul.

In Scenario 1 of Lake Sarez, the volume and depth of potential rockslide were predicted from a physically-based slope stability model, Scoops3D using the geotechnical parameters assigned from the past literature. The outputs were then coupled with the Heller-Hager model which estimated the impulse wave characteristics. The optimistic and pessimistic range of parameter values from past studies were chosen in Scenario 2 and Scenario 3 respectively. These parameter values were assigned to Heller-Hager model to estimate the wave run-up heights, overtopping volume and duration. Simple hydrographs were constructed from the outputs of the Heller-Hager model which could be coupled with the flood model.

For the Lake Rivakkul, an ideal rotational slip was assumed for the potential rockslide in Scenario 1 from which the volume and depth were predicted. Heller-Hager was used to estimate the wave run-up heights. In Scenario 2, the dam impounding Lake Rivakkul was assumed to breach and completely empty the lake. The peak discharge and time to peak were estimated from the empirical equations to construct the input hydrograph for the two-dimensional flood modelling in the HEC-RAS. Terrain data was extracted from SRTM DEM (30 m) with the computational mesh size of 50 m. A full momentum scheme with the timestep of 5 seconds and a uniform roughness coefficient of 0.06 was used. The resulting flood was routed at 24 km and 60 km downstream of the lake outburst till Rivak village and Khorugh respectively.

Scenario 1 and Scenario 3 generated the run-up heights that overtopped the Usoi dam impounding Lake Sarez in the expense of several limitations. However, the Usoi dam was considered stable by numerous studies so downstream flood modelling was not done but the hydrograph was constructed from the overtopping volume and duration demonstrating its plausibility of coupling with the flood model. Scenario 1 of Lake Rivakkul did not generate enough run-up height to overtop the dam therefore, it was not able to couple with the flood model. In Scenario 2 of Lake Rivakkul, the peak flood reached at the Rivak village and Khorugh at 2.25 hours and 4.45 hours respectively. The average inundation depths at these places reached about 3.6 m and 4 m accordingly. The results of the chain modelling were represented only as the first-pass hazard assessment. Uncertainties and limitations of each process models along with the challenges of modelling the lake outburst hazard chain were highlighted. Modelling of the lake outburst hazard cascade will inherit some uncertainties and quantification of uncertainties are recommended for a range of acceptable results. To overcome these challenges in the data-scarce mountainous environment, recommendations were made regarding the selection of advanced numerical models complemented by field investigations and the future use of physically-based multi-hazard models which can analyse the entire event within a single run.

Keywords: Lake outburst, modelling, mountainous, rockslide, impulse waves, flood

ACKNOWLEDGEMENTS

"Challenges are what make life interesting. And overcoming them is what makes life meaningful". - Buddha

First of all, I am grateful to my parents and brother. Their relentless love and support drove me to this achievement.

I would like to extend my sincere gratitude to my first supervisor, Professor Dr. Cees van Westen for providing me with all support and knowledge, since the phase of choosing the research topic to the internship and to polishing the final product of this thesis. I am also extremely thankful to my second supervisor, Ir. Gabriel Parodi for his crucial guidance and insights. It is with their mentoring and constructive feedback that I could complete this work.

I would like to acknowledge the Multi-hazard risk assessment project at district level in Tajikistan for providing me with essential thematic data for the study.

I am grateful to all the teachers of NHR domain from whom I gained indispensable skills and knowledge to excel in my career. My gratitude goes to ITC Student Affairs for encouraging us to go through the tough times.

To all my international friends from NHR and other domains as well, I am thankful for all the memories that we have shared. We faced a lot of challenges and most importantly, we overcame together and shared our cultures.

Finally, I would like to thank my Nepalese friends in ITC, with whom I got to share my experiences and got to enjoy some quality time together. Their company made me feel homely.

TABLE OF CONTENTS

LIST OF FIGURES

LIST OF TABLES

LIST OF ANNEXES

1. INTRODUCTION

1.1. Background

Naturally-dammed lakes can be formed in many ways such as by obstruction of a river by landslides, volcanic processes (lava, pyroclastic flows and lahars) or by melting of glaciers. Hazards and risks linked to dam outburst floods have been recorded in mountainous regions all over the world and have been an important research topic for many years. Out of numerous types of dams that are formed naturally, the dams made from landslides, glacial ice and moraines pose the most significant risk to society (Costa & Schuster, 1988).

Lake outburst floods are catastrophic events releasing a high volume of water and sediments with peak discharges that are several orders of magnitude larger than perennial flows (Carrivick, 2006; Quincey & Carrivick, 2015). Worni et al. (2014) argued that the term "lake outburst flood" just defines the final event but there are several underlying events that can cause a dam failure resulting in a flood. Landslide dams can fail due to seismic activity, catastrophic overtopping caused by a landslide entering the lake at high velocity, surface erosion caused by natural overtopping of the lake water, internal erosion (piping), instability caused by lake pressure against the dam or slope instability of the dam faces (Fan et al., 2012; Schuster & Alford, 2004). The glacial ice dams and moraine dams can fail due to ice/snow avalanches or calving glaciers that produce flood waves (Byers et al., 2018). Similarly, rising lake levels causing erosion of moraines, enhanced groundwater flow (piping) through moraines or hydrostatic failures of the ice dams (Mergili et al., 2011) result in disastrous outburst flood downstream. Therefore, the lake outburst floods are the outcomes of multiple hazards and their interactions.

Kappes et al. (2012) have mentioned several complications of multi-hazard assessment; one of them is the interaction between different hazards. Multi-hazard interactions can be classified into several types (Bell & Glade, 2004; Kappes et al., 2010; Gill & Malamud, 2014; Van Westen & Greiving, 2017) as 1) Independent events: two processes acting independent of one another, 2) Compounding events: disposition of one hazard altered by another, 3) Coupled events: processes sharing the same trigger and affecting the same area, 4) Cascading events: one hazard triggering the other and 5) Conditional events: processes in which susceptibility or intensity of other hazard increases substantially, either abruptly or cumulatively. Lake outburst floods are often the results of cascading hazards, also known as domino effect, follow-on event, knock-on effect or triggering effect (Kappes et al., 2012). In most cases, these interactions are not considered at all or too difficult to consider because of their spatial and temporal variability, which result in an underestimation of the actual hazard risk (Kappes et al., 2010; Marzocchi et al., 2012).

Approaches and frameworks for such multi-hazard assessment are scarce in literature because of their complex interactions and difficulties in quantification (Kappes et al., 2012; Gallina et al., 2016). Certain tools have been developed to analyse the interaction between multi-hazards such as CAPRA, ARMAGEDDON, and HAZUS (Kappes et al., 2012). For instance, the CAPRA tool uses different modules for different hazards that are related according to triggering effects between hazards. Besides these tools, the interaction between hazards has been investigated using matrices and scores (Tarvainen et al., 2006; De Pippo et al., 2008). Event tree analysis (ETA) is another approach where the multi-hazard interactions are linked and characterized by the defined value of the probability of occurrence under different scenarios. Thus, ETA reveals all possible results at a higher degree of details (Lacasse et al., 2008; Marzocchi et al., 2012). However, the modelling of each cascading process is done rarely.

1.2. Literature review

1.2.1. Longevity and stability of natural dams

Several studies regarding the longevity and stability of landslide dams revealed that landslide dams have lasted from several minutes to several thousand years after their formation (Costa & Schuster, 1988; Ermini & Casagli, 2003; Peng & Zhang, 2012; Fan, 2013). Table 1.1 shows the results of studies on the longevity of landslide dams for different study cases all over the world.

Table 1.1: Studies related to landslides dam longevity

Reference	Study cases	Description
Costa & Schuster (1988)	187	35% failed within 1 day, 55% failed within 1 week or less, 68% failed within 1 month, 89% failed within 1 year.
Ermini & Casagli (2003)	205	40% failed within 1 day, 70% failed within 1 month, 80% failed within 1 year.
Peng & Zhang (2012)	204	34% failed within 1 day, 71% failed within 1 month, 87% failed within 1 year.

The stability of landslide dams depends upon several controlling factors including geometry, internal structure, material properties, grain size distribution, volume and rate of sediments that flow into the lake and seepage (Costa & Schuster, 1988; Korup, 2002). However, the particle size distribution and internal structure are only exposed after the dam failure, making dam stability prediction a challenging task (Fan, 2013). Costa & Schuster (1988) also documented the longevity of glacier dams, which can fail annually or non-annually, catastrophic or non-catastrophic, depending on the local climate conditions, filling rates of lake and temperature change. On the other hand, the longevity of the moraine dams range from years to centuries and their stability relates to retreating glaciers. The mountain glaciers have continued to recede since late Holocene period and the rate of recession has increased due to global warming in the last few decades (Kattelmann, 2003; Clague & O'Connor, 2015; Harrison et al., 2017). These moraines contain ice cores and debris transported by the glaciers and with the increase in temperature, the stability of moraine dams are compromised as the ice core melts.

1.2.2. Large Landslide-Tsunami generation

Impulse waves or tsunami waves usually occur in oceans, bays, lakes, fjords and reservoirs when the mass movement impacts the water body or due to tectonic activities. Landslides of large volumes with extremely high speed along the subaerial slopes generate destructive water waves. These generated waves are classified as gravity waves and are capable of overtopping the dams and embankments in extreme cases, causing fatalities and destruction of properties (Heller & Hager, 2011). One of such major events caused due to a mass movement was the Vajont landslide that occurred on 9th October 1963. The landslide of 270 million m^3 slid from Mount Toc in northern Italy into an artificial reservoir impounding 115 million m^3 of water by a concrete double-arched dam (Bosa & Petti, 2013; Genevois & Tecca, 2013). The wave run-up swept across the dam reaching over 245 m above its crest and down to the Piave river along the Vajont gorge, where the water level reached up to 70 m (Fritz, 2002; Crosta et al., 2016). The catastrophe claimed about 2000 lives and destroyed numerous villages along the river valley, however, the dam did not collapse in the event which would have caused more destruction.

Several rockslides falling into the Norwegian fjords have generated tsunamis in the 20th century. The Tafjord disaster in 1934 occurred due to a rock avalanche of 3 million m^3 volume which generated a tsunami of 62 m high, claiming 41 lives and destroying the neighbouring villages (Blikra et al., 2005). Similarly, rockslides plunging in Loen in 1905 and 1936 claimed the lives of 133 people by a tsunami with heights between 40.5 and 74.2 m (Harbitz et al., 2014). The authors also asserted that Norway had experienced

about two to three catastrophic tsunami events every century from the historical records of the past 400 years.

The Lituya Bay in Alaska has recorded frequent giant water waves in the last two centuries. In 1958, an earthquake of 8.3 Richter scale triggered a rockslide with a volume of 30.6 million m^3 that slid into the bay. The impact of the rockslide generated waves with a run-up height of 524 m which was seven times higher than the run-up of the Loen event in 1936 and approximately double of the Vajont event in 1963 (Fritz, 2002; Ward & Day, 2010).

The Three Gorges Dam at Yangtze River in China is one of the largest hydropower projects in the world impounding 40 km^3 of water (Yin et al., 2016) in a highly landslide-prone area. The Qianjiangping landslide, for example, with a volume of 20 million m^3 which occurred in 2003, was one of the largest landslides in the Three Gorges area which claimed 11 lives due to tsunami wave height of 30 m (Wang et al., 2008; Crosta et al., 2016). Likewise, the 2008 Gonjiafang landslide (vol. 0.38 million m^3) in the Yangtze River generated a tsunami with a maximum run-up height of 13.1 m (Wang et al., 2015).

1.2.3. Modelling approaches of natural dam outburst flood

Various modelling approaches have been adopted to study the processes of natural dam outburst flood in mountainous regions all over the world. Some studies incorporated all the relevant processes whereas some included only a part of the hazard chain during modelling (Figure 1.1). The types of models include slope stability models, impulse wave models, dam breach models, flood models, experiment-based scale models and complex integrated numerical models. The list of process models is shown in Table 1.2.

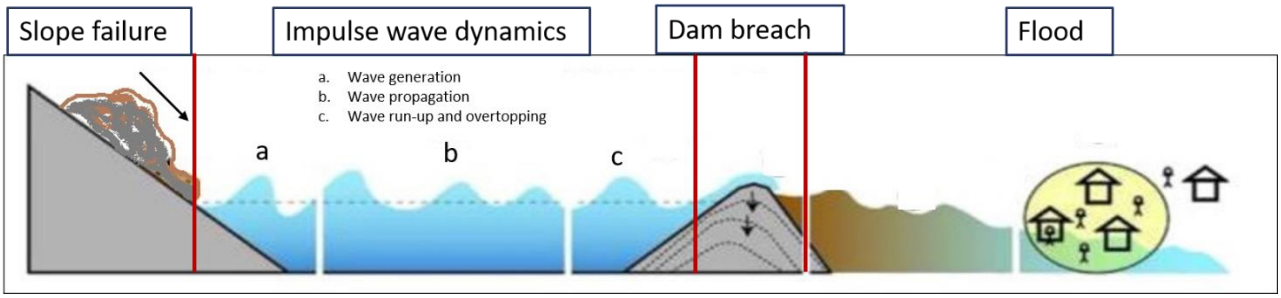

Figure 1.1: Schematic diagram of lake outburst process chain triggered by a slope failure [Modified from Worni et al. (2014)]

Table 1.2: List of process models used for modelling lake outburst flood

Process	Models	Reference
Slope Stability (Runout model)	RAMMS	Mergili et al. (2011); Schneider et al. (2014); Somos-Valenzuela et al. (2016); Lala et al. (2018)
Impulse wave dynamics	Experiment-based physical models	Synolakis (1987); Müller (1995); Fritz (2002); Fritz et al. (2003); Heller et al. (2009); Wang et al. (2015); Heller et al. (2016)
	BASEMENT	Worni et al. (2012); Byers et al. (2018); Lala et al. (2018)
	DualSPHysics	Wang et al. (2015); Heller et al. (2016)
	FLOW-3D	Somos-Valenzuela et al. (2016)
	IBER	Schneider et al. (2014)
Dam breach	BASEMENT	Worni et al. (2012); Byers et al. (2018); Lala et al. (2018)
	BREACH	Fan et al. (2012)

	DAMBRK	Alford et al. (2000)
Flood	BASEMENT (2-D)	Worni et al. (2012); Somos-Valenzuela et al. (2016); Byers et al. (2018); Lala et al. (2018)
	Denlinger Model (1D)	Risley et al. (2006)
	FLDWAV (1D)	Bajracharya et al. (2007)
	FLO-2D	Mergili et al. (2011)
	HEC-RAS (1D)	Bajracharya et al. (2007), Alho & Aaltonen (2008); Osti & Egashira (2009); Butt et al. (2013); Hermanns et al. (2013); Klimeš et al. (2013)
	HEC-RAS (2D)	Anacona et al. (2015); Kougkoulos et al. (2018); Sattar et al. (2019)
	MIKE-11 (1D)	Aggarwal et al. (2013)
	SOBEK 1D-2D	Fan et al. (2012)
	STREAM-2D	Kidyaeva et al. (2017)
	TELEMAC-2D	Alho & Aaltonen (2008)

Slope stability model (Runout model)

Physically-based mass movement runout models, such as the Rapid Mass Movement Simulation (RAMMS), has been used to model the potential mass movement volume impacting into the lake. RAMMS uses the finite volume method for solving two-dimensional, depth-averaged mass and movement equations for granular flow (Christen et al., 2010). Lala et al. (2018) used RAMMS to model a potential avalanche in Imja Tsho, Nepal. Schneider et al. (2014) and Somos-Valenzuela et al. (2016) reconstructed the rock-ice avalanche that fell into the Lake 513 and Lake Palcacocha in Peru which caused the outburst floods. However, it is often difficult to locate the source of the avalanches, the time of its occurrence and a detailed investigation of the remote study area is often required, which is not always possible after the events.

Impulse wave dynamic model

Most of the modelling works on the impulse wave resulting from a rapid mass movement entering a lake have been done using empirical and analytical equations derived from laboratory experiments (Fritz, 2002; Fritz et al., 2003; Heller et al., 2009; Heller et al., 2016) based on simplified assumptions. Analytical equations for impulse wave overtopping and run-up have been developed considering reservoir geometry (channel form or basin form) which often simplify the irregular shapes of natural water bodies (Synolakis, 1987; Müller, 1995). Wang et al. (2015) used physical experiments and numerical simulation to model the potential landslide-generated impulse waves from Gongjiafang slope in the Three Gorges reservoir, China. They used DualSPHysics for numerical modelling which required more accurate topography and slide characteristics data as compared to empirical modelling. DualSPHysics is based on smoothed particle hydrodynamics (SPH) which uses a discrete element method to simulate the slide-water interaction.

Heller et al. (2016) presented a novel experimental-numerical approach for wave generation where the output generated from the experimental methods was used to calibrate the numerical model, DualSPHysics. Another numerical model, Basic Simulation Environment for Computation of Environmental Flow and Natural Hazard Simulation (BASEMENT) which solves the shallow water equations (SWE) has been used to model the wave generation, propagation and run-up (Worni et al., 2012; Byers et al., 2018; Lala et al., 2018). Lala et al. (2018) calibrated the BASEMENT model with the wave heights generated from the analytical Heller-Hager model for avalanche-induced impulse waves. Schneider et al. (2014) used the IBER

model for wave propagation after the estimation of wave generation from the Heller-Hager model. IBER is based on a finite volume non-structured mesh made up of triangular or quadrilateral elements which solve SWE to simulate turbulent, free surface unsteady flow. Somos-Valenzuela et al. (2016) modelled the impulse wave dynamics in the Lake Palcacocha, Peru using a three-dimensional hydrodynamic model called FLOW-3D. They have also pointed out that the 3D simulation of wave dynamics represent the full effects of waves and their magnitudes. FLOW-3D is advantageous over the empirical and 2D SWE models attributing to the inclusion of vertical accelerations during wave generation which is not accounted for in the latter models.

Dam breach model

Dynamic dam breaching is a very complex phenomenon to model due to the combination of various processes such as hydrodynamics, erosion, sediment transport, boulder movement, slope failures etc. (Westoby et al., 2014; Worni et al., 2014; Somos-Valenzuela et al., 2016). BASEMENT is one of the popular hydrodynamic models used to model dam breach process in lake outburst hazard chain (Worni et al., 2012; Somos-Valenzuela et al., 2016; Byers et al., 2018; Lala et al., 2018). It consists of a sediment transport module which applies the SWE scheme to respond to the shear stress from hydrodynamic forces and use empirical functions of non-cohesive sediment transport to estimate drifting, suspended transport, bed-load transport and deposition of sediment (Somos-Valenzuela et al., 2016). Fan et al. (2012) used the physically-based BREACH model (Fread, 1991) to simulate the outflow hydrograph for the Tangjiashan landslide-dammed lake in China. BREACH couples the conservation of mass of the reservoir inflow, spillway outflow and breach outflow with the sediment transport capacity along a breach channel formed by the erosion. Parametric dam breach model DAMBRK (Fread, 1991) was used by Alford et al. (2000) to model the seiche and breach flood scenarios of Lake Sarez, Tajikistan but the results from this study were more indicative than predictive.

Flood model

Flooding is the outcome of the lake outburst hazard chain which comprises of highly turbulent, unsteady flow of different flow transformations (Mergili et al., 2011; Worni et al., 2012). The outburst floods entrain the sediments from the dam material along with the deposits from the valley floor and sides. Such kind of flood has runout distances further than the clearwater flows, due to its increased momentum from the combination of fluid and solid forces and continuous addition of bed and bank erosion (Westoby et al., 2014). One-dimensional hydrodynamic models have been widely used in modelling the downstream flood propagation, which solves the St. Venant equations. For example: Risley et al. (2006) used Denlinger model to route the seiche and breach flood in Lake Sarez, Tajikistan; Bajracharya et al. (2007) used FLDWAV to model the potential GLOF in Imja Tsho, Nepal and the output discharge from FLDWAV was used in HEC-RAS to estimate the flood depth; Osti & Egashira (2009) used HEC-RAS to route the flood in Tam Pokhari, Nepal; Aggarwal et al. (2013) used MIKE-11 to model the potentially dangerous Lake 410 in India to obtain the flood hydrograph; Butt et al. (2013) used HEC-RAS to model the potential flood from the outburst of the landslide dam in Attabad, Pakistan; Hermanns et al. (2013) modelled the scenario-based breach and consequent flood in Rauma river in Norway using HEC-RAS; Klimeš et al. (2013) reconstructed the GLOF in Lake 513 in Peru using HEC-RAS.

Two-dimensional flow simulations are required to represent the complex flow routes which are characteristics of mountainous regions, where 1D model underestimates the actual hazard (Alho & Aaltonen, 2008; Risley et al., 2006). Examples include: Mergili et al. (2011) modelled the flood water as hyperconcentrated flow and debris flow from the outburst of Khavrazdara in Tajikistan. FLO-2D was used to predict the hyperconcentrated flow runout whereas RAMMS was used to model the runout as debris flow using the parameter values from a past lake outburst event in Dasht. They argued that there would be

a flow transformation from hyperconcentrated flows to debris flows as the flood water entrain the sediments along the channel and modelling such kind of phenomena is challenging. Likewise, Schneider et al. (2014) also used RAMMS to model the flood as debris flow whereas Somos-Valenzuela et al. (2016) used FLO-2D for flood routing in Peru.

Fan et al. (2012) used 1D-2D SOBEK to calculate the spatio-temporal variation of flood parameters of Tangjiashan Lake in China. 1D-2D SOBEK model combines 1D river flow in channel and 2D overland flow and can switch the simulation into either dimension during normal and flood conditions. Kidyaeva et al. (2017) used a 2D model called STREAM-2D to model the potential flood from the same landslide-dammed lake outburst in China. Fan et al. (2012) coupled the dam breach model (BREACH) outputs with the flood model to simulate the outburst flood from different scenarios which include natural breach and rainfall as a trigger but not the mass movement. Kidyaeva et al. (2017) only used the flood model to simulate the lake outburst resulting from a mass movement as a trigger to Lake Tangjiashan.

HEC-RAS 2D was used amongst others to simulate the outburst floods in the Chilean Patagonia by Anacona et al. (2015), in the Bolivian Andes by Kougkoulos et al. (2018) and in the Indian Himalayas by Sattar et al. (2019). BASEMENT was used by Worni et al. (2012) to simulate different scenarios of potential flood from three glacial lakes in Indian Himalayas. Byers et al. (2018) and Lala et al. (2018) used BASEMENT to simulate the GLOFs in the Nepalese Himalayas. Worni et al. (2014) claimed BASEMENT as one of the most complete and integral GLOF modelling approach currently available, attributing to its ability to model the impulse wave dynamics in the lake, dam erosion and breach followed by downstream flooding.

Alho & Aaltonen (2008) compared the simulation of extreme glacial outburst floods (Jökulhlaups) using HEC-RAS 1D and TELEMAC-2D to find out the possibilities and the limitations of 1D simulation. They concluded that both models simulated the identical inundation area except in the gorges where HEC-RAS 1D underestimated the flow depths. HEC-RAS 1D performed a stable simulation of extreme events with the calibration of Manning's values from TELEMAC-2D and changes in implicit weighting factor.

1.3. Problem statement and scientific significance

Lake outburst floods of natural dams are much larger in extent and have a shorter peak time than floods caused by rainfall or snowmelt (Costa & Schuster, 1988). Outburst floods are sudden events which have high magnitude discharge with high erodibility power that can transport and deposit the sediments over large areas, making them a serious threat to life and property (Carrivick, 2006). A single major event triggers several processes in a chain of events, which need to be identified and studied in detail. Therefore, understanding the cause of outburst and subsequent modelling of the hazard chain is an important topic to investigate.

Modelling tools can be used to study the lake outburst flood hazards from natural dams, which provide insight regarding the cascading processes. However, obtaining data in the high altitude terrain is quite difficult. According to Chen et al. (2016), lack of inventories related to landslides and reliable hydro-meteorological data for model validation limits the modelling of multi-hazards in mountainous areas. Likewise, subsurface data such as bathymetry of high altitude lakes, rock discontinuities, geotechnical properties are challenging to obtain and represent high heterogeneity and therefore have high uncertainties. Also, modelling multi-hazards is often hampered by the strict separation of disciplines which have different approaches, conflicting definitions and domain-specific tools (Kappes et al., 2012; Worni et al., 2014). Despite several attempts to study the chain processes of lake outburst hazards, a study on the selection and applicability of an appropriate sequence of models in a data-poor mountainous environment is still limited.

To fill this void, single process modelling of outburst flood would not be enough and integrated process chain modelling needs to be adopted to deal with the uncertainties involved in each process (Worni et al., 2014). Therefore, this study attempts to evaluate different sequences of hazard that leads to a lake outburst flood. This model chain could be replicated in any case study of naturally-dammed lakes to study the associated hazards. Thus, among the four major processes of the lake outburst hazard chain, this study aims to address three major components:

1) Slope stability modelling
2) Impact wave generation, propagation and run-up modelling
3) Downstream flood modelling

The scientific challenge of this study is its attempt to find out the interaction between different hazards in lake outburst hazard cascade in a mountainous environment. Modelling individual hazard processes gives insights into the inherent uncertainties which can be identified and quantified to develop future research on multi-hazard interactions. The results of this study can be used as a preliminary hazard assessment approach that will help in the wider goal of assisting local communities, disaster risk management and concerned stakeholders adapt to the risks associated with naturally-dammed lakes.

1.4. Research objectives and research questions

1.4.1. General objective

The main objective of this research is to evaluate the outburst flood hazard chain of naturally-dammed lakes in a mountainous region by integrated process chain modelling under different scenarios. The model outcomes will show the range of relevant possible sequences of hazards and aims to support to disaster risk mitigation planning.

1.4.2. Specific objectives and research questions

Sub-objective 1: To evaluate the hazard interactions and design the sequences of hazards (scenarios) that will lead to natural lake dam breach and subsequent flooding

1) What are the various triggering events, focusing especially on mass movements that can initiate the outburst flood?
2) What are the possible dam breach scenarios that could be modelled in the hazard chain?

Sub-objective 2: To evaluate suitable models to analyse the interaction of various hazard processes

1) What are the appropriate models to be applied for the processes in a lake outburst hazard chain?
2) What are the inputs and outputs of the models adopted in the study?
3) How to couple these models? Is the result of one model compatible with the next model as input?

Sub-objective 3: To identify and, wherever possible, quantify the uncertainties involved in parameterization and scenario design

1) What are the assumptions that need to be made during parameterization?
2) To what extent is it possible to calibrate and validate each process model with existing data?
3) What are the sensitive factors of each process in a hazard chain?

1.5. Organization of thesis and workflow

This thesis is divided into 7 chapters which are as follows:

Chapter 1-Introduction presents the background of the study, a literature review on important topics, problem statement, scientific significance of the study, research objectives and relevant questions.

Chapter 2-Study area and data collection describe the two case study areas: Lake Sarez and Lake Rivakkul and the earlier research work in these areas.

Chapter 3- Description of the model presents the theoretical background of the three models used in this study: Scoops3Di, Heller-Hager model and HEC-RAS. The approach of coupling the models are also described in this chapter.

Chapter 4- Hazard modelling of Lake Sarez describes the scenario design for Lake Sarez. It presents the methods to model the area in the Scoops3D and to couple the outputs with Heller-Hager model concluding with the analysis and discussion of the results.

Chapter 5- Hazard modelling of Lake Rivakkul describes the scenario design for Lake Rivakkul. The methods for modelling the impact waves in Heller-Hager model are described followed by the modelling of downstream flood in HEC-RAS. Finally, results and discussions are presented.

Chapter 6- Discussion presents the limitations and uncertainties of the models used. It also discusses the challenges of modelling the outburst flood hazard chain.

Chapter 7- Conclusion and recommendation contain the main findings of the study and recommendations to improve the modelling of outburst hazard chains in future.

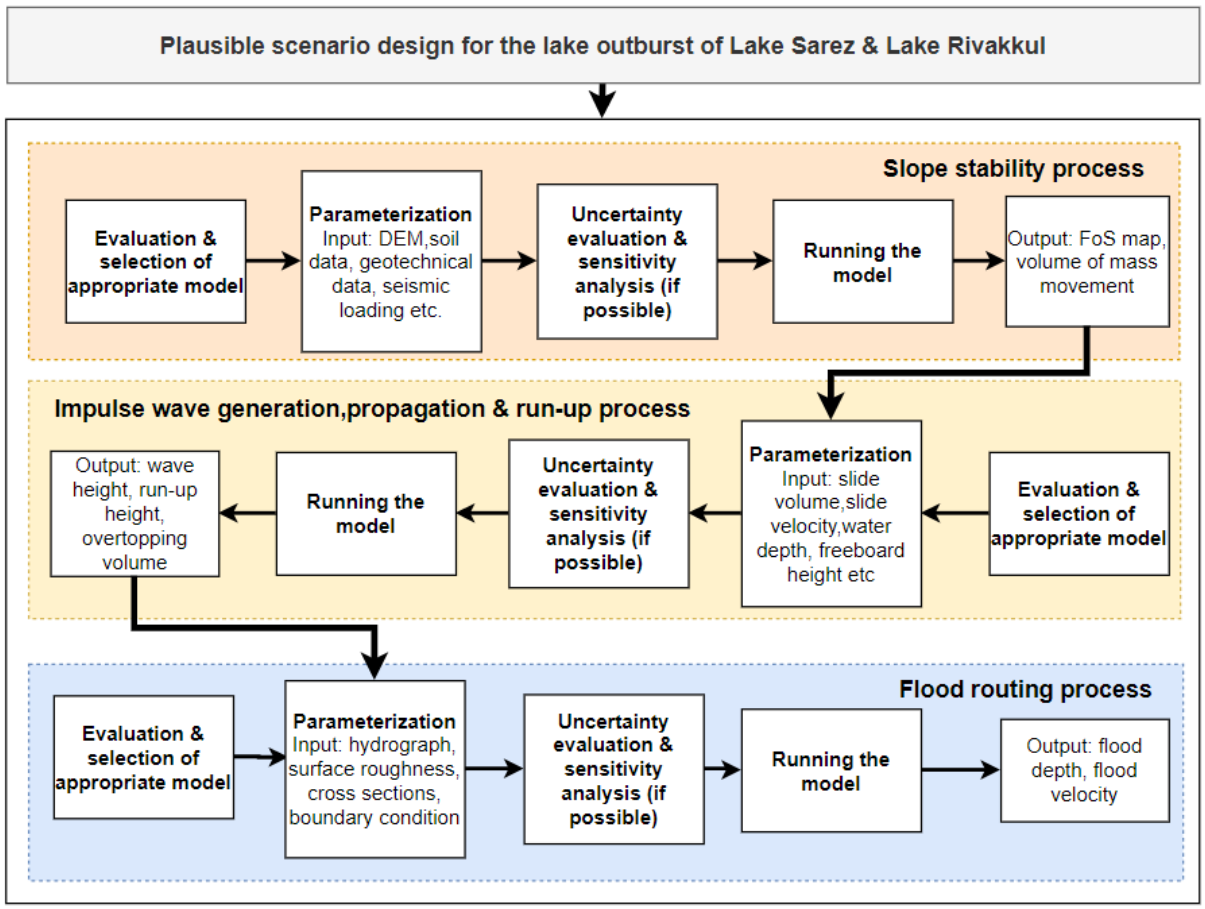

Figure 1.2: Workflow of the study

2. STUDY AREA AND DATA COLLECTION

In this chapter, the general characteristics of the study areas are discussed along with the previous investigations done in these study areas.

Tajikistan is a landlocked, mountainous country located in Central Asia which is divided into four administrative provinces: Sughd, Khatlon, Districts of Republic Subordination (DRS) and Gorno-Badakhshan Autonomous Oblast (GBAO) as shown in Figure 2.1. Both the study areas lie in the GBAO region. GBAO contains one of the highest mountain ranges in the world, known as the Pamir, with mountain peaks higher than 7000 masl. Besides, the region comprises of other smaller mountain ranges such as Shugnan Range, Shakhdara Range etc. Because of its geographic settings, GBAO region is prone to natural hazards: earthquakes, mass movements such as rockslides and mudslides, floods and multi-hazard events such as earthquake-triggered rockslides. These natural events block rivers and streams and along with the recession of glaciers in the mountains, they form high altitude lakes of different dimension and different levels of hazard. As a result, GBAO region consists of many glacial, erosion and landslide-dammed lakes.

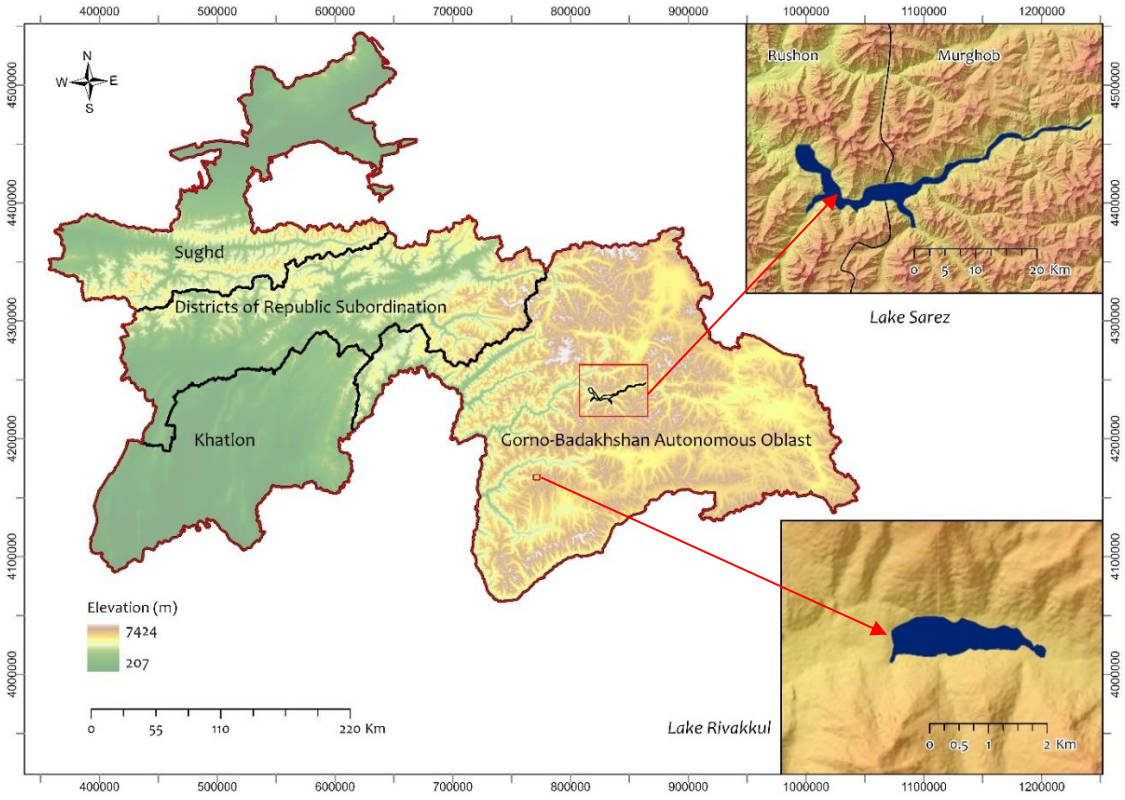

Figure 2.1: Location map of Lake Sarez and Lake Rivakkul in the GBAO region of Tajikistan

Regional-scale analysis of lake outburst hazards was done by Mergili & Schneider (2011) in southwestern Pamir using empirical modelling and remote sensing. 6 lakes were rated very highly hazardous and 34 lakes were rated highly hazardous among the 428 lakes considered (greater than 2500 m^2) in the study region. The regional-scale analysis was done based on available medium resolution satellite images which compromised the detail of the surrounding area and applied coarse estimations of modelling parameters. Nevertheless, they provided the baseline for the detailed studies in future.

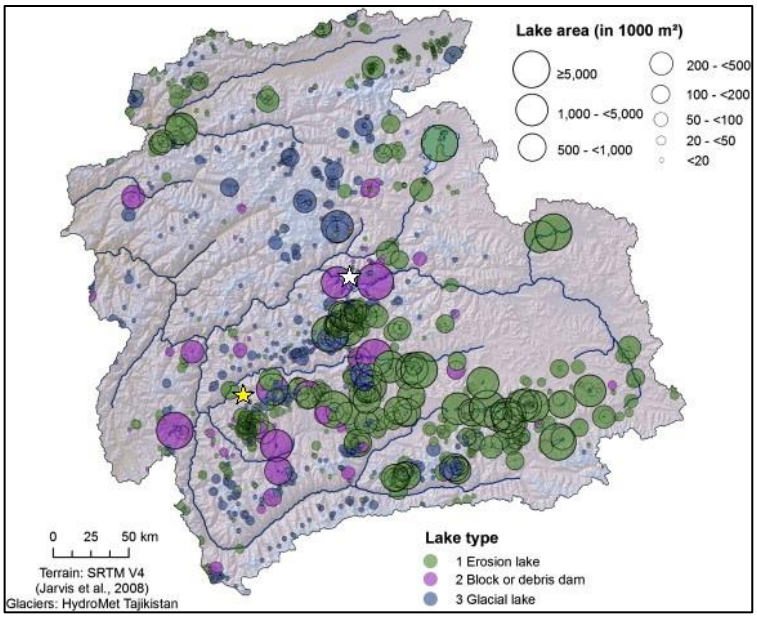

Figure 2.2: Distribution of lakes of various origin and size in the GBAO region; white and yellow star represents the location of Lake Sarez and Lake Rivakkul respectively [Modified from Mergili et al. (2013)]

Mergili et al. (2013) prepared a multi-temporal inventory of the high mountain lakes in the Pamir as shown in Figure 2.2. They delineated 1642 lakes, among which 652 were glacial lakes with a higher growing trend in size and number, compared to lakes of other origins.

2.1. Case study area 1: Lake Sarez

Lake Sarez is located at coordinates 38°12'06" N and 72°45'27" E at 3268 masl. The lake is located in both Murghob and Rushon districts of the GBAO region in Tajikistan (Figure 2.1). An earthquake of M7.2 with epicentre at 38.2°N/72.8°E struck the Pamir Mountains of eastern Tajikistan, north of the Murghab River on February 18, 1911, which resulted in a huge rockslide as shown in Figure 2.3.

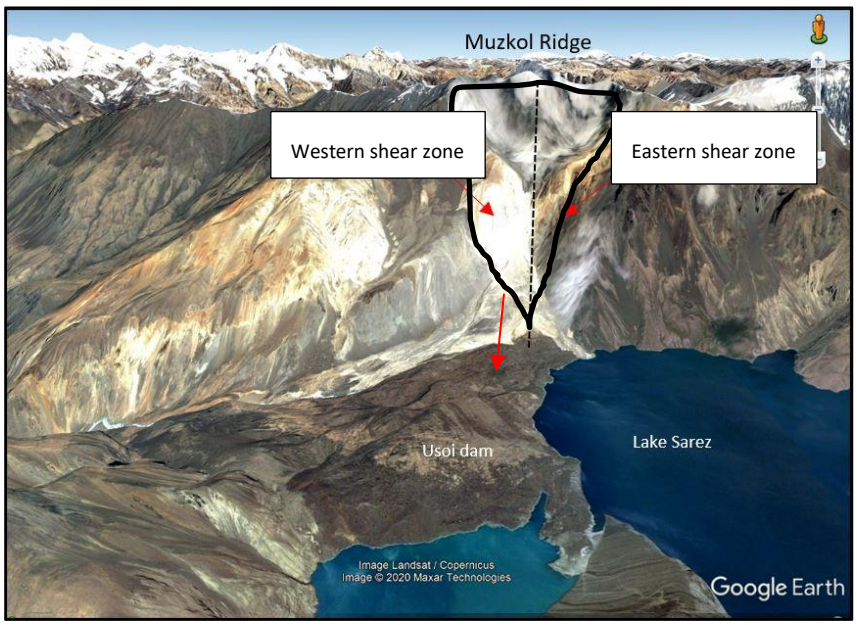

Figure 2.3: Illustration showing the two shear zones of an active wrench fault (dashed line) forming a wedge of failure (black polygon) from Muzkol Ridge resulting rockslide and formation of Usoi dam [adapted from Hanisch & Söder (2000)]

The rockslide dammed the Murgab river and impounded Lake Sarez, forming a 670 m high embankment, also known as Usoi rockslide dam named after the village of Usoi which was buried under it. The Usoi dam is the highest among the natural or man-made dams in the world (Papyrin, 2001; Schuster & Alford, 2004). The volume of the Usoi dam is 2.2 km^3 which slid from the southern ridge of Muzkol Ridge (Ischuk, 2006). The failure of the Usoi dam was due to a combination of unfavourable tectonic activities including a high degree of rock fracturing due to past tectonic movements, presence of a major thrust fault, presence of intensive shear zones setting up for wedge failure as shown in Figure 2.3 (Hanisch & Söder, 2000; Droz & Spacic-Gril, 2002). The visible part of the Usoi dam is composed of quartzites and schists (Carboniferous age) and marbles and shales (Permian-Triassic age) with secondary gypsum, anhydrite and dolomite (Hanisch & Söder, 2000; Ischuk, 2006). The dam is divided into three parts as shown in Figure 2.4 (Hanisch & Söder, 2000; Papyrin, 2001):

1) southern section: highest part of the dam with a freeboard of 250-270 m (3515-3535 masl) which contains blocks of various sizes without any visible fines (silt).
2) central section: has a freeboard of approximately 100 m (3365 masl) and contains a large amount of silts with extremely irregular surface, cracks and openings in the ground.
3) northern section: has the lowest freeboard of 50 m (3315 masl) and consists of blocks with an average diameter of 2-5 m. No fine materials are visible. There are several active rock avalanches, mudflows and debris flows in this section and one of the rock avalanches has diverted its sediment towards the lake.

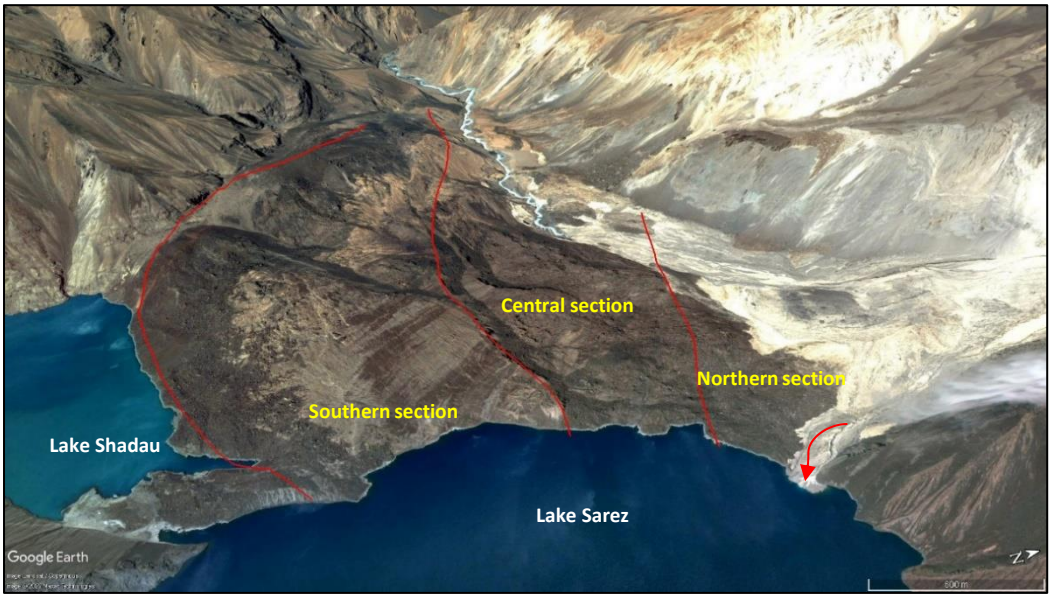

Figure 2.4: Different sections of Usoi dam, the flow of sediments (white granular texture) in the northern section directing towards Lake Sarez from the wedge failure and seepage stream at the background [adapted from Hanisch & Söder (2000); Papyrin (2001); Google Earth (n.d.)]

Lake Sarez is approximately 60 km long, with around 550 m depth, a lake area size of 79.7 km^2 and impounding a water volume of 17 km^3. Figure 2.5 shows the filling curve of Lake Sarez from February 1911 to early 1944 prepared by Delaney & Evans (2011) based on geophysical investigations carried out by Preobrajensky (1920) and Stucky Consulting Engineers (2001). The filling curve indicated that there was a rapid filling of the lake up to 3102 masl till August 1912, completely blocking the river. Seepage only started in May 1914 when the lake level reached 3050 masl. The lake filling rate decreased after 1915 dramatically when the lake level reached about 3100 masl as the outflow through seepage increased. The authors also indicated that the water filling in Lake Sarez occurred in three different time periods:

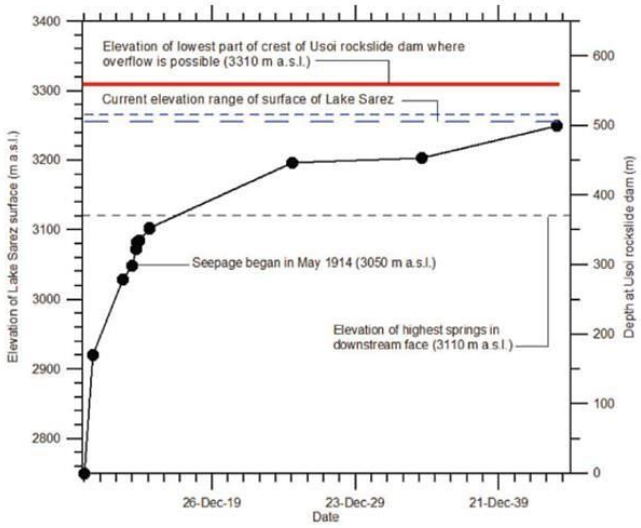

Figure 2.5: Filling curve of Lake Sarez from 1911 to early 1944 summarized from Preobrajensky (1920) and Stucky Consulting Engineers(2001) (Delaney & Evans, 2011)

1) 1911-1914 where there was rapid fill up without any seepage, 2) 1914-1944 where filling rate decreased as outflow counterbalanced the inflow and 3)1944-till present where the water level is at about 3265 m with annual fluctuation and with lake depth of approximately 500 m. According to Droz & Spacic-Gril (2002), the average lake level increased at the range of 8 to 25 cm/year in the 20 year study period between 1949 to 1999. The increase in lake level was attributed to the slow clogging process of the filtration channels which indicated the immature hydrogeological behaviour of the dam. The discharge of the seepage through the dam has an average value of 45 m^3/s with an annual variation of 35-80 m^3/s (Hanisch & Söder, 2000; Droz & Spacic-Gril, 2002).

The dam stability assessment done by several studies indicated that the Usoi dam is highly stable (Droz & Spacic-Gril, 2002; Hanisch & Söder, 2000; Ischuk, 2006). The mechanical stability of the dam in the upstream and downstream part is attributed to its rugged foundation which resists the entire sliding of the dam and the slope is also insignificant (10% gradient). A pseudo-static earthquake analysis on Usoi dam claimed that it could withstand horizontal acceleration up to 0.5g even with lower bound strength of geotechnical parameters. The external erosion of the head of the canyon controlled by the seeping springs was considered as a possible mode of causing the dam instability. But it was unlikely as the headward progression of the canyon would require to penetrate the blocky bedrock and it would even have a positive effect on the water drainage if it succeeds to penetrate (Droz & Spacic-Gril, 2002).

Another possible hazard identified was the internal erosion of the dam. The internal structure of the dam is not known. However, there were no sediments or erosion found in the seeping springs in the downstream slope and it was supported by the fact that the spring had a fairly constant discharge since 1943 (Hanisch & Söder, 2000). Besides, Ischuk (2006) supported that the water was seeping through a complex inter-block hydraulic pathway with a negligible velocity (in range of decimeters per second) which was not sufficient to cause any internal erosion. The possible overflowing of lake water over 3310 masl and subsequent erosion of the dam was also discarded as it would require an additional of 3.2 Gm^3 of water (Delaney & Evans, 2011).

Strom (2014) argued that the Usoi dam was one of the geomorphic and hydrological anomalies among the landslide dams in the world attributing to a fortunate balance between inflow and outflow of the lake water. Nevertheless, morphological and structural features of the dam such as its enormous height, relative compactness, distinct evidence of the downstream face deformations and deep erosional canyons made the dam favourable for failure, for which the long-term safety could not be guaranteed. He also suggested implementing necessary measures while the conditions remain stable for permanent safety.

The so-called Right Bank Landslide (RBL) at about 5 km east from the Usoi dam, has been identified as the most possible slope failure that can slide and generate displacement waves that might overtop or erode the

dam or at least change the seepage system (Figure 2.6). According to Droz & Spacic-Gril (2002), the RBL comprised loose material (silty-sandy-blocky material along with some glacial till deposits) showing certain cementation due to harsh climatic conditions. The bedrock that outcrops along the lakeshore showed the composition of hard and fractured detritic carboniferous rocks of the Sarez formation (sandstones, schists, slates). Besides RBL, Papyrin (2001) argued that there was another possible slope failure in the left bank which has not been accounted for and studied in detail but could be more hazardous to Usoi dam than the RBL, despite its smaller size (0.15 km^3). However, there has been a lot of studies suggesting different volumes and depths of RBL and its hazard to Lake Sarez outburst.

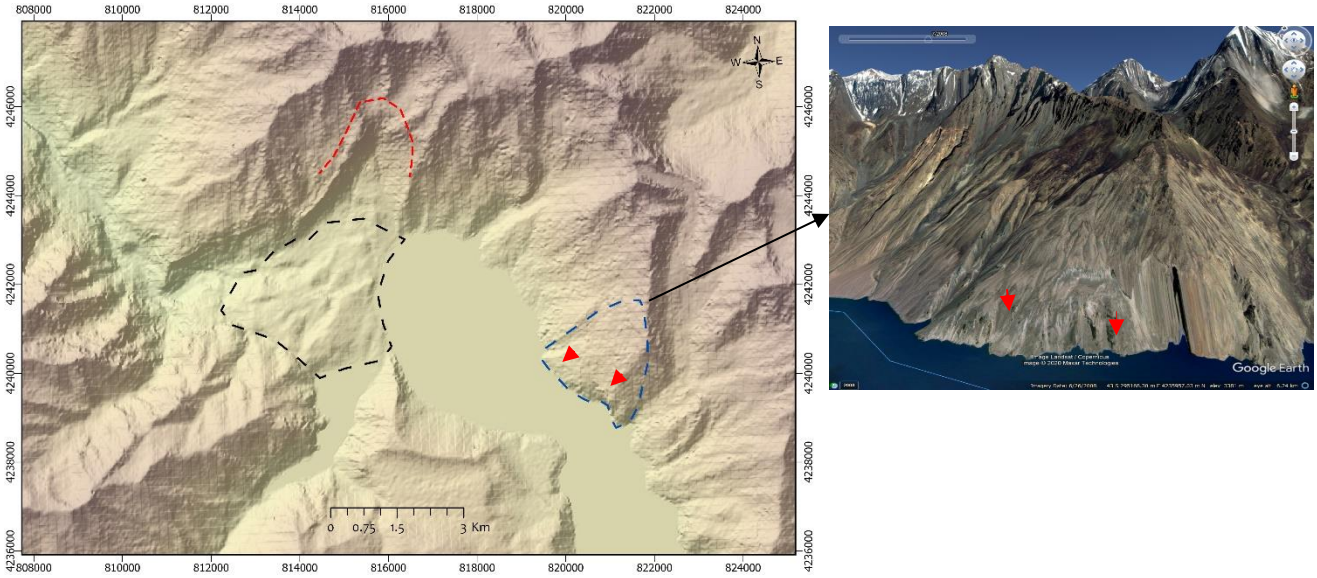

Figure 2.6: Illustration showing location of Right bank landslide (blue dash) along with the landslide scarp from Muzkol ridge (red dash) which formed the Usoi dam (black dash); red arrows indicating the active slide zones in RBL [adapted from Ischuk (2006); Raetzo (2006); Google Earth (n.d.)]

Based on a single seismic survey of the RBL slope bedrock in 1986, the total volume of loose deposits was estimated to be 1.25 km^3 with a thickness of 250 m (Papyrin, 2001). Hanisch & Söder (2000) and Droz & Spacic-Gril (2002) have estimated the volume of the RBL in the range of 0.1 km^3 to 2 km^3 from their field investigations. However, Ischuk (2006) has estimated different volumes dividing the RBL slope into two sections: north-western mass of 0.6 km^3 and south-eastern mass of 0.3 km^3, with a total of 0.9 km^3 and depth ranging from 60 to100 m. He also claimed that the south-eastern part was active and had a high chance of collapsing compared to the north-western part and it was unlikely for the entire slope to fail. Raetzo (2006) divided the RBL into four sections based on specific geologic conditions and slope processes: south, central, north and upper parts. The south part described by Raetzo (2006) corresponds to the south-eastern mass described by Ischuk (2006) dominated by loose material and exposed bedrocks and having high susceptible to slide into the lake compared to other parts. Raetzo (2006) claimed that the monolithic instability of RBL with an estimated volume of 0.5 km^3 with depth estimate of 100 m was not realistic and slides would occur in a succession of smaller volumes rather than a single event.

Several studies have indicated the displacement of the RBL but there were no robust data to prove if the movement corresponded to the loose deposits at the upper surface or to deep-seated movement. Hanisch & Söder (2000) mentioned that the RBL displaced by 1 - 2 cm in the period of nine months recorded by two rod extensometers installed in 1998 whereas Russian investigators found movements up to 10 cm/ year. Ischuk (2006) argued that the displacement of 10 cm/year was restricted to the movement of shallow surface deposits recorded by survey benchmarks located at the depth of 1.5-1.8 m and did not represent the deep-

seated movement. Droz et al. (2008) monitored the historical movement of unstable mass in RBL using GPS measurements and Permanent Scatterer Interferometry (PSInSAR) technique, as part of Lake Sarez Risk Mitigation Project (LSRMP). They found that the movement of the slope was directed toward the lake and displacements measured ranged from 6-16 cm/year between 2004 and 2006 with no clear indication of deep-seated movement. Using PSInSAR, permanent scatterers such as rock outcrops were monitored from the 23 SAR images dated 2003-2006 with a reference GPS point. The authors found that the permanent scatterers were displaced in range of -120 mm/year to 20 mm/year and the results corresponded with GPS measurements in the RBL. The results of terrestrial and spatial measurements indicated that the instability of the entire RBL was negligible.

Lake Sarez was chosen as the study area because of the following reasons:

- Several reconnaissance surveys have been done in Lake Sarez including geotechnical surveys (Hanisch & Söder, 2000; Papyrin, 2001; Droz & Spacic-Gril, 2002). So, the information regarding the formation and present conditions of the lake and the dam are ample.
- From past studies, the Right Bank Landslide (RBL) located at about 5 km east from the Usoi dam had been identified as the potential rockslide that could fall into the lake. The Pamirs are the part of Alpine-Himalayas transorogenic belt characterized by complex geologic structure, extremely high seismic activity and numerous active mass movements (Droz & Spacic-Gril, 2002). Therefore, Lake Sarez represents the scenario where an earthquake-triggered mass movement could occur and the impact waves overtop the dam or erode the dam and cause flood downstream.
- The worst-case scenario of flooding from Lake Sarez will not only affect Tajikistan but also neighbouring countries along the Amu-Darya River basin such as Afghanistan, Uzbekistan, and Turkmenistan. Risley et al. (2006) modelled the worst-case flood scenario with a complete breach of the Usoi dam releasing 17 km^3 of impounded water. Simulated peak flows ranged from 20,000-60,000 m^3/s at distance ranging from 50-530 km downstream of the Usoi dam.

2.2. Case study area 2: Lake Rivakkul

Lake Rivakkul is located at coordinates 37°36'57.00"N and 72° 4'25.43"E at 3820 masl in the Shugnan district of GBAO region in Tajikistan. The lake area is approximately 1.2 km^2. There is no detailed bathymetric information on the depth of the lake however, empirical equations estimate the depth of about 35 m (Mergili & Schneider, 2011). Based on this, the lake volume is estimated at around 0.045 km^3. Lake Rivakkul is fed by glacier meltwater and proglacial lakes from the mountains beneath Yurievskij Pass (5325 masl) as shown in Figure 2.7. A small stream (Bijondara) flows through the dam into the incised Rivak valley until it joins the Gunt River 25 kilometres downstream. The annual average precipitation as snow measured from seven meteorological stations in the Gunt basin was found to be 208 mm/yr. With an average elevation of 4300 masl, the snow cover in the area is greater than 50% in the months of November to March and a distinct transition from snow to glacier melt occurs during July and August, which feed most of the water bodies in the region (Pohl et al., 2015). The region is classified as a cold climate with hot and dry summers (Dsa) according to Köppen–Geiger classification (Peel et al., 2007; Pohl et al., 2015).

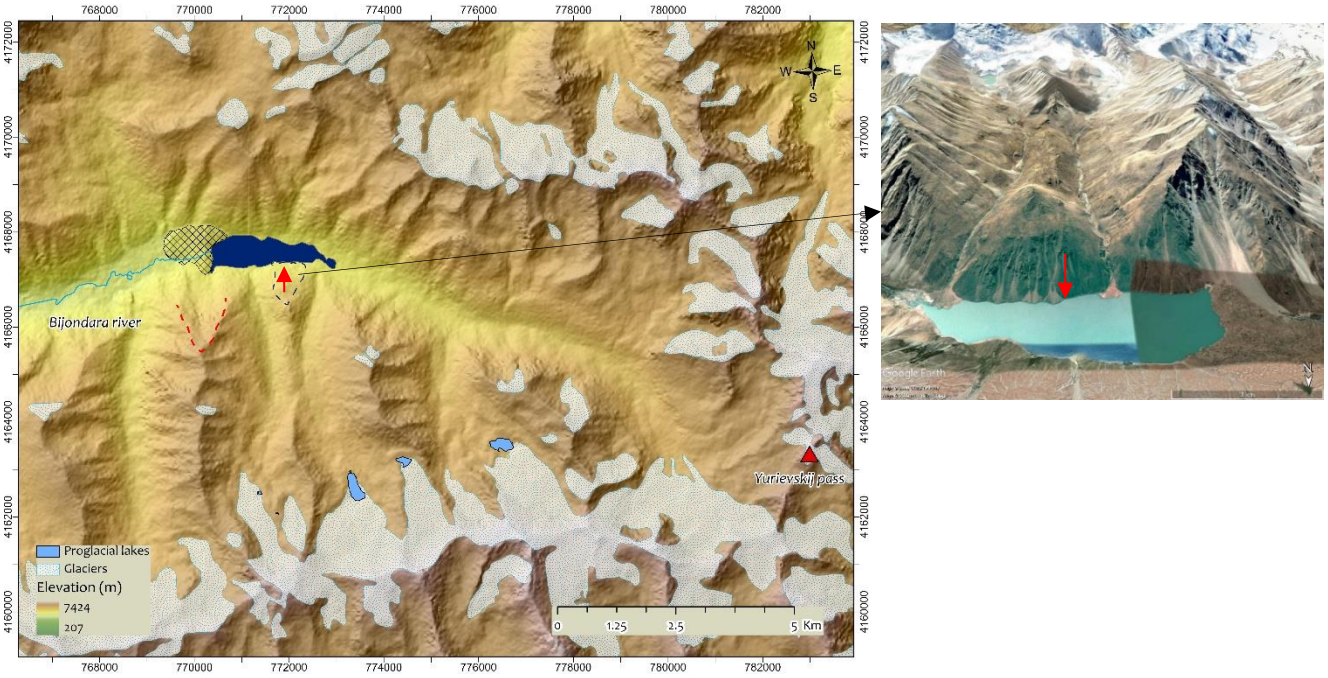

Figure 2.7: Illustration showing Rivakkul dam (cross-hatch) formed due to rockslide (scarp zone in red dash) and series of proglacial lakes draining into Lake Rivakkul. Red arrows showing a potential landslide zone into the lake [Google Earth (n.d.)].

There were contradicting opinions on the origin of the dam that impounds Lake Rivakkul among the authors (Strom, 2010; Ischuk, 2011). Ischuk (2011) claimed that the Rivakkul dam and other lake dams in Central Asia such as Yashikkul, Shiva, Kudara-Pasor were formed by the end moraines of the small cirque (niche) glaciers or pre-glacial nivation hollows or the combination of end moraines as main damming features accompanied by rock slope failures. Ischuk & Saidov (2016) had classified the Rivakkul dam as the final moraine arched ridge formed in the narrow valleys of Pamir. They also mentioned the difficulties in estimating the volume and outbreak potential of such lakes as the valleys were surrounded by cliffs with ice-saturated loose sediments. Strom (2013) disagreed and argued that the dams were formed by rockslides as their head scarps were comparatively fresher than the contemporary niche glaciers. He added that if there were niche glaciers present at one site, then there should exist similar and same-aged geomorphic features in the adjacent slopes at the same elevation, which was not the present in case of Lake Rivakkul. Presence of moraine materials was due to remnants of past glaciers which were overturned and overlaid by the large scale slope failures (Strom, 2006). The dam is about 776.5 m long, 1 km wide and has a freeboard of about 43 m.

Lake Rivakkul is chosen as the study area because of the following reasons:

- Lake Rivakkul is surrounded by steep mountains with snow. It is susceptible to snow avalanches, mudflows and rockslides. Lake Rivakkul falls under the high hazard category with moderate susceptibility according to Mergili & Schneider (2011) attributing to its larger size (greater than 1 km^2) and location (high altitude). The susceptibility rating was based on internal forces (dam material, lake drainage, lake development, downstream slope of the dam) and external forces (topographic susceptibility, calving possibility, seismic hazards, freeboard). The lake size area was used as a surrogate for the potential event magnitude from which lake volume and peak discharge would be estimated using empirical equations and hazard was devised from the combination of magnitude and susceptibility rating. However, the study was done on a regional-scale and field investigation for validation is required.

- Any sudden breach of the Rivakkul dam can cause a huge flood that immediately affects the Rivak village (24 km downstream). After the flood combines with the Gunt river, it flows along villages like Barsem, Manem, Bogev, Bidurd and towards the GBAO region's capital city, Khorugh (60 km downstream of Lake Rivakkul) located at the confluence of Gunt and Panj river. Khorugh is the economical and social hub of the region with a population of 29,900 (Statistics Agency Tajikistan, 2019). Furthermore, there are two small-hydropower plants (Pamir 14 MW and Khorugh 7 MW) and the Pamir highway along the Gunt river towards Khorugh which would be at high risk from the outburst flood. Possible flood routing path is shown in Figure 5.8.

3. DESCRIPTION OF THE MODELS USED

This chapter summarizes the process models used in the study. First, it discusses the different types of methods or models that exist at present and then focuses on the choice of a particular model to analyse the processes in a hazard cascade.

Mass movements such as rockslides are one of the main triggering events in the lake outburst hazard chain. Estimating or predicting the magnitude of the event, such as its volume and velocity provide insights into its consequences on subsequent hazards. Generally, landslide volumes are predicted in two ways: field investigation and physically-based modelling. Field investigations majorly include geotechnical techniques and geophysical techniques (Jongmans & Garambois, 2007; Pazzi et al., 2017). The details of geotechnical methods to assess the stability of natural slopes are discussed by Fell et al. (2000). The advantages of geophysical methods over geotechnical methods include its non-invasive method with flexibility and usability in slopes where large volumes can be investigated. However, drawbacks include the decreasing resolution of the methods with increasing penetration depth, indirect information and non-unique solution for which the geotechnical data has to be known with a precise degree of certainty (Hack, 2000; Jongmans & Garambois, 2007).

Physically-based models are based on physical laws that replicate the underground conditions of the potential failure slope. It requires input data such as terrain data, soil parameters (soil cohesion, soil internal friction angle, bulk density, soil thickness), hydrological parameters (saturated hydraulic conductivity, infiltration capacity) etc. These models adopt two different principles to analyse the stability of the slope: Limit Equilibrium Model (LEM) and Finite Element Model (FEM). In FEM, the model domain is split into a finite number of elements where the force and strain are calculated for each element using constitutive equations. These models are advanced as they can account for site-specific features such as tension cracks and external loads. However, these models require advanced geological boundary conditions and accurate input parameters. Most of the physically-based models use LEM where potential failure surfaces are predefined and equilibrium of forces or moments of predefined failure surfaces are calculated. The LEM can be applied in 1D, 2D or 3D slope stability analysis.

Actual slope failures are three dimensional (3D) in nature and analysis using 3D models give comparatively more accurate estimation or prediction of failure volume (Reid et al., 2015). 3D models such as OpenLISEM (Bout et al., 2018), Scoops3D (Reid et al., 2015), r.slope.stability (Mergili et al., 2014) are capable of modelling the slip surface in a GIS environment and are suitable for simulating the volume of potential large slope failures. They account for the pre-defined slip surface geometry as circular or elliptical and are applicable for deep-seated landslides. Scoops3D was used in this study to predict the volume from the potential failure slope attributing to its efficient user interface, open-source and capability to simulate in a GIS environment along with the inclusion of horizontal force as seismic loading. The failure volume and depth obtained from the model are used as inputs for the following impact wave dynamics model.

Generally, in practice, the landslide impulse waves are assessed through 3 methods (Heller et al., 2009, 2016):

1) General applicable equations derived from the physical model tests
2) Case-specific numerical simulations
3) Case-specific physical model tests

General applicable equations require the unknown wave parameters to be expressed through generic equations as a function of slide characteristics and wave propagation parameters. The equations are derived

through rigorous experimental set-ups in the laboratory in a 2D wave channels or 3D wave channels. All the experiments are based on the idealization of a horizontal bottom which limits the use of this method in a reservoir with complex geometry. However, this method allows a cost-effective preliminary hazard assessment within a limited time-span and moderate resources and expertise.

Numerical methods are more accurate in predicting the wave characteristics but it requires high computation power, longer time and skilled expertise along with detailed data resources. Case-specific physical model tests replicate the prototype or study area in terms of its complex geometry providing the most accurate method in assessing the impulse wave characteristics at present. Nevertheless, this method requires a substantial amount of resources and logistics with a timeframe of more than a year.

Heller-Hager model was chosen for this study because of its low computational time yet precise and clear estimations compared to high resolution, data demanding numerical models and prototype specific physical models. The outputs from the model such as overtopping volume and duration can be used to construct hydrograph to couple the flood model.

Seiche wave or breach of the dam results in a large flow of impounded water with high discharge in the downstream community. As the water entrains the sediment from dam and valley floor, the flow characteristic varies significantly. Therefore, the flood water can be routed as clear water or modelled as debris flow or combination of both to represent different scenarios of disaster.

HEC-RAS is widely used in modelling the lake outburst flood as clear water to assess the hazard in downstream communities (Bajracharya et al., 2007; Alho & Aaltonen, 2008; Osti & Egashira, 2009; Butt et al., 2013; Hermanns et al., 2013; Klimeš et al., 2013; Anacona et al., 2015; Kougkoulos et al., 2018; Sattar et al., 2019). Because of its free availability and improved stability with the 2D hydraulic calculation for a steep river such as in our case, HEC-RAS was chosen to model the downstream flood.

3.1. Slope stability model: Scoops3D

Scoops3D was originally developed by Reid et al. (2015) to analyse the volcanic edifice failures and subsequent hazard analysis. Later Scoops3D-i was further developed in a computer software by U.S. Geological Survey (USGS) for slope stability analysis throughout a digital landscape represented by a DEM. Scoops3D can incorporate complex topography along with 3D distribution of subsurface properties, pore-water pressures and seismic loading. Scoops3D uses the 3D " method of columns" limit-equilibrium analysis with a spherical potential slip surface.

The detailed Factor of Safety (FoS) calculation in Scoops3D can be found in Reid et al. (2015). The potential landslide volume can be calculated in Scoops3D by following steps:

1) The potential slip surfaces are searched in the terrain (DEM) using a complete search method with user-defined options such as box search, single surface search or file search. These options are chosen to limit the permutation of infinite searches in DEM. The search method generates millions of spheres that intersect the DEM also known as trial surfaces. These spatially distributed spheres are defined by several internal model parameters discussed below.
2) The stability of each trial surface is calculated using two different LEMs: Ordinary method (Fellenius, 1936) and Bishop's simplified method (Bishop, 1955). Single FoS is determined for all the pixels that contain the trial surface. Each pixel will be intersected by the number of trial surfaces until the lowest FoS is determined.

3) As the pixels are cut by the number of spheres, the trial surface with the minimum FoS will be determined as the potential slip surface for that pixel. Final slip surface for an individual landslide is determined by the combination of pixels containing the least stability.
4) A new terrain map is generated with all the materials of potential slip surfaces removed based on the cutoff FoS value assigned by the user. Then, the failure height map is produced by subtracting the new terrain by previous terrain map and pixel size is multiplied with the failure height map to calculate the potential landslide volume.

Scoops3D uses several internal parameters during search method which influence the final volume. Model internal parameters include search lattice extent, search resolution and volume limit. Two landslide triggers can be assigned in Scoops3D: pore water pressure due to groundwater and seismic loading. The internal parameters and triggers in Scoops3D are further discussed in Annex 1.

3.2. Impulse wave generation, propagation and run-up model: Heller-Hager model

The Heller-Hager model is a combination of generally applicable empirical equations derived from several physical experiments that investigate the landslide generated impact wave in lakes and reservoirs (Heller et al., 2009). In this model, the mass movement as a triggering event is modelled as a granular, sub-aerial landslide.

Figure 3.1 illustrates the three phases of landslide generated impact wave over a horizontal bed reservoir. Impacts waves are generated due to sub-aerial landslides and get propagated towards the dam through wave transformation. The final phase is represented by the wave run-up and force transfer into the dam and in some cases, the transferred wave overtops the dam and floods downstream. In narrow reservoirs, the second phase i.e. wave propagation may not occur at all.

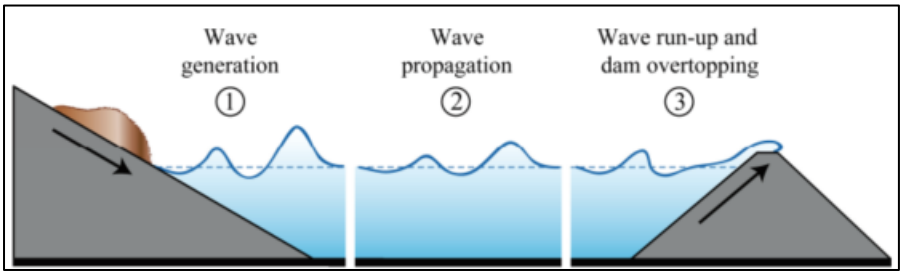

Figure 3.1: Three phases of landslide generated impact wave: 1) slide impact generating wave, 2) wave propagation with wave transformation, 3) run-up of impact wave, load transfer to the dam and/or overtopping [Heller (2007)]

Figure 3.2 shows the computation method of the landslide induced impact waves in Heller-Hager model. In the first phase i.e. wave generation and propagation phase, the generally applicable equations are used to differentiate the generation of the wave from a prismatic wave channel (2D) or that from a rectangular wave basin (3D). Heller (2007) developed the 2D equations based on Zweifel (2004) and Fritz (2002) whereas 3D equations were developed based on Huber & Hager (1997). The second phase computes the run-up and overtopping of the waves through a method devised by Müller (1995). Based on the wave profile and internal water movement, the wave forces on the dam are computed by two different methods in the third phase. Non-linear water waves are of different types such as 1) Stokes wave: waves whose trough are flatter and longer than the crest capable of slight transfer of the fluid mass, 2) Solitary wave: non-linear tsunami-like wave capable of large transfer of the fluid mass, 3) Cnoidal wave: wind-generated waves in shallow water with flat troughs and crests and 4) Bore waves: shallow-water waves with horizontal particle movement and having a large fluid transport capacity.

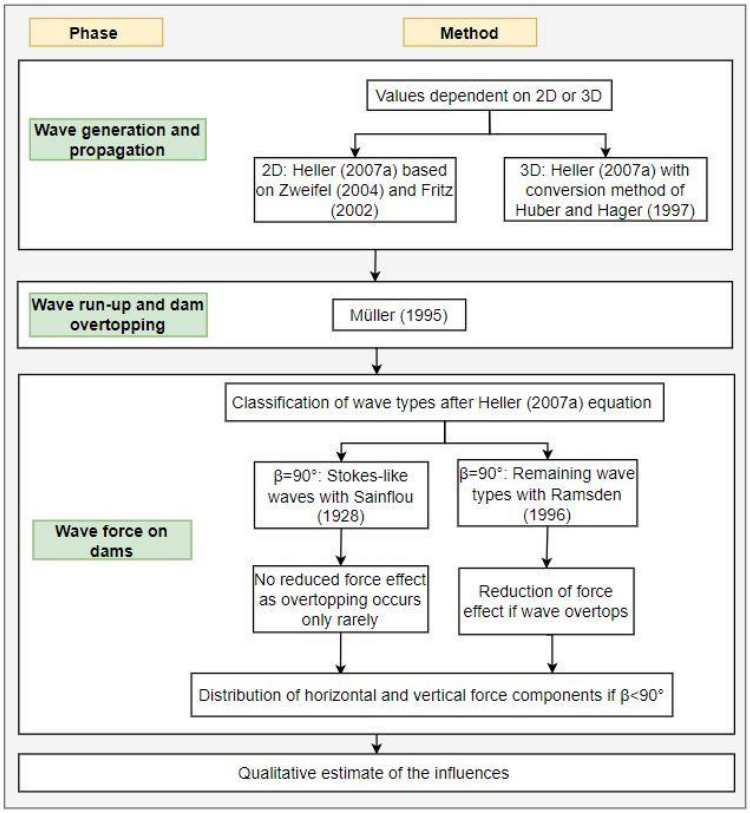

Figure 3.2: Computation procedures of landslide induced impact waves with different phases in Heller-Hager model [Modified from Heller et al. (2009)]

The Stokes waves are computed by Sainflou (1928) method and remaining wave types (Solitary, Cnoidal, and Bore waves) are computed following the method by Ramsden (1996). In the first step of wave force calculation, the dam wall is considered vertical (β=90°) for both methods with full force effect without overtopping. The remaining waves are more likely to overtop so a corresponding force reduction method is applied. If the dam is not vertical (β<90°), wave force into the dam is resolved into horizontal and vertical components. After the computation of these generally applicable equations, the effects of variation from an idealized reservoir geometry are accounted for and described qualitatively.

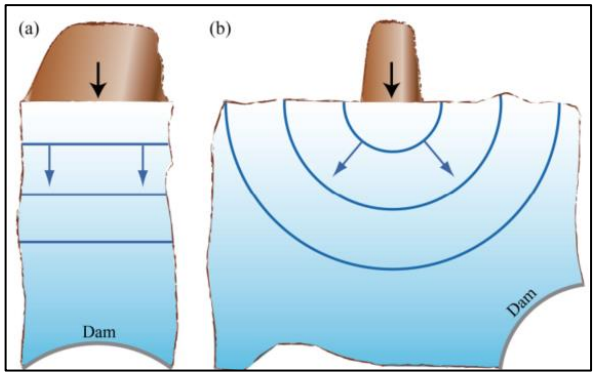

Figure 3.3: Idealized reservoir geometries showing different positions of dams and impacting slides. a) Extreme case with longitudinal impact slide and confined transverse wave propagation, b) Extreme case with impact slide and free radial wave propagation [Heller et al. (2009)]

The generally applicable equations for wave generation are derived from laboratory tests either in a 2D prismatic channel or in a 3D rectangular wave basin. Figure 3.3 shows the extreme cases of 2D and 3D tests. In the extreme case a), the slide which is equal to or greater than the reservoir width impacts the reservoir longitudinally and confined wave propagates into the dam. In extreme case b), the slide is smaller than the width of the reservoir and impacts at any possible location and the waves can propagate radially and freely from the impact zone. Any model tests that deviate from these two idealized geometries will increase the model effects and will have the potential to exceed the limitations of the model. The exceedance of the limitations is not desirable as it increases the model uncertainty. The exceedance of limitations might be caused due to dissimilarity of the 2D or 3D reservoir geometry between the model and the real-world prototype, which result due to wave phenomena such as diffraction, reflection, refraction, shoaling, constriction etc. These phenomena are not accounted for during computations in the initial phases of the model. The details of the governing equations, limitations and sensitive parameters of the Heller-Hager model are further discussed in Annex 2.

3.3. Flood routing model: HEC-RAS 5.0.7

HEC-RAS (Hydrologic Engineering Centre - River Analysis System) is an integrated system of software which allows performing 1D, 2D and/or a combined 1-2D steady and unsteady flow in open channels including sediment transport computations (no detachment), temperature and water quality monitoring. HEC-RAS software was developed by Hydrologic Engineering Center at Institute for Water Resources (IWR), U.S. Army Corps of Engineers. It is free hydraulic software with a friendly graphical user interface.

In this study, 2D unsteady computation is adopted to model the downstream flood. HEC-RAS 2D flow modelling has several advantages or capabilities such as 1) flexibility in using 2D Diffusion Wave equations or full 2D Saint Venant equations, 2) combined modelling of 1D and 2D flow computations at the same time, 3) uses the underlying detailed terrain (high-resolution sub-grid model) to represent the model outputs, 4) faster computations and integrated GIS with RAS Mapper.

Numerical simulation

The new version of HEC-RAS solves either 2D Saint Venant equations or 2D Diffusion wave equations for the hydrodynamic simulation. Let us assume the bottom surface elevation is given by z (x, y), h (x, y, t) is the water depth such that the water surface elevation be H(x, y, t) = z (x, y) + h (x, y, t) as shown in Figure 3.4.

The unsteady differential form of the mass conservation (continuity), assuming incompressible flow is shown by equation 3-1.

$$\frac{\partial H}{\partial t} + \frac{\partial (hu)}{\partial x} + \frac{\partial (hv)}{\partial y} + q = 0 \qquad [3\text{-}1]$$

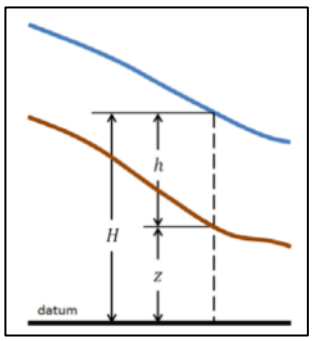

Figure 3.4: Illustration of water surface profile for numerical simulation

where H (m) is surface elevation, h (m) is the water depth [h (x, y, t)], t (s) is time, u and v (both m /s) are the velocity components in the x- and y-direction respectively and q (m/s) is the source and sink flux term. Neglecting the vertical velocity and vertical derivatives from the Navier-Stokes equation for fluid motion, the unsteady differential form of the momentum conservation equations are shown by equations 3-2 and 3-3.

$$\frac{\partial u}{\partial t} + u\frac{\partial u}{\partial x} + v\frac{\partial u}{\partial y} = -g\frac{\partial H}{\partial x} + v_t\left(\frac{\partial^2 u}{\partial x^2} + \frac{\partial^2 u}{\partial y^2}\right) - c_f u + fv \qquad [3\text{-}2]$$

$$\frac{\partial v}{\partial t} + u\frac{\partial v}{\partial x} + v\frac{\partial v}{\partial y} = -g\frac{\partial H}{\partial y} + v_t\left(\frac{\partial^2 v}{\partial x^2} + \frac{\partial^2 v}{\partial y^2}\right) - c_f v + fu \qquad [3\text{-}3]$$

where u and v (both m/s) are the velocity components in the x- and y-direction respectively, g (m^2/s) is the acceleration due to gravity, v_t (m^2/s) is horizontal eddy viscosity coefficient, c_f (m/s) is the bottom friction coefficient, and f (s^{-1}) is Coriolis parameter. When diffusive equations are chosen, the inertial terms such as unsteady, advection, Coriolis and turbulence terms of the momentum equations are neglected which makes the simulation faster and simpler.

To solve the above-mentioned equations in HEC-RAS, implicit finite volume algorithm is used as a solver which approximates the average integral on a reference volume and allows a more general approach to unstructured computational cells. The model domain must be sub-divided into computational structured or unstructured meshes or grids or cells. The boundary cells of the model domain vary with shape and size. The cells can be three-sided up to eight sides. Figure 3.5 represents an example of a triangular computational cell with its components. The water surface elevation is calculated in the cell centre. Cell faces are the straight

lines, but also can be multi-point lines and cell face points are the end of cell faces joining adjacent cells. Each cell represents a detailed elevation-volume relationship with the help of underlying terrain data. The cell faces in HEC-RAS contain the hydraulic properties information such as cross-sections, wetted perimeter, elevation, roughness etc. Thus, this approach makes the use of larger cell size and yet accurately represent the underlying terrain. The equations are solved with an iterative scheme with a maximum of 40 iterations.

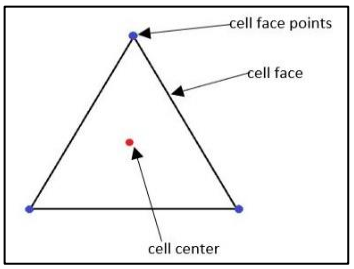

Figure 3.5: Example of a triangular computational cell with its components used for solving the hydrodynamic equation

Selecting an appropriate computational time step is as important as assigning an appropriate computational cell for the model stability and accurate solutions. Diffusion Wave equations and Saint Venant equations are the two options in HEC-RAS to solve for the fluid motion over the computational mesh. Generally, the Diffusion Wave equations are numerically lenient compared to the Saint Venant equation although large time steps can be used with the former. The following equations 3-4 and 3-5 guide the user for picking a computational time interval for the Diffusion Wave equations and the Saint Venant equations respectively.

$$\mathbf{C} = \frac{\mathbf{V}\Delta\mathbf{T}}{\Delta\mathbf{X}} \leq \mathbf{2.0}\ (\text{with a max}\, \mathrm{C} = 5.0) \quad \text{Or} \quad \mathbf{\Delta T} \leq \frac{\mathbf{2}\Delta\mathbf{X}}{\mathbf{V}}\ (\text{with C} = 2) \qquad \textbf{[3-4]}$$

$$\mathbf{C} = \frac{\mathbf{V}\Delta\mathbf{T}}{\Delta\mathbf{X}} \leq \mathbf{1.0}\ (\text{with a max}\, \mathrm{C} = 3.0) \quad \text{Or} \quad \mathbf{\Delta T} \leq \frac{\Delta\mathbf{X}}{\mathbf{V}}\ (\text{with C} = 1) \qquad \textbf{[3-5]}$$

where C is Courant number, ΔT is the computational time interval (s), V is the flood wave velocity (m/s), and ΔX is the average cell size (m). The general steps to perform 2D modelling in HEC-RAS is shown in Annex 3.

3.4. Coupling of models

Figure 3.6 shows the input and output parameters of different process models used in this study and the general idea of coupling the models. The output from Scoops3D such as failure volume map gives the volume of mass failure from each pixel. The new terrain data is subtracted from previous terrain data to obtain a failure depth in ArcMap. The failure depth map is then multiplied with the pixel size to obtain the final failure volume map using the zonal statistical tool in Arcmap.

The obtained depth and volume of mass failure are assigned as input parameters for Heller-Hager model (shown in red colour) whereas other parameters are assigned independently. The subsequent outputs from the Heller-Hager model (shown in green colour) such as overtopping volume, duration and discharge are used to construct a simple triangular hydrograph, which is one of the main input parameters for HEC-RAS flood model. Other input parameters of the flood model are assigned accordingly with respect to the model domain.

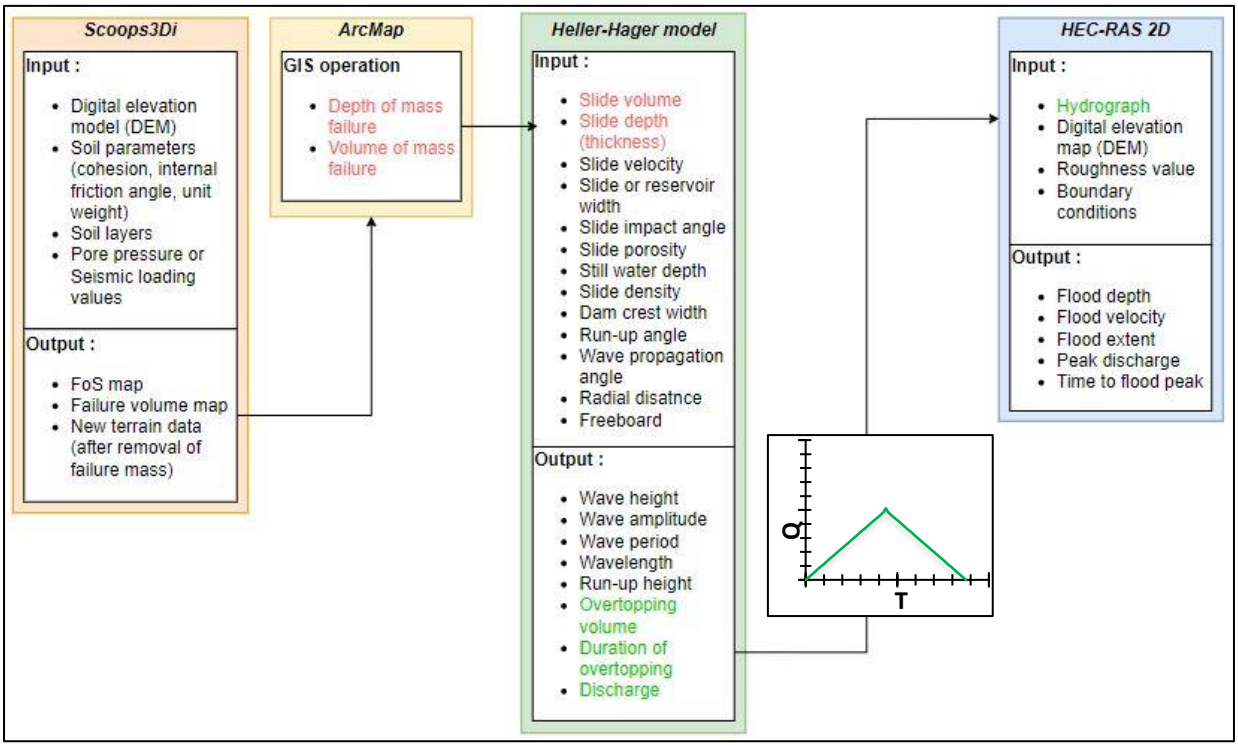

Figure 3.6: Inputs and outputs of different process models and approach to couple the models (colored parameters are only used as for coupling the models and rest are independently assigned)

4. HAZARD MODELLING OF LAKE SAREZ

In this chapter, Lake Sarez is modelled for possible mass movement events that might lead to dam break or overtopping of its dam depending upon different scenarios as well as its topographical, geological and hydrological conditions. The first part focuses on designing possible scenarios for lake outburst. The second part focusses on the organization of the input data preparation for the Scoops3D and Heller-Hager model with data obtained from the literature, empirical equations, satellite imageries, and digital elevation model (DEM). The results of the Heller-Hager model are used to construct a hydrograph to test its plausibility for a subsequent flood model. Finally, the results are analysed and discussed.

4.1. Scenario design

As mentioned in chapter 2, the so-called right bank landslide (RBL) had been identified as a potential rockslide area by various authors. It is located at approximately 5 km east of Usoi Dam, and this landslide has a potential to catastrophically fail into the lake as shown in Figure 2.6 (Hanisch & Söder, 2000; Droz & Spacic-Gril, 2002; Ischuk, 2006; Raetzo, 2006; Strom, 2014). Papyrin (2001) argued about another potential landslide on the left bank of Lake Sarez but the exact location is not known and its investigations in the literature are scarce compared to RBL. During the scenario design for the Scoops3D and Heller-Hager model, only the RBL was used as the potential mass movement that could fall into the lake and generate the impact waves in the lake. Three scenarios were designed:

1) In Scenario 1, Scoops3D was used to predict the potential mass failure (volume and depth) which was then assigned to Heller-Hager model to analyse the impact wave generation, propagation and run-up. The geotechnical properties such as cohesion, internal friction angle and unit weights were assigned from past studies and empirical data, as such information of RBL was scarce in the literature compared to the Usoi dam. Initially, the hypothetical set of geotechnical parameters were used without seismic loading. The idea was to make the FoS value more or less equal to 1 for maintaining the near metastable state. The geotechnical parameters were varied by trial and error method until the slope reached the near metastable state. Once the optimal parameters were chosen, the seismic loading was added as a trigger to calculate FoS and subsequently the volume of failure mass. Scenario 1 was divided into Scenario 1a and Scenario 1b representing the mass failure of entire RBL and the region having the lowest FoS respectively.
2) In Scenario 2, the optimistic range of values of slide characteristics of RBL were acquired mainly from past studies and modelled in Heller-Hager model. Likewise, satellite images and DEMs were used to support the values of the parameters required for the model. The outputs of the model were then analysed and discussed.
3) In Scenario 3, the pessimistic range of slide characteristics from the past studies were used to model to check if the output such as run-up height exceeded the freeboard of the dam or not. However, this scenario was very unlikely without any external trigger such as earthquake but this scenario gave an idea about the impact waves created due to such large magnitude failure. Only two input parameters of Heller-Hager model i.e. slide volume and slide depth/thickness were modified because other parameters could be estimated from satellite images, DEM, Google Earth, empirical equation. All three scenarios were assigned with the same values.

4.2. Input data preparation

4.2.1. Scoops3D

Scoops3D assumes the potential slip surface as spherical resembling a rotational slide (Reid et al., 2015). No information on groundwater and soil layers were available for the RBL, so a homogenous, dry condition of the soil was assumed. The soil properties are related to their parent material and their formation mechanisms and hence, present a wide range of spatial heterogeneity. Considering limited literature on the RBL, the geotechnical parameters required for Scoops3D were assigned from past studies at different regions as shown in Table 4.1.

Table 4.1: Geotechnical parameters of rockslides from literature

Description		**Geotechnical parameters**			**Reference**
Location	**Geology**	**cohesion, c (kPa)**	**internal friction angle, Ψ(°)**	**unit weight, γ' (kN/m³)**	
Vaiont rockslide, Italy	composed of breccia and clay interbeds	na	12	na	Hendron & Patton (1987)
Riou-Bourdoux Valley, France	bedrock consists of dark marls, chalky flysch	0-14.1	23	16.1	Caris & Van Asch (1991)
Usoi rockslide dam, Tajikistan	wedge failure; composition of glacial deposits, breccia, quartzites, schists, marbles, shales	0-10	25	22	Hanisch & Söder (2000)
Guinsaugon rock slide-debris avalanche, Philippines	dominant rocktypes: sandstone and breccia	0.45-0.78	22.9	20.7-21.8	Catane et al. (2008)
St. Catherines Point, England	weakly cemented sandstone with clay seams, rotational slumping of active wedge. Likely retrogressive behaviour	0	7.5-20	na	Glastonbury & Fell (2008)
Ventnor, England	weakly cemented sandstone over thick consolidated clay, rotational slumping of active wedge. Likely retrogressive behaviour	0	10	na	Glastonbury & Fell (2008)
Diezma, Betic Cordillera, Spain	complex movement initiated by rotational slide; quartzite, sandstone, limestone, dolostone	0.3	12	na	Azañón et al. (2010)

Advanced Land Observation Satellite-Phased Array type L-band Synthetic Aperture Radar (ALOS-PALSAR) DEM was used for the terrain data. At first, the cohesion (c) value was assumed to be 0 kPa to provide the least soil strength. The internal friction angle (Ψ) was assumed to be 10° and unit weight (γ') of 25 kN/m³, which corresponded to the lithology present in the RBL (further described in section 4.2.2). The internal model parameters for Scoops3D and their recommended values are discussed in Annex 1. The volume limit used in the study ranged from 10^5 m³ to 10^{10} m³ considering the estimated volume of RBL from past studies (Table 4.6). Table 4.2 summarizes the internal model parameters used to search trial surfaces for Scenario 1.

Table 4.2: Search parameters for Scoops3D

Search lattice extent (m)		**Search resolution (m)**			**Volume limit (m³)**
Horizontal	Vertical	Horizontal	Vertical	Radius increment	
DEM extent	3300-5000	12.5	12.5	2	10^5-10^{10}

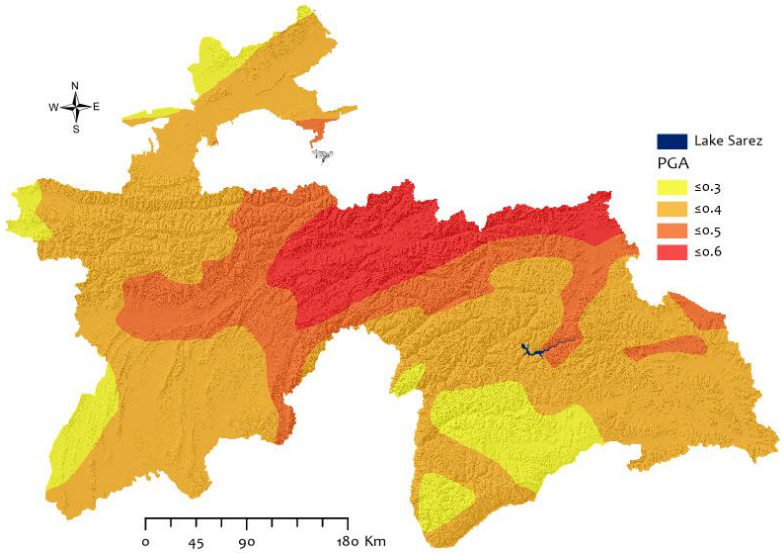

Figure 4.1: Peak ground acceleration (PGA) values for return period of 475 years for Tajikistan

Figure 4.1 shows the Peak Ground Acceleration (PGA) values for the return period of 475 years. PGA value of 0.4 was chosen as seismic loading since the RBL was located at that range. Detailed analysis of an earthquake triggering event is out of the scope of this study.

Prediction of failure volume and depth

A metastable state for the entire RBL was unable to achieve even with the maximum range of geotechnical values from Table 4.1, which could be attributed to the steep slope of the RBL. Table 4.3 shows the series of FoS values obtained from different combinations of geotechnical parameters. The strongest combination of geotechnical parameters (Run 5) yielded FoS in range of 0.35-1.47. So, this range was used for further analysis in our study. The southeastern part of the slope remained the most unstable as shown in Figure 4.2 because that section had the steepest slope, which was also described by Ischuk (2006) and (Raetzo, 2006) as the unstable section and likely to fail into the lake.

Table 4.3: Combination of different geotechnical parameter values with giving different range of FoS

Trials	c (kPa)	Ψ(°)	γ' (kN/m³)	Min FoS	Max FoS
Run 1	0	10	25	0.1	0.5
Run 2	0	15	25	0.15	0.77
Run 3	5	15	25	0.18	0.84
Run 4	10	20	25	0.26	1.15
Run 5	15	25	25	0.35	1.47

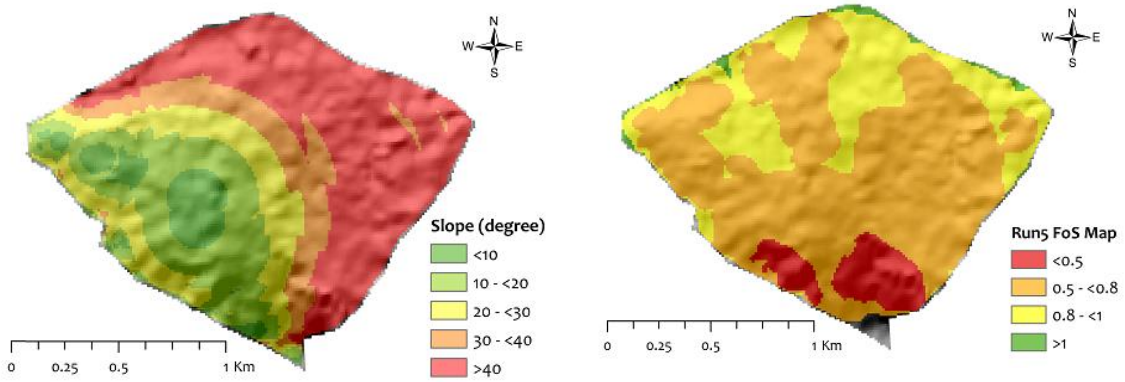

Figure 4.2: Illustration showing the slope of RBL (left) and FoS map for the Run 5 combination of geotechnical parameters

Table 4.4 shows the geotechnical parameters and seismic loading value used to predict the volume and depth of failure mass. A failure height map was prepared by subtracting the new terrain from the pre-slip terrain. The new terrain was obtained by removing the failure mass from each pixel for a given cut off value of FoS (FoS cutoff =1 in our case). Then, the volume and depth were calculated using zonal statistic tool as Table in ArcMap expressed by equation 4-1:

$$\mathbf{V} = \boldsymbol{R^2} \sum_{\boldsymbol{k=0}}^{\boldsymbol{n}} \boldsymbol{h_k} \qquad \textbf{[4-1]}$$

where V (m^3) is volume of the failure mass, R (m) is the pixel size and h (m) is the depth of failure mass. Figure 4.3 shows the factor of safety map with regions having the lowest FoS values and the failure height map.

Table 4.4: Geotechnical parameters and earthquake loading value used in Scoops3D

Parameters	cohesion, c (kPa)	internal friction angle, Ψ(°)	unit weight, γ' (kN/m³)	seismic loading (-)
Value	15	25	25	0.4

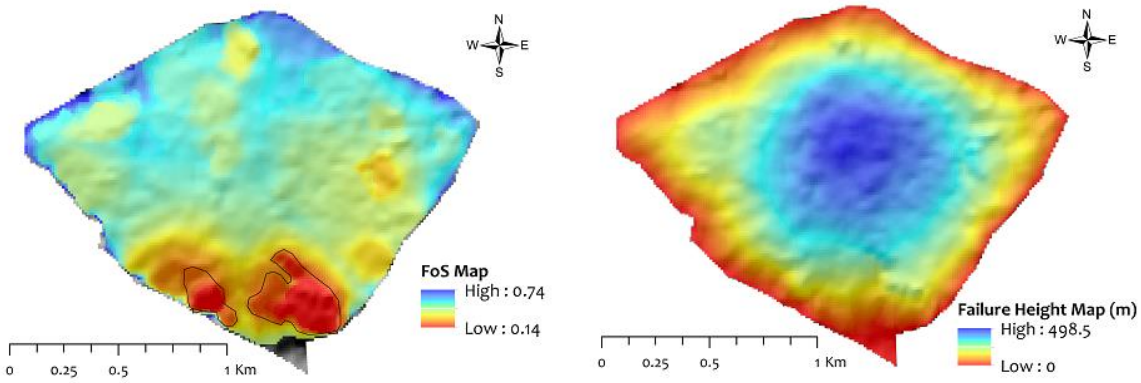

Figure 4.3: Factor of Safety (FoS) map and Failure height map as a result of seismic loading along with sections with the lowest FoS values

The mean depth for the entire RBL failure was found to be 234 m which corresponded to the value estimated by Papyrin (2001) and the volume was 0.4 km^3 which was smaller compared to their estimation (1.25 km^3). But our predicted volume of the entire RBL came close to volume assumed by Raetzo (2006)

which was 0.5 km³. For the sections with the lowest FoS values in the southeastern side of RBL, the volume predicted was about 0.02 km³ with a mean depth of 155 m. The volume estimated by Ischuk (2006) and Raetzo (2006) at the same slope was about 0.3 km³ and 0.1 km³ which was higher than our prediction. However, the slope at the southeastern side was indeed the most unstable and has a high chance of failure with a minimal trigger. Table 4.5 summarizes the volume and depth values that was used in the subsequent Heller-Hager model to calculate the impact wave characteristics.

Table 4.5: Final volume and depth of failure mass for Scenario 1a and 1b

Scenario / Parameters	Max depth (m)	Mean depth (m)	Total volume (km³)
Entire RBL (Scenario 1a)	498.5	234	0.4
Sections with lowest FoS (Scenario 1b)	360	155	0.02

4.2.2. Heller-Hager model

The Heller-Hager model can be divided into three parts: Slide characteristic\Wave generation, Wave propagation and Wave run-up and overtopping. Eight parameters represent the slide characteristics that would generate the wave, two parameters influence the wave propagation in 3D and four parameters influence the run-up and overtopping of the wave. The parameter values were obtained from multiple studies on Lake Sarez and RBL along with estimation from DEMs, Google Earth and satellite images. The parameter values of Lake Sarez and RBL from the past studies are shown in Table 4.6.

Table 4.6: List of parameter values for RBL obtained from past studies. Remarks include main comments from past studies and methods used in this study to estimate the parameters except for slide volume and thickness

Parameters	Values	Reference	Remarks
Wave Generation			
Slide impact velocity V_s (m/s)	25-35	Ischuk (2011)	was calculated using the Körner equation (1976)
Bulk slide volume V'_s (km³)	1.25	Papyrin (2001)	author estimated from field investigation (seismic survey)
	0.35-2	Hanisch & Söder (2000)	authors estimated from field investigation
	0.1	Droz & Spacic-Gril (2002)	authors estimated from field investigation
	0.1 (South landmass); 0.5 (for entire RBS)	Raetzo (2006)	author divided into four zones: South, Central, North and Upper parts; altitude ranges from 3600 masl to greater than 4300 masl
	0.3 (SE mass); 0.6 (NW mass)	Ischuk (2011)	author divided into two blocks; unlikely that the both blocks slide simulatneously forming 0.9 cubic km volume
	0.3-2	Strom (2014)	author estimated from compilation of different literature
Slide thickness s (m)	250	Papyrin (2001)	author estimated from field investigation (seismic survey)
	>100	Raetzo (2006)	author considered 200-300 m thickness unrealistic estimate
	60-100	Ischuk (2011)	author considered uncertain estimate
Slide or reservoir width b (m)	~1000	Hanisch & Söder (2000)	was estimated from satellite image
Bulk slide density ρ_s (kg/m³)	1575		was estimated with help from lithology map
Bulk slide porosity n (%)	37		was taken as the average value from Table 3.2
Slide impact angle α (°)	35-40	Hanisch & Söder (2000)	was estimated from DEM (ALOS PALSAR)

	~ 35	Droz & Spacic-Gril (2002)	
	40-60	Raetzo (2006)	
Still water depth h (m)	~500	Alford & Schuster (2000)	authors estimated from compilation of different literature
	480-490	Papyrin (2001)	author estimated from field investigation
Wave Propagation (3D)			
Radial distance r (m)	3000-5000	Alford & Schuster (2000)	was estimated from satellite image and DEM
	~3000	Risley et al. (2006)	
Wave propagation angle γ (°)	80		was estimated from satellite image and DEM
Wave Run-up and Overtopping			
Still water depth h (m)	480-490	Papyrin (2001)	was estimated from compilation of different literature
Run-up angle β (°)	23	Risley et al. (2006)	was estimated from satellite image and DEM
Freeboard f (m)	~50	Alford & Schuster (2000)	was estimated from DEM (ALOS PALSAR, SRTM)
	~250 (southern part),~100 (central part),~50 (northern part)	Hanisch & Söder (2000)	
	45-55	Papyrin (2001)	
	~50	Risley et al. (2006)	
	~38-45	Ischuk (2011)	
Crest width b_K (m)	~3700	Raetzo (2006)	was estimated from DEM (ALOS PALSAR, SRTM)
	~3200	Ischuk (2011)	

Different authors have estimated the volume of the potential slides from right bank ranging from 0.1 km^3 to 2 km^3. Some authors have sub-divided the RBL into different regions depending upon their characteristics and also claimed that the southern landmass of RBL is more susceptible to fall into the lake rather than the whole RBL landmass (Ischuk, 2006; Raetzo, 2006). Therefore, the slide volume of the southern landmass of RBL i.e. 0.1 km^3 at the elevation of about 3600 masl was used for Scenario 2. For Scenario 3, it was assumed that the whole landmass of the RBL would fall into the lake so, the maximum volume of 2 km^3 was selected. According to Korup et al. (2007), giant landslides in the Tienshan-Pamir region were in the range of kilometre-scale events that occurred during periods of late Quarternary, late Pleistocene and Holocene age. The largest ancient landslides recorded in Central Asia were Beshkiol and Karakudjur rockslides having volumes of around 10 km^3 each in Tienshan Mountain region triggered by strong earthquakes (Strom & Korup, 2006). Usoi rockslide dam that impounded Lake Sarez was about 2.2 km^3 triggered by Pamir Earthquake of M7.2 (Strom, 2010).

Likewise, the estimated slide thickness from different past studies varied in the range of 60-250 m. Scenario 2 assumed only the sliding of the upper loose surface of RBL with a depth of 60 m. Scenario 3 assumed the deep-seated failure of RBL with a maximum depth of 250 m which was obtained from the single seismic profile in 1986 (Papyrin, 2001). Hanisch & Söder (2000), Ischuk (2006) and Raetzo (2006) disagreed with the depth value obtained from Papyrin (2001) and considered as a misinterpretation of the geophysical and drilling result.

The slide impact angle ranged from 35° to 60° according to various sources depending upon the different sections of the Usoi dam. From the profile shown in Figure 4.4 constructed from ALOS PALSAR DEM, the slide impact angle of 35° was considered for this study.

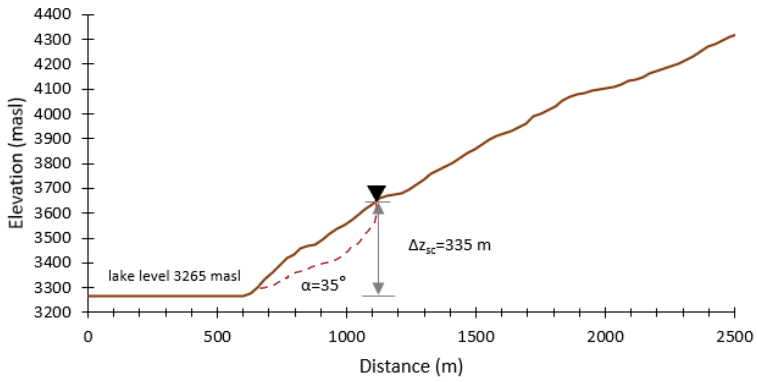

Figure 4.4: Profile of RBL showing the slide impact angle and elevation of potential sliding (black arrow) along with potential slide surface (orange dash)

The slide velocity was estimated from the Körner (1976) equation, which depended upon slide impact angle, the vertical drop height, and dynamic friction angle (Eq. B-1, Annex 2). The vertical drop height of 335 m was assigned considering the elevation of potential failure surface at 3600 masl (Raetzo, 2006) and lake level at 3265 masl. A dynamic bed friction angle of 20° was used as mentioned in McKinnon et al. (2008) for rockslides such as in our case. Slide velocity was estimated to be 56.34 m/s, which was higher than estimated by Ischuk (2006) for the entire RBL landmass.

According to the available lithology map of Tajikistan at 1:200,000 scale, the RBL was dominated by sedimentary rocks such as schist, siltstone and sandstone as shown in Figure 4.5. The density (granulate) of the rocks present in RBL are shown in Table 4.7. Assuming equal composition of the rocks, the density was estimated to be approximately 2500 kg/m^3. The bulk slide porosity was assumed to be 37% taking an average from the values within the limitation range given in Table B 1. The average rock density had to be converted into bulk slide density using the conversion formula given by equation 4-2:

$$\varrho_s = (1-n)\varrho_g \qquad [4\text{-}2]$$

where ϱ_s (kg/m^3) is bulk slide density, n (%) is porosity and ϱ_g is granulate density (kg/m^3). Therefore, the bulk slide density of 1575 kg/m^3 was used in the model.

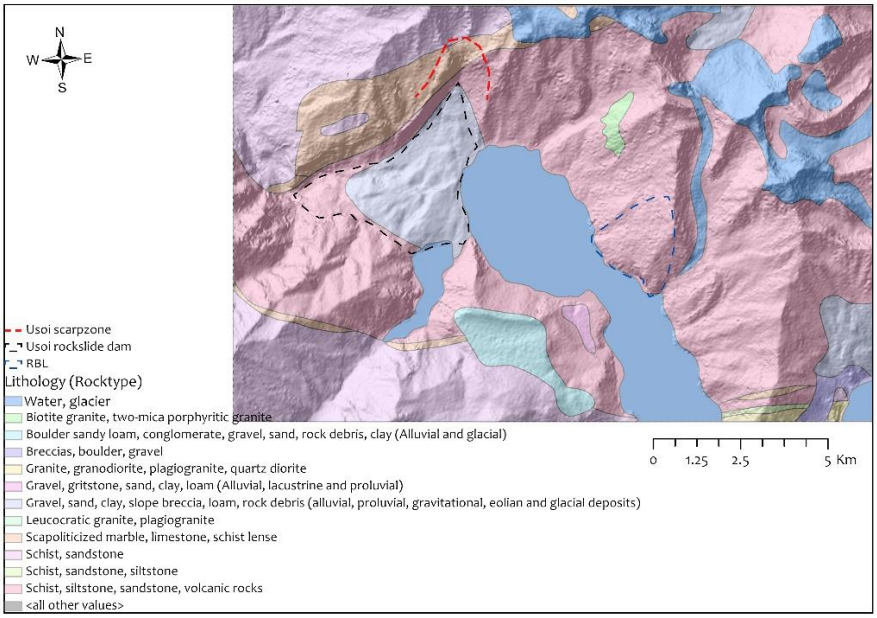

Figure 4.5: Lithological characteristics at the RBL indicated by blue dashed polygon(Map scale: 1:200,000)

Table 4.7: Mean densities of rocks at the RBL

Rock type	Mean density (kg/m³)	Reference
Schist	2732	Dorren & Seijmonsbergen (2003); Tenzer et al. (2011)
Siltstone	2347	
Sandstone	2463	
Volcanic	2362	

Lake Sarez was filled at different time periods (see Figure 2.5) with an average increment of 8-25 cm/year (Droz & Spacic-Gril, 2002). Uniform lake depth of 500 m was used in our study for simplification. The lake depth corresponded to the bathymetric works done by several scientists compiled in Papyrin (2001), Raetzo (2006) and Delaney & Evans (2011).

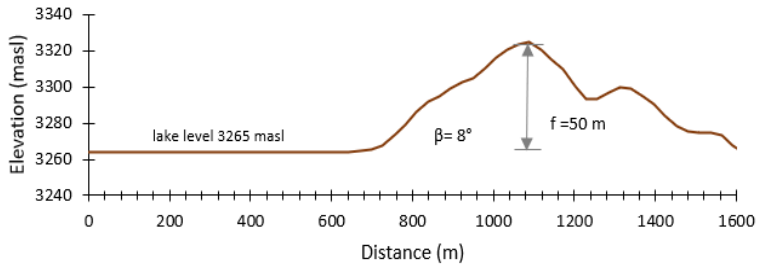

Figure 4.6: Profile of the northern section of the Usoi dam showing lake level, run-up angle and freeboard

Hanisch & Söder (2000) found different freeboard heights along the Usoi dam; approximately 250 m in the southern part, 100 m in the central part, and the lowest 50 m in the northern part (see Figure 2.4). In our study, the profile of northern section of the Usoi dam was used which had the lowest freeboard and run-up angle of 8° as shown in Figure 4.6.

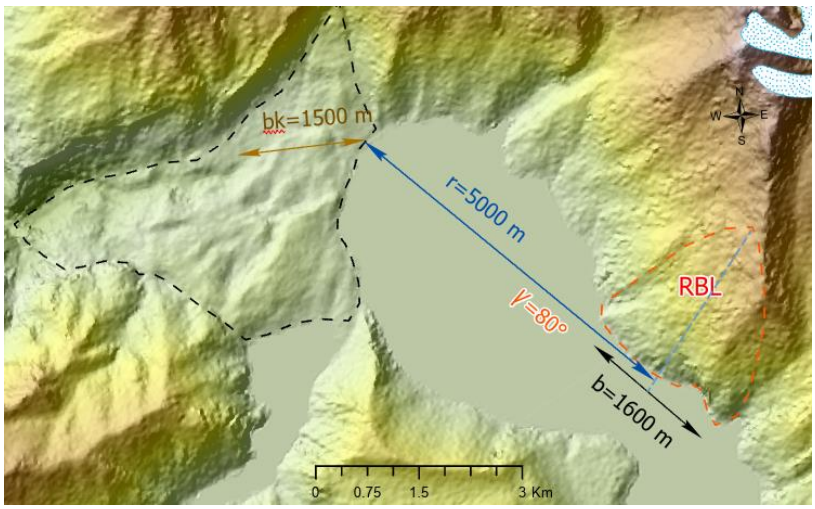

Figure 4.7: Parameters of Heller-Hager model obtained from DEM and satellite images (b_k= dam crest width, r= radial distance, γ= wave propagation angle, b= slide width) and profile line on RBL

Parameters such as slide width, wave propagation angle, radial distance and dam crest width were estimated from DEM profiles and verified with Google Earth and satellite imageries as shown in Figure 4.7. Dam crest width was measured for the northern section of dam until it reached the canyon formed by the stream. The wave propagation angle of 80° was used with a slide width of 1600 m.

The input parameters of all the scenarios are shown in Table 4.8. The slide volume and slide depth or thickness for Scenario 1a (entire RBL) and Scenario 1b (slope with lowest FoS) were obtained from Table 4.5, whereas the rest of the parameters were kept similar for all three scenarios.

Table 4.8: Summary of input parameters in Heller-Hager model for Lake Sarez

Lake Sarez scenarios	Scenario 1a	Scenario 1b	Scenario 2	Scenario 3
Wave Generation/Slide Characteristics				
Slide impact velocity V_s (m/s)	56.34	56.34	56.34	56.34
Bulk slide volume V'_s (km^3)	**0.4**	**0.02**	**0.1**	**2**
Slide thickness s (m)	**234**	**155**	**60**	**250**
Slide or reservoir width b (m)	1600	1600	1600	1600
Bulk slide density ρ_s (kg/m^3)	1575	1575	1575	1575
Bulk slide porosity n (%)	37	37	37	37
Slide impact angle α (°)	35	35	35	35
Still water depth h (m)	500	500	500	500
Wave Propagation (3D)				
Radial distance r (m)	5000	5000	5000	5000
Wave propagation angle γ (°)	80	80	80	80
Wave Run-up and Overtopping				
Still water depth h (m)	500	500	500	500
Run-up angle β (°)	8	8	8	8
Freeboard f (m)	50	50	50	50
Crest width b_K (m)	1500	1500	1500	1500

4.3. Results and discussion

This section shows the results of different scenarios of modelling the RBL falling into the Lake Sarez using Heller-Hager model coupled with Scoops3D in terms of slide volume and slide depth.

In Scenario 1, the volume and depth of RBL were calculated from the Scoops3D with seismic loading of 0.4g. Scenario 1a depicted the entire failure of the RBL whereas Scenario 1b depicted the failure of the southeastern part of RBL which had the lowest FoS values. Scenario 1a resulted in wave height of 37 m and run-up height of 79 m whereas Scenario 1b resulted in 17.2 m high wave height and run-up height of 33 m. The lowest freeboard of the Usoi dam was 50 m so the impact water wave from Scenario 1a would overtop the dam whereas Scenario 1b did not have enough height to overtop. The results of Scenario 1a and 1b accounted for six and two limitations in the Heller-Hager model respectively. The overtopping volume of water surpassed $2.2 \cdot 10^6$ m^3 for Scenario 1a with an average discharge of about 281,550 m^3/s considering no freeboard. In general, the average discharge and the overtopping duration i.e. 71 seconds would be much lesser in our case than the abovementioned values.

Scenario 2 and Scenario 3 represented the optimistic and pessimistic set of governing parameters from existing literature respectively for analysing the impact waves in Lake Sarez due to failure of the RBL. Scenario 2 generated the wave height of about 16 m but did not have enough wave run-up height (approx. 31 m) to overtop the dam. It accounted for two limitations in the model. Likewise, Scenario 3 resulted in the generation of about 52 m high wave height and wave run-up height of about 118 m which overtopped the dam. The overtopping volume was about $9.8 \cdot 10^6$ m^3 with an average discharge of 449,550 m^3/s which lasted for a short time of 74 seconds considering no freeboard. Scenario 3 exceeded six limitations in the Heller-Hager model. Table 4.9 summarizes the results of all the scenarios of impulse wave analysis in Heller-Hager model.

Table 4.9: Summary of the results for all the scenarios in Heller-Hager model

Results	Scenario 1a	Scenario 1b	Scenario 2	Scenario 3
Wave height H (m)	36.9	17.2	16.2	52.3
Wave amplitude (m)	29.6	13.8	13	41.9
Wave period T (s)	55.8	46.1	45.5	60.9
Wave length L (m)	4024.1	3274.6	3225.3	4441.1
Run-up height (m)	79	33	30.9	117.5
Overtopping volume V_o per unit length dam crest for f=0 (m^3/m)	13373.7	no value	no value	22194.3
Duration of overtopping t_o for f=0 (s)	71.2	no value	no value	74
Overtopping volume V'_o per unit length dam crest (m^3/m)	1471.8	no value	no value	6560.4
Average discharge q per unit length dam crest for f= 0 (m^2/s)	187.7	no value	no value	299.7
Maximum discharge q_M per unit length dam crest for f= 0 (m^2/s)	375.5	no value	no value	599.5
Number of not satisfied limitations out of 23 (2D) or 24 (3D)	6	4	4	6

In a similar study by Risley et al. (2006), three scenarios were constructed for Lake Sarez overtopping due to landmass impact. The landslide volumes of 0.2, 0.5 and 1 km^3 were assumed to impact over the lake generating overtopping volumes of $2 \cdot 10^6$, $22 \cdot 10^6$ and $87 \cdot 10^6$ m^3 in the duration of 70, 90 and 110 seconds respectively. Also, they mentioned about the investigations done in the Lake Sarez by Stucky Consulting Engineers (2001). The overtopping volume generated from 0.1 and 0.5 km^3 of slides were about 9000 and $1.6 \cdot 10^6$ m^3 of overtopping volume. The difference between the overtopping volumes was attributed to the different methods of calculation of the flood wave amplitude. In our case, wave amplitude was estimated as a function of impulse product parameter, lake depth at the site of impact, radial distance and wave propagation angle as shown by equations B-3 to B-5, Annex 2 (Heller et al., 2009). Risley et al. (2006) used equations by Walder et al. (2003), where wave amplitude depended upon slide volume, water depth, lake width and duration of landslide motion. Whereas, Stucky Consulting Engineers (2001) estimated the wave amplitude by assuming a constant ratio of landslides to wave energies from the historic observations of lakes with shallower depths than Lake Sarez (Risley et al., 2006).

The two large landslide-generated tsunami events were the Lituya Bay 1958 event generating the run-up height of 542 m when an earthquake-induced rockslide (0.03 km^3) fell into the bay (Fritz, 2002) and the Vajont 1963 event with a wave run-up of 235 m high triggered by the landslide of estimated 0.27 km^3 volume (Crosta et al., 2016). Compared to the past events, the wave run-up heights from our study were smaller despite a large volume assumption of the landslide, attributed to several factors such as the depth of the reservoir at impact zone, the distance between impact zone and dam, magnitude of the triggering event (earthquake) etc. The wave generated by the slide attenuates as it travels farther distance and if the depth of the reservoir is shallower compared to the slide, the water displaces extensively creating a large splash or high wave height such as in Vajont event.

For the calculation of the impulse waves, all the scenarios had their parameter values within the range provided by the model except for the Froude number as shown in Table 4.10 indicated by the red colour. Froude number is the ratio of inertial force to gravity force and is one of the important parameters in impulse wave generation as the Heller-Hager model is based on Froude similitude (Heller & Hager, 2009). In Froude similitude, the scale effects of other force ratios such as Reynolds number (inertial force to viscous force) and Weber number (inertial force to surface tension force) are negligible compared to Froude number. The scale effects result when these force ratios are not kept constant between the model and prototype (Heller, 2011). The scale effects are inherent in physical modelling attributing to inability to scale the real-world governing parameters but scale effects must be kept within the range.

Table 4.10: Limitations of calculation of impulse waves for all scenarios

Parameter	Description	Range	Scenario 1a	Scenario 1b	Scenario 2	Scenario 3
Slide Froude number	$F=V_s/(gh)^{0.5}$	$0.86 \le F \le 6.85$	0.8	0.8	0.8	0.8
Relative slide thickness	$S=s/h$	$0.09 \le S \le 1.64$	0.47	0.31	0.31	0.5
Relative slide mass	$M=\rho_s V'_s/(\rho_w bh^2)$	$0.11 \le M \le 10.02$	1.58	0.08	0.63	7.88
Relative slide density	$D=\rho_s/\rho_w$	$0.59 \le D \le 1.72$	1.58	1.58	1.58	1.58
Relative granulate density	ρ_g/ρ_w	$0.96 \le \rho_g/\rho_w \le 2.75$	2.5	2.5	2.5	2.5
Relative slide volume	$V=V'_s/(bh^2)$	$0.05 \le V \le 5.94$	1	0.05	0.25	5
Bulk slide porosity	n	$30.7\% \le n \le 43.3\%$	37	37	37	37
Slide impact angle	α	$30° \le \alpha \le 90°$	35	35	35	35
Relative slide width	$B=b/h$	$0.74 \le B \le 3.33$	3.2	3.2	3.2	3.2
Relative radial distance	r/h	$5 \le r/h \le 30$	10	10	10	10
Wave propagation angle	γ	$-90° \le \gamma \le +90°$	80	80	80	80
Relative streamwise distance	$X=x/h$	$2.7 \le X \le 59.2$	no value	no value	no value	no value
Impulse product parameter	$P=FS^{0.5}M^{0.25}\{\cos[(6/7)\alpha]\}^{0.5}$	$0.17 \le P \le 8.13$	0.57	0.22	0.23	0.89

Impulse product parameter, a dimensionless parameter which is the combination of all governing parameters for impulse wave generation depends on the Froude number. In our case, the values of other parameters compensated the limitations caused by the Froude number for all the scenarios.

Likewise, for the calculation of wave run-up, all the scenarios were limited by the relative angle which depended upon run-up angle (β) of the dam as shown in Table 4.11. The slope in the northern profile of Usoi dam (see Figure 2.4) was undulating and did not have steep slopes compared to other sections. Wave run-up tests were conducted using three slopes having run-up angles (β= 90 °, 45° and 18.5°) which set the basis of limitations in the Heller-Hager model (Heller et al., 2009).

Table 4.11: Limitations of calculation of wave run-up for all scenarios

Parameter	Description	Range	Scenario 1a	Scenario 1b	Scenario 2	Scenario 3
Relative wave height	H/h	$0.011 \le H/h \le 0.521$	0.074	0.034	0.032	0.105
Wave steepness	H/L	$0.001 \le H/L \le 0.013$	0.009	0.005	0.005	0.012
Relative angle	90°/β	$1.0 \le 90°/\beta \le 4.9$	11.3	11.3	11.3	11.3

Scenario 1a and Scenario 3 were limited by the relative period, relative angle and relative duration of overtopping for the calculation of wave overtopping and its duration as shown in Table 4.12 (indicated by the red colour). Relative period is the function of wave period (T), acceleration due to gravity (g) and still water depth (h) in front of the dam. Wave period further depends upon wave height (see equation B-6, Annex 2) in front of the dam which was within the range. So, the lower relative period value was influenced by the higher still water depth considered in our case.

Table 4.12: Limitations of calculation of wave overtopping and duration of overtopping for all scenarios

Parameter	Description	Range	Scenario 1a	Scenario 3
Relative wave height	H/h	$0.019 \le H/h \le 0.488$	0.074	0.105
Non-linearity	a/H	$0.59 \le a/H \le 0.95$	0.8	0.8
Wave steepness	H/L	$0.001 \le H/L \le 0.023$	0.009	0.012
Relative period	$T(g/h)^{0.5}$	$9.0 \le T(g/h)^{0.5} \le 21.0$	7.82	8.53
Relative wave celerity	$c^2/(gh)$	$0.83 \le c^2/(gh) \le 1.40$	1.06	1.08
Relative wavelength	L/h	$6.0 \le L/h \le 24.0$	8	8.9
Relative angle	90°/β	$1.0 \le 90°/\beta \le 4.9$	11.3	11.3
Parameter	**Description**	**Range**	**Scenario 1a**	**Scenario 3**

Relative period	$T(g/h)^{0.5}$	$14 \leq T(g/h)^{0.5} \leq 22$	8	9
Relative duration of overtopping	$t_o(g/h)^{0.5}$	$10.5 \leq t_o(g/h)^{0.5} \leq 13.5$	10	10.4

The overtopping volume and duration of overtopping (for f = 0) from Scenario 1a and Scenario 3 results were used to construct a simple triangular hydrograph to show how the outputs of Heller-Hager model could be coupled with flood model. Scenario 1b and Scenario 2 did not have enough run-up heights to overtop the dam so these were not included. The duration of overtopping as well as the estimated peak discharge would be much lower in our cases because of the presence of the freeboard. The peak discharge estimated from the overtopping volume and overtopping duration for no freeboard sets up the upper limits of discharge produced from such events. The peak discharge estimated were 281,550 m^3/s and 449,550 m^3/s for Scenario 1a and Scenario 3 respectively. Figure 4.8 shows the simple triangular hydrograph constructed from the results of Scenario 1a and Scenario 3.

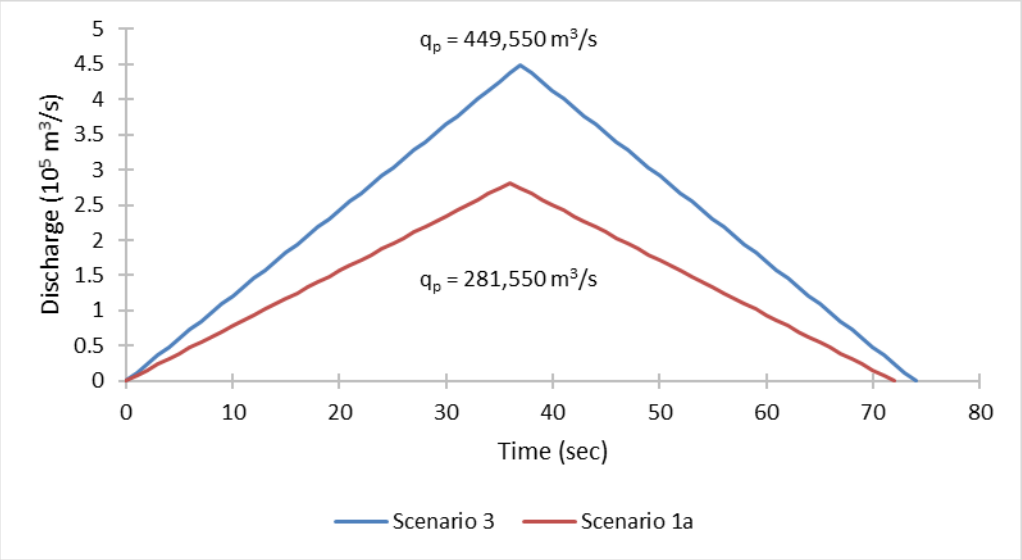

Figure 4.8: Simple triangular hydrograph constructed from the outputs of Heller-Hager model

Because of the high freeboard, broad crest width along with the balance between the inflow and outflow of the water through Usoi dam, it was considered highly stable by many studies and suggested that it would not outburst soon (Alford & Schuster, 2000; Hanisch & Söder, 2000; Droz & Spacic-Gril, 2002; Ischuk, 2006; Raetzo, 2006; Strom, 2014). So this study only analysed the run-up height of the impulse waves for Lake Sarez by coupling a slope stability model with an impulse wave model and further dam breach flood modelling was not performed.

5. HAZARD MODELLING OF LAKE RIVAKKUL

In this chapter, various scenarios are designed for Lake Rivakkul with respect to the potential dam failure as a result of a rockslide in the lake as described in chapter 2. Next, the temporal change of Lake Rivakkul is analysed using Landsat images. The input data are prepared for the Heller-Hager model which are obtained from engineering drawings, past literature, empirical equations, satellite imageries, and digital elevation model (DEM). The results of the Heller-Hager model are discussed and checked for plausibility to couple with the HEC-RAS model. Finally, the downstream flood modelling is executed with HEC-RAS along with the discussion.

5.1. Scenario design

Lake Rivakkul has not been studied in detail as compared to Lake Sarez. The origin of Lake Rivakkul is contradicted among the authors. Ischuk (2013) claimed Lake Rivakkul to be the remnant lake from a cirque glacier, whereas Strom (2010) and Mergili & Schneider (2011) argued it to be a rockslide-dammed lake or the combination of both. The lake is located below an incised valley with steep mountains which accumulate a large amount of snow in winter. The potential sources of mass movement that could affect the lake are snow avalanches, debris flows from the upstream proglacial lakes and a rockslide (see Figure 2.7). Lake Rivakkul is located in the tectonically active Pamir mountains (Pamir-Shugnan sub-range) which could trigger rockslides from the surrounding steep slopes. However, because of the limitation of the Heller-Hager model as well as the complex hazard interactions, the occurrence of snow avalanches and debris flows were not modelled in our case although these are likely triggers as their run-out might spread into the lake.

We assumed the rockslide situated at the southern slope at a distance of approximately 1.7 km from the Rivakkul dam to be the trigger for a potential dam break scenario (Figure 5.1). The mountains surrounding Lake Rivakkul are dominated by boulders, gravel, and biotite granite (Pamir Shugnan type) and have a slope of around 35°. The Google Earth satellite images showed the slope had multiple scarps with run-out zones directing towards the lake.

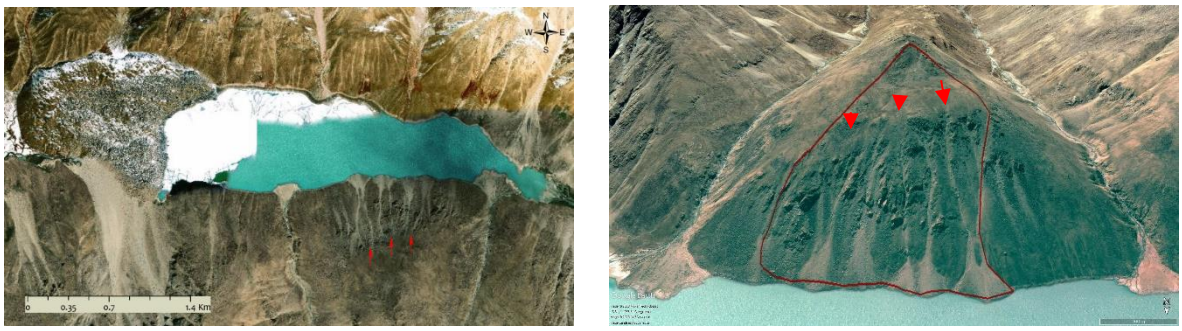

Figure 5.1: Satellite image and Google Earth image showing Lake Rivakkul and potential rockslide area with scarps denoted by red arrows

Two scenarios were devised in case of Lake Rivakkul:

1) In Scenario 1, a deep-seated potential rockslide was assumed to fall into the lake and generate the impact waves that might or might not overtop the Rivakkul dam. Lack of literature limited the use of Scoops3D in this case to determine the potential failure depth. So, a perfect rotational failure was assumed from the profile line drawn in the slope to estimate the volume and depth of the slide which were then used in the Heller-Hager model. The results of the Heller-Hager model were then checked to construct an input hydrograph for the HEC-RAS.

2) Scenario 2 was the worst-case scenario for Lake Rivakkul. Here, we assumed a complete breach of the dam and complete emptying of the lake, consequently, releasing a large volume of water. The hydrograph constructed from the empirical equations was used for downstream flood modelling in HEC-RAS.

5.2. Temporal change analysis of Lake Rivakkul

Before modelling the impact wave in the Heller-Hager model, the area of Lake Rivakkul was investigated for its temporal change using satellite images. Changes in the lake water level or lake area is an important measure of lake water volume as it influences the local hydrology and regional climate (Qiao et al., 2019). There have been several studies that relate the lake area to lake volume and depth (O'Connor et al., 2001; Huggel et al., 2002; Cook & Quincey, 2015). Remote sensing images are essential tools to monitor the temporal changes in lakes, especially in high mountainous regions where accessibility is often difficult.

In our case, Landsat Multispectral Scanner (MSS), Thematic Mapper (TM), Enhanced Thematic Mapper Plus (ETM+) and Operational Land Image (OLI) images were acquired from the period 1976 to 2019. The summer months of July-September were chosen for the cloud-free and snow-free images of the study area. The area of the lake was digitized manually and the rate of change was calculated as shown in Table 5.1. A drawback in visual interpretation compared to automatic methods is that delineation of the lake area can vary subjectively from person to person.

Table 5.1: Landsat image acquisition date and rate of change of Lake Rivakkul area

Date	Area (sq km)	Rate (sq km/yr)	Resolution(m)
28/08/1976	1.294		60
29/07/1980	1.185	-0.02725	60
20/08/1993	1.245	0.00462	30
04/09/2001	1.137	-0.01350	30
12/08/2010	1.401	0.02933	30
22/09/2019	1.112	-0.03211	15
Mean	**1.229**		

It was found that the area of Lake Rivakkul fluctuated temporally with a mean size of 1.229 km^2 from 1976 through 2019. Lake Rivakkul is mainly fed by glacier meltwater and discharge from proglacial lakes. Snow as precipitation dominated the winter months in this region with approximately 50% snow cover and the water bodies in the Gunt basin were mostly fed by glacier snowmelt in the months of July and August (Pohl et al., 2015). However, the fluctuation of lakes was partly affected by the mudflows or debris flows fanning out in the lake vicinity as well as in the upstream inflow path. Figure 5.2 shows a mudflow disruption at the inflow of Lake Rivakkul in the images of 2001 and 2019, hence affecting its size. The presence of a mudflow phenomenon is an indication that the upper watershed has active mass movements in part of the year.

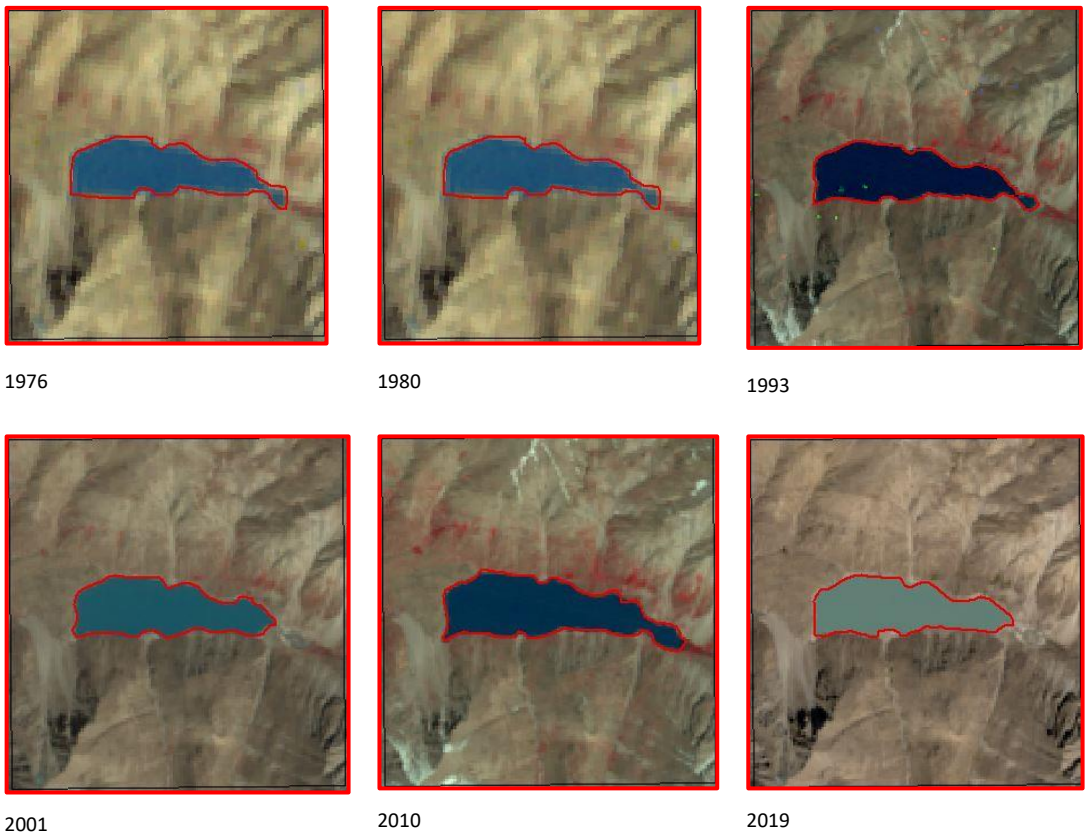

Figure 5.2: Landsat images showing the temporal change in the Rivakkul Lake area from period 1976-2019

Strozzi et al. (2012) mapped Lake Rivakkul and surrounding proglacial moraine-dammed lakes using Synthetic Aperture Radar (SAR) data from TerraSAR-X, ALOS PALSAR, ENVISAT and Radarsat-2. The advantages of SAR data over optical data are that they can be used in any weather condition, suitable in the mountainous environment and areas affected by the monsoon along with high temporal and spatial resolution. However, the backscattering intensity can be influenced by features such as wet sand, wet snow, icebergs, ice debris which could resemble the backscattering of lake water and hence, misclassify and vary the size of the lake. A combination of SAR images complemented by optical imageries, DEMs and field data can be used for detailed monitoring of the development of high altitude lakes which are hazardous to outburst floods.

5.3. Input data preparation

5.3.1. Heller-Hager model

The lack of literature for Lake Rivakkul made it difficult to parameterize the Heller-Hager model. The input parameters such as slide volume and lake depth were estimated from simplified engineering drawing from the profile line drawn along the potential slope for Scenario 1. Estimation of landslide volumes by relating it with landslide-related factors such as surface area, length, width and triggering factors have been done extensively in past studies (Keefer, 1994; Dai & Lee, 2001; Korup, 2005; Guzzetti et al., 2009; Larsen et al., 2010; Tseng et al., 2013; Amirahmadi et al., 2016). However, prediction of landslide volumes from the unstable slope is accompanied by several uncertainties and lack of geotechnical data and ground information restrict the use of Scoops3D in this case. From satellite images and DEM, the surface area of the potential

rockslide was delineated which approximated to 422,000 m². A profile line was drawn from top of the slope to the toe as shown in Figure 5.3 using ALOS PALSAR DEM.

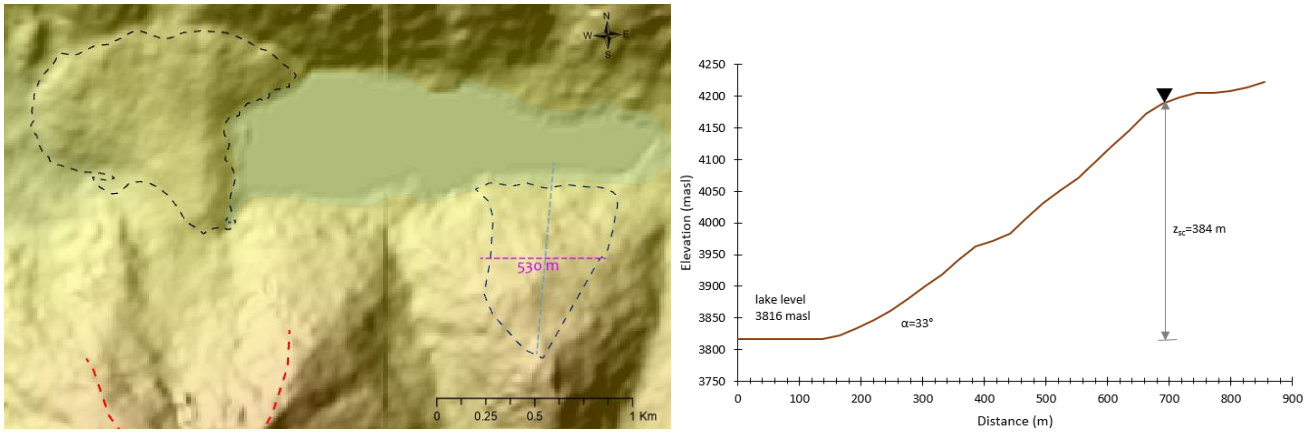

Figure 5.3: Illustration of the profile (blue line) and average width (purple line) drawn in the potential rockslide area; black triangle indicates the elevation of slope failure

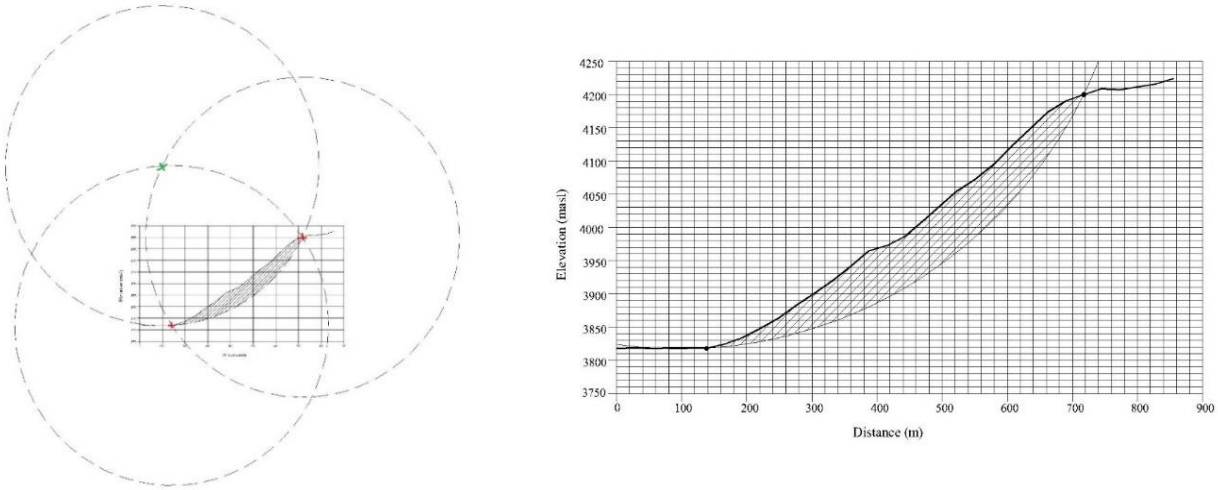

Figure 5.4: Schematic illustration of circle fitting for landslide volume estimation (left) and ideal rotational slip surface from top to toe of the slope with each grid equivalent to 200 m²(right)

The elevation of the slope failure point was considered to be at 4200 masl which had a slide impact angle of 33°. For the estimation of volume in Scenario 1, a circle was fitted that passed through the top and toe of the slope representing an ideal rotational slip. Initially, the slope profile from the middle of the rockslide area was divided into scale grids with a horizontal and vertical spacing of 20 m and 10 m respectively in a graph. Circles were drawn making the top point (4200 masl) and toe point (3817 masl) as their corresponding centres represented by red crosses as shown in Figure 5.4. The intersection of these two circles represented by a green cross was then used to construct a circular arc that passed both the toe and top points. Each scale grid was equivalent to the area of 200 m². The area cutting the profile line was calculated by counting the grids in the graph which was about 34,200 m². The volume of the rotational slip was obtained by multiplying the mentioned area with the average width of the slope measured at the middle elevation of the slope (530 m) denoted by a purple dashed line in Figure 5.3.

The predicted volume of the rotational slip surface was about 0.018 km^3. The average depth of about 43 m was obtained by dividing the volume with the surface area. The final representation of the ideal slip surface for Scenario 1 is shown in Figure 5.4.

Using the Körner (1976) formula (Eq. B-1, Annex 2), the slide velocity was estimated which depended upon the slide impact angle, vertical drop height, and dynamic friction angle. The vertical drop height of 384 m (Figure 5.3) was assigned considering the elevation of the potential failure surface at 4200 masl and the lake level at 3816 masl which was verified using the DEM and Google Earth. The dynamic bed friction angle and slide impact angle were assigned 20° and 33° respectively. Thus, the slide velocity was estimated to be 57.5 m/s.

The depth of the lake was another uncertain parameter as there was no bathymetry data of the lake. The empirical equation by Huggel et al. (2002) relates the lake surface area with lake depth as shown in equation 5-1. The regression equation was derived from 15 ice-dammed and moraine-dammed lakes in the Swiss Alps and has been used in several studies (Huggel et al., 2004; Mergili & Schneider, 2011; Byers et al., 2013).

$$\mathbf{D = 0.104A^{0.42} \quad (r^2 = 0.916)} \qquad \mathbf{[5\text{-}1]}$$

where D (m) is lake depth and A (m^2) is lake surface area.

However, Cook & Quincey (2015) argued that lake depth and lake area were only moderately correlated (r^2 = 0.38) compared to the correlation between lake area and volume (r^2 = 0.91). They also questioned the applicability of these empirical equations across a wide range of locations and in the lakes with complex bed surface characterized by multiple deep areas and sedimentation from the surrounding environment. Using equation 5-1, the lake depth corresponded to 36 m in our study area considering the recent lake area of 1.112 km^2 (Table 5.1). Uniform depth of 36 m was used for the simplification of the study.

Bulk porosity was assumed to be 37% as the average value from the range given in Table B 1. The lithological composition of the potential rockslide is shown in Figure 5.5. The densities of various types of rocks are shown in Table 5.2. Heller-Hager model requires density in terms of bulk slide density so the rock (grain) density was converted to bulk slide density using equation 4-2. Considering the equal composition of rocks in the area, the average density was found to be 2500 kg/m^3. After conversion, the bulk slide density was estimated to be 1575 kg/m^3.

Table 5.2: Mean densities of the rocks found in potential rockslide zone

Rock type	Mean density (kg/m^3)	Reference
Biotite	2650	Dorren & Seijmonsbergen (2003); Tenzer et al. (2011)
Granite	2640	
Boulder	2400	
Gravel	2309	

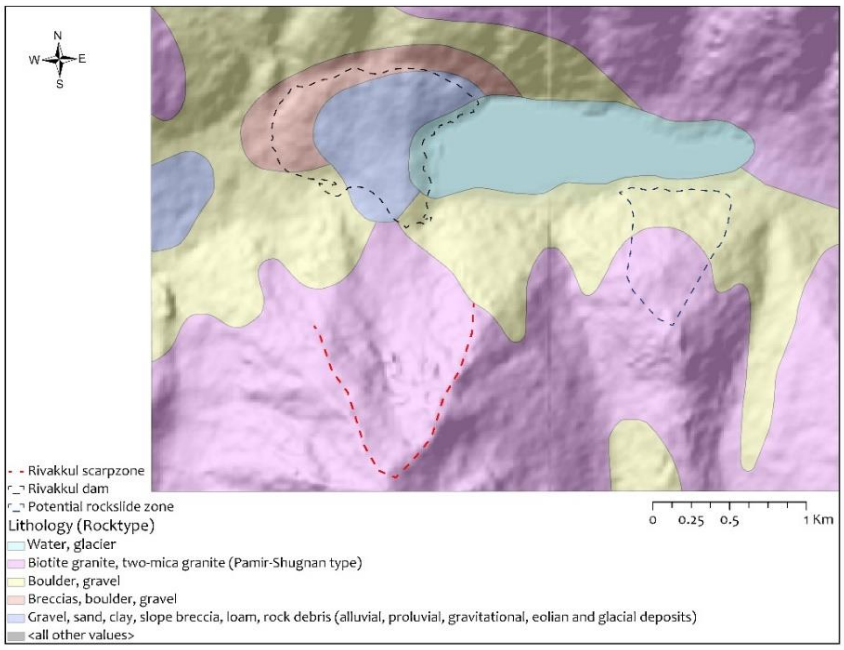

Figure 5.5: Lithological characteristics at the potential rockslide indicated by blue dashed polygon (Map scale: 1:200,000)

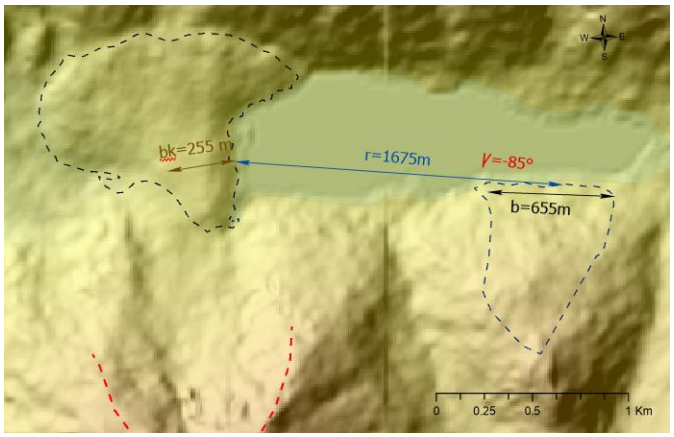

Figure 5.6: Governing parameters of Heller-Hager model

Parameters such as slide width, wave propagation angle, radial distance, freeboard, dam crest width, and run-up angle were estimated from the DEM and satellite images as shown in Figure 5.6. The slide width at the foot was 655 m and wave propagation angle of -85°. Depending upon the location of the dam and slide direction, a sign convention was adopted in the model. If the dam was located on the right side with respect to the slide direction, then positive sign was used and vice-versa. Figure 5.7 shows the profile of Rivakkul dam near along the seepage zone. Rivakkul dam had the run-up angle of 12° in the front slope and steep distal slope towards the valley. The crest width corresponded to 255 m with a freeboard of 43 m.

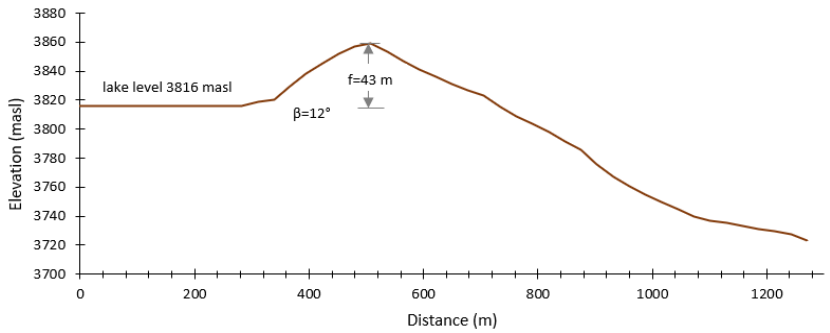

Figure 5.7: Profile of Rivakkul dam showing lake level, freeboard and run-up angle

The input parameters of the Scenario 1 are shown in

Table 5.3.

Table 5.3: Summary of input parameters in Heller-Hager model for Lake Rivakkul

Lake Rivakkul scenarios	Scenario 1
Wave Generation/Slide Characteristics	
Slide impact velocity V_s (m/s)	57.5
Bulk slide volume V'_s (km^3)	**0.018**
Slide thickness s (m)	**43**
Slide or reservoir width b (m)	655
Bulk slide density ρ_s (kg/m^3)	1575
Bulk slide porosity n (%)	37
Slide impact angle α (°)	33
Still water depth h (m)	36
Wave Propagation (3D)	
Radial distance r (m)	1675
Wave propagation angle γ (°)	-85
Wave Run-up and Overtopping	
Still water depth h (m)	36
Run-up angle β (°)	12
Freeboard f (m)	43
Crest width b_K (m)	255

5.3.2. HEC-RAS

HEC-RAS 5.0.7 was used for the analysis of Scenario 2, where the entire volume of lake water was assumed to be emptied due to the complete breach of the dam. HEC-RAS has modules to analyse dam breach and route the flood in one or two dimensional under steady state or unsteady state conditions. The dam breaching module was not used in this study though it is a relevant process in a lake outburst hazard chain.

Rivakkul dam breach flood was modelled up to 24 km downstream at Rivak village and 60 km downstream at Khorugh town. Khorugh is the capital and economical hub of GBAO region. The loss and risk estimation are out of the scope of the study, so we just focused on the preliminary hazard assessment.

Initially, 1D unsteady flow simulations were run to model the flood downstream, but the following issues occurred :

1) ALOS-PALSAR (12.5m) and SRTM (30m) DEMs were used to extract terrain data. The available terrain data did not represent the stream channel in detail attributing to its smoothening of terrain and acquisition methods, further discussed in chapter 6. Though the resolution was coarser for the SRTM, it gave better results than the ALOS PALSAR DEM.
2) HEC-RAS 1D was limited to 10% slope gradient, but our study area was very steep in some stretches. As a result, there were a lot of warnings under unsteady flow conditions regarding the energy balance and conveyance ratio. The solution was to increase the cross-sections in the river reach within a few meters of distance. On doing so, the model became unstable.
3) In the second approach, the river reach was divided into shorter reaches and 1D unsteady flow conditions were applied. The improvement in the result was not significant, attributed to the steep slope and most probably terrain data as well. The warnings persisted.
4) 1D steady flow analysis could be done and has been done in some previous studies, but an outburst flood will not have constant flow in all time steps and might not replicate the phenomenon. So, 2D unsteady flow computation was applied to improve the stability of the model.

2D unsteady flow modelling

2D unsteady flow condition was performed applying the full momentum equation which was recommended for dam breach flood (Brunner, 2016a). The other option was applying diffusion wave equation which considered fewer force components compared to a full momentum approach. SRTM DEM was used to extract topographic information of the study area. A 2D flow area was delineated with a computational mesh of 50 m.

Manning's roughness coefficient was assigned a value of 0.06 for the mountainous streams as mentioned in Brunner (2016b). However, the channel and the floodplains have different roughness values but due to lack of in-situ data, a uniform roughness value of 0.06 was assigned. Different roughness values have been assigned by different authors in the mountainous condition like in our case. For examples: Risley et al. (2006) used the uniform roughness value of 0.038 for predicting outburst flood in Lake Sarez, Tajikistan; Butt et al. (2013) assigned uniform roughness of 0.04 for Attabad landslide-dammed lake outburst flood in Pakistan; Klimeš et al. (2013) used roughness value ranging from 0.035 to 0.13 for different reaches in Lake 513 outburst flood in Peru; Anacona et al. (2015) used roughness values ranging from 0.04 to 0.1 for modelling GLOF in Chilean Patagonia; Kougkoulos et al. (2018) used the roughness value ranging from 0.03-0.05 for predicting outburst flooding in the Bolivian Andes.

The upstream boundary condition was set with an input hydrograph. Peak discharge and dam breach time were the important parameters to construct an input hydrograph, for which empirical equations were used. The lake volume was estimated using Huggel et al. (2002) equation which related the surface area with volume. Mathematically, it is expressed as:

$$\mathbf{V = 0.104A^{1.42} \quad (r^2 = 0.916)} \qquad \mathbf{[5\text{-}2]}$$

where V (m^3) is the lake volume and A (m^2) is the lake surface area. Lake surface area was delineated from the satellite image and was found to be $1.112 \cdot 10^6$ m^2 and volume estimated approximated to $4 \cdot 10^7$ m^3. Depth of the lake was estimated from equation 5-1.

Table 5.4: Empirical equations for estimating peak discharge of Lake Rivakkul with volume ($V=4.10^7$ m^3), depth (D=36 m), ρ_w=density of water, g=acceleration due to gravity

Equation for Q_p	Reference	Q_p Rivakkul (m^3/s)
$1.175(V.D)^{0.41}$	MacDonald & Langridge-Monopolis (1984)	6606
$672(10^{-6}\ V)^{0.56}$, $r^2=0.76$	Costa (1985)	5303
$6.3D^{1.59}$, $r^2=0.76$	Costa (1985)	1796
$181(10^{-6}\ VD)^{0.43}$, $r^2=0.76$	Costa (1985)	4079
$0.0158(\rho_w.g.V.D)^{0.41}$	Costa & Schuster (1988)	3847
$1.6V^{0.46}$, $r^2=0.73$	Walder and O'Connor (1997)	5024
$6.7D^{1.73}$, $r^2=0.53$	Walder and O'Connor (1997)	3143
$0.99(D.V)^{0.40}$, $r^2=0.76$	Walder and O'Connor (1997)	4509
	Mean	4300

Table 5.4 shows the list of empirical equations used for estimating the peak discharge of Lake Rivakkul. The peak discharge values ranged from 1796 m^3/s to 6606 m^3/s. For the dam breach time, Froehlich (1995) and Froehlich (2008) empirical formula were used, attributed to their smaller uncertainty range (Wahl, 2004; Anacona et al., 2015) as shown in Table 5.5. A triangular hydrograph with an average peak discharge of 4300 m^3/s at about 1 hour was used as an upstream boundary condition for our study area. Several studies have used simple triangular hydrographs in hydrodynamic models as an input, attributing to the lack of gauging

stations and unpredictability of an outburst (Risley et al., 2006; Anacona et al., 2015; Kougkoulos et al., 2018).

Table 5.5: Empirical equations for dam breach time relating to impounded lake volume ($V=4.10^7$ m^3), the height of breach ($h_b=43$ m) and acceleration due to gravity (g)

Equation for T	Reference	T (hr)
$0.00254V^{0.53}h_b^{-0.90}$	Froehlich (1995a)	1.1
$63.2(V/(gh_b^2))^{0.5}$	Froehlich (2008)	1.01

The downstream boundary condition was assigned with an estimated friction slope 0.033 for both sites (Rivak village and Khorugh) as shown in Figure 5.8. The small stream (Bijondara) from Lake Rivakkul merges with Gunt River at Rivak village having an average annual discharge of 105 m^3/s (Pohl et al., 2015), which then converged to Panj River at Khorugh. So, a boundary condition with inflow hydrograph having a constant discharge of 105 m^3/s was added at the Gunt River-Rivakkul stream junction to embed the inflow from Gunt River while routing the flood up to Khorugh. The discharge information of Bijondara was not available and assumed to be lower than the Gunt River. After assigning the boundary conditions, the model was executed with a computational time step of 5 seconds. The summary of the inputs of the study areas are shown in Table 5.6.

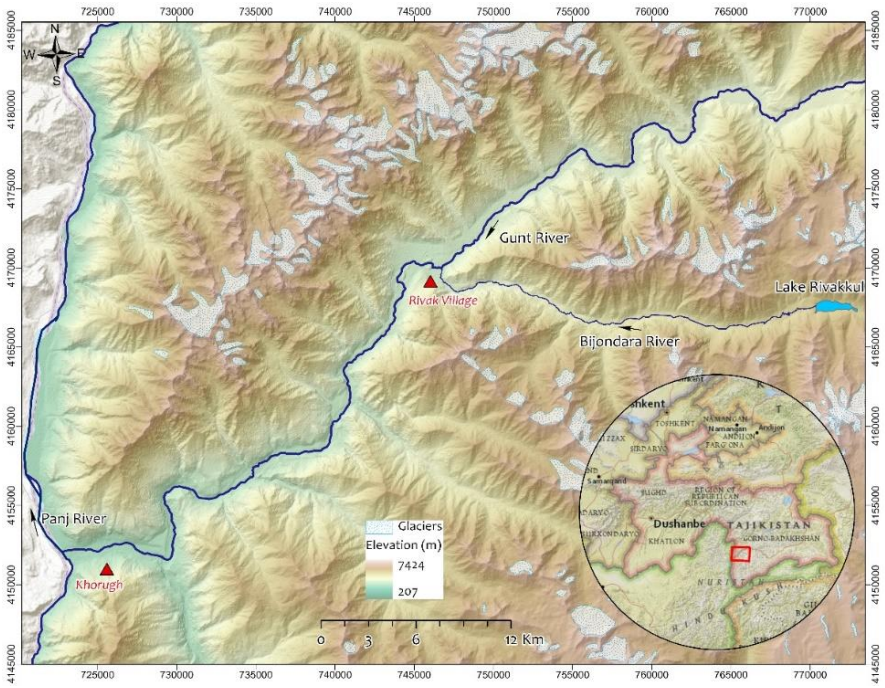

Figure 5.8: Study area showing the routing path of potential outburst flood from Lake Rivakkul

Table 5.6: Summary of the inputs for modelling Lake Rivakkul outburst flood in HEC-RAS

Inputs/Study area	Rivak	Khorugh
Distance from the lake (km)	24	60
Terrain data	SRTM 30 m	SRTM 30 m
Computational mesh size (m)	50	50
Computational mesh cells	19339	48010
Number of boundary conditions	2	3
Manning's roughness coefficient	0.06	0.06
Computation time step (s)	5	5
Equation set	Full momentum	Full momentum

5.4. Results and discussion

This section discusses the results of Scenario 1 of Heller-Hager model. The outputs are analysed for the coupling with the HEC-RAS. Finally, flood routing results from HEC-RAS are analysed and discussed for the worst-case in Scenario 2.

The volume and depth of Scenario 1 were obtained assuming an ideal rotational slip surface. Scenario 1 generated the wave height of 6.3 m and a run-up height of 14.2 m, which was not enough to overtop the Rivakkul dam with a freeboard of 43 m. Scenario 1 accounted for six limitations in the model. Table 5.7 summarizes the results for Scenario 1.

Table 5.7: Summary of the results for Scenario 1 in Heller-Hager model

Results	Scenario 1
Wave height H (m)	6.3
Wave amplitude (m)	5.1
Wave period T (s)	18.6
Wavelength L (m)	373.8
Run-up height (m)	14.2
Overtopping volume V_o per unit length dam crest for f=0 (m^3/m)	no value
Duration of overtopping t_o for f=0 (s)	no value
Overtopping volume V'_o per unit length dam crest (m^3/m)	no value
Average discharge q per unit length dam crest for f=0 (m^2/s)	no value
Maximum discharge q_M per unit length dam crest for f=0 (m^2/s)	no value
Number of not satisfied limitations out of 23 (2D) or 24 (3D)	6

Relative slide mass and relative slide volume exceeded the range provided in the model for the generation of impulse waves. Both parameters depend upon the slide volume and the volume prediction in our case was very simplistic due to unavailability of data. The volume prediction method did not take into account any of the geotechnical properties or seismic acceleration which made the predicted volume to be highly uncertain. The other limitations exceeded were the relative slide width and relative radial distance. These parameters are functions of the still water depth. The lower the depth of the lake, the higher the deviation from the allowed range in the model. It can be considered that the Lake Rivakkul was not deep enough to generate the proper wave dynamics due to the falling of a rockslide of large volume. The Heller-Hager model is limited to the slide volumes that are significantly smaller than the volume of the lake. Displacement of water dominated over the wave generation in our case. Table 5.8 shows a summary of the limitation range for the generation of an impulse wave with red colour indicating the values exceeding the allowed range.

Table 5.8: Limitations of calculation of impulse waves

Parameter	Description	Range	Scenario 1
Slide Froude number	$F=V_s/(gh)^{0.5}$	$0.86 \le F \le 6.85$	3.06
Relative slide thickness	S=s/h	$0.09 \le S \le 1.64$	1.19
Relative slide mass	$M=\rho_s V'_s/(\rho_w bh^2)$	$0.11 \le M \le 10.02$	33.4
Relative slide density	$D=\rho_s/\rho_w$	$0.59 \le D \le 1.72$	1.58
Relative granulate density	ρ_g/ρ_w	$0.96 \le \rho_g/\rho_w \le 2.75$	2.5
Relative slide volume	$V=V'_s/(bh^2)$	$0.05 \le V \le 5.94$	21.2
Bulk slide porosity	n	$30.7\% \le n \le 43.3\%$	37
Slide impact angle	α	$30° \le \alpha \le 90°$	33
Relative slide width	B=b/h	$0.74 \le B \le 3.33$	18.19
Relative radial distance	r/h	$5 \le r/h \le 30$	46.5
Wave propagation angle	γ	$-90° \le \gamma \le +90°$	-85
Relative streamwise distance	X=x/h	$2.7 \le X \le 59.2$	no value

Impulse product parameter	$P=FS^{0.5}M^{0.25}\{\cos[(6/7)\alpha]\}^{0.5}$	$0.17 \leq P \leq 8.13$	7.54

The other two limitations exceeded were relative wave steepness and relative wave angle as shown in Table 5.9. Wave steepness is the function of wave height and wavelength, which in turn depend upon several governing parameters for impulse wave generation. The exceedance of limitations in Table 5.8 inherently affected the wave run-up limitations. For relative angle exceedance, the Heller-Hager model was tested with the range of 18.5°- 90° whereas the run-up angle in the Rivakkul dam was just 12°.

Table 5.9: Limitation of calculation of wave run-up

Parameter	Description	Range	Scenario 1
Relative wave height	H/h	$0.011 \leq H/h \leq 0.521$	1.76
Wave steepness	H/L	$0.001 \leq H/L \leq 0.013$	0.017
Relative angle	90°/β	$1.0 \leq 90°/\beta \leq 4.9$	7.5

Since Scenario 1 did not have enough run-up height to overtop the dam, we were not able to construct the hydrograph for modelling the flood due to the seiche wave caused by the falling of the rockslide in Lake Rivakkul. To make the wave to overtop the Rivakkul dam, some unrealistic modifications of the parameters could be done such as increasing the lake depth to compensate the water displacement from the large volume of the slide. Consequently, a higher number of limitations than Scenario 1 are expected in the Heller-Hager model, which would make the estimation of wave generation more uncertain.

The overtopping duration of the seiche wave as a result of a potential rockslide was very short even for the larger Lake Sarez (Figure 4.8). Lake Rivakkul is 425 times smaller than Lake Sarez in terms of water volume impoundment. It can be expected that even if there was overtopping of the wave over Rivakkul dam, it would have a very small overtopping duration though it may have large discharge. HEC-RAS cannot execute if the input hydrograph has a very small timestep. It was thus, assumed that the overtopped water gets absorbed into the dam crest or gets attenuated within a short stretch of stream, not producing a significant flood downstream.

Scenario 2 was modelled using HEC-RAS at two locations downstream (Rivak village and Khorugh) assuming a complete breach of the dam and emptying of the entire lake. The maximum flood depth for Rivakkul-Rivak village simulation reached up to 26.5 m, with a mean depth of 5.04 m whereas the average velocity was 5.04 m/s with the maximum velocity reaching up to 19.7 m/s (Table 5.10). The flood depth at Rivak village reached up to 5 m and velocity up to 12 m/s as shown in Figure 5.9 and Figure 5.10.

The maximum flood depth in Rivakkul-Khorugh simulation had a mean depth of 6.2 m. The maximum velocity reached up to 29.17 m/s, with an average velocity of 3.9 m/s (Table 5.10). The modelling results showed the flood depth at Khorugh reached up to 10 m and velocity up to 8 m/s as shown in Figure 5.11 and Figure 5.12.

Table 5.10: Outputs of the HEC-RAS flood modelling at Rivak and Khorugh

Parameters/ Study Area		Rivak	Khorugh
Max. Depth (m)	Maximum	26.5	26.8
	Mean	5.3	6.2
	Std Deviation	3.55	4.15
Max. Velocity (m/s)	Maximum	19.7	28.17
	Mean	5.04	3.9
	Std Deviation	3.26	2.73
Flood Extent (km^2)		4.85	12.93
Time to reach peak discharge downstream (hr)		2.25	4.45

Considering a narrow valley, steep near-vertical cliffs, loose sediments at different stretches and sharp river bends, the flood depth higher than 15 m seems realistic in our case. In a similar mountainous set-up, a GLOF simulated in South Lhonak lake, Sikkim by Sattar et al., (2019) found the downstream flood with inundation depth of 8 m and velocity up to 9 m/s in Chungthang town at 62.5 km downstream. Likewise, Anacona et al. (2015) reconstructed the GLOF in Chilean Patagonia in which the outburst flood had a mean velocity of 2.1 m/s and depth of 1.5 m in a town located at 26 km downstream from outburst volume of $12 \cdot 10^6$ m^3.

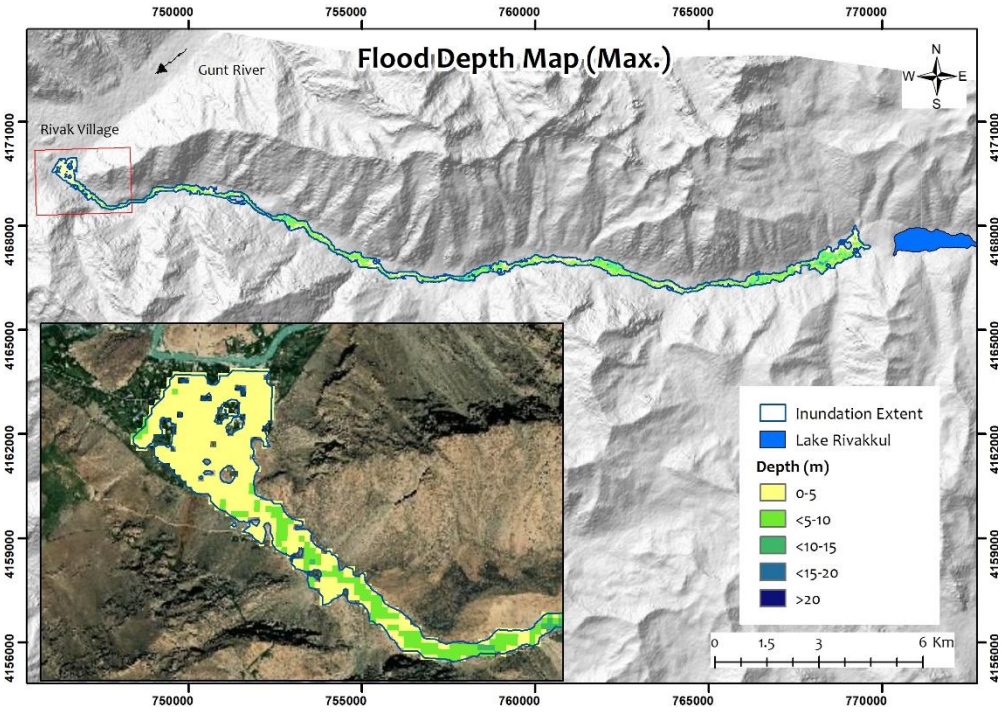

Figure 5.9: Maximum flood depth map of Rivak village

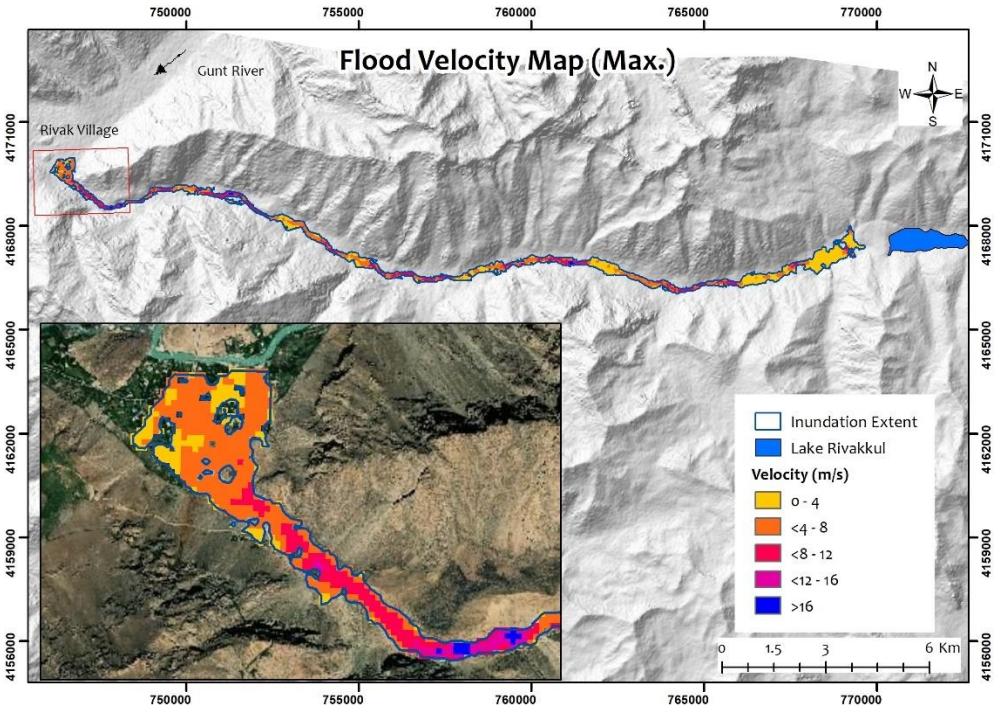

Figure 5.10: Maximum flood velocity map of Rivak village

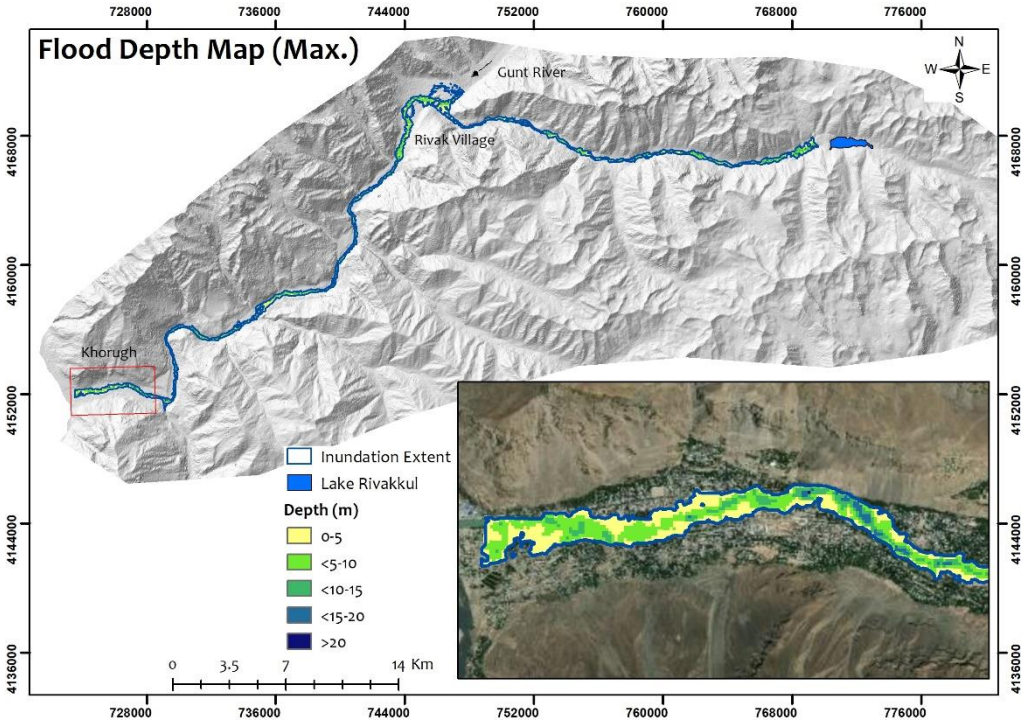

Figure 5.11: Maximum flood depth map of Khorugh

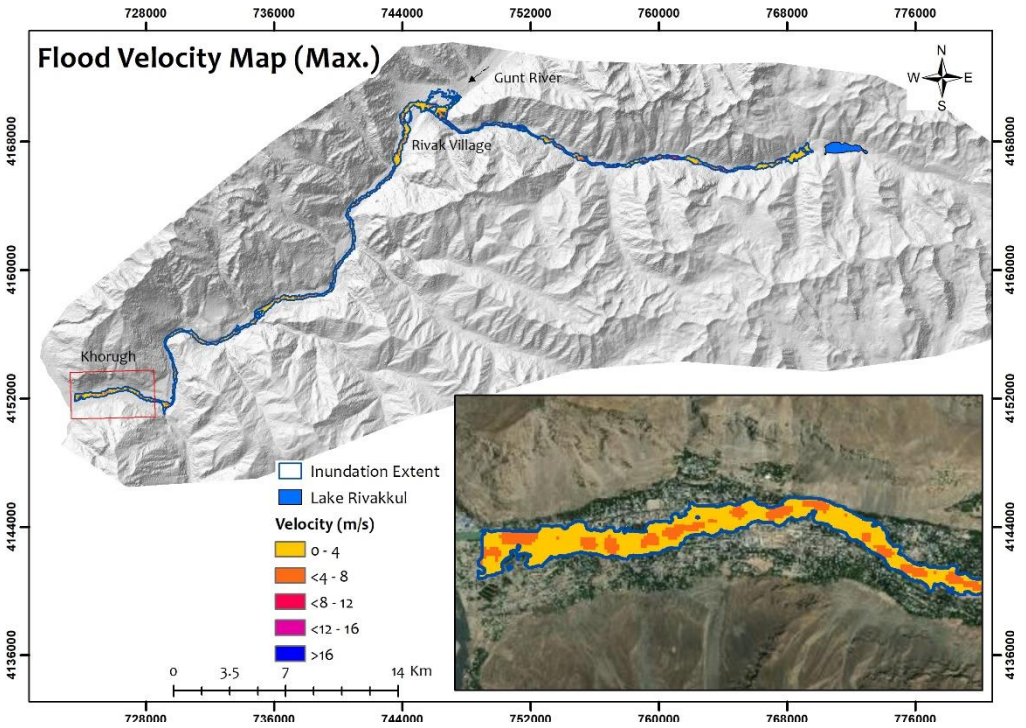

Figure 5.12: Maximum flood velocity map of Khorugh

Figure 5.13 shows the input and output hydrographs for Rivakkul-Rivak village and Rivakkul-Khorugh simulation. In the Rivak village simulation, the peak discharge of 4300 m^3/s was attenuated by 2.5 % to 4192 m^3/s. The modelling results showed that it took 2.25 hours for peak discharge to travel 24 km reach at Rivak village from the outburst of Lake Rivakkul. The inundation extent was about 5 km^2. Likewise, the peak discharge of 4083 m^3/s reached at the Khorugh town after 4.45 hours. The peak discharge attenuated by 5.05% from the input hydrograph while reaching to Khorugh with an inundation extent of 13 km^2.

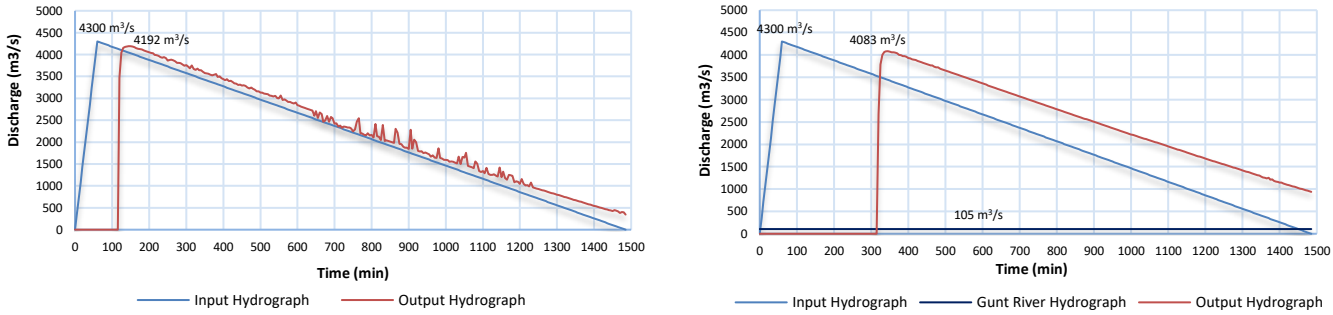

Figure 5.13: Input and output hydrographs used at Rivak (left) and Khorugh (right) simulation in HEC-RAS

Within the 60 km reach downstream to Khorugh, there were many small villages and two hydroelectric power stations which would be affected by the outburst flood. A complete risk assessment is out of the scope of the study attributing to the requirement of detail elements at risk and vulnerability data. Besides, the simulations were influenced by several uncertainties related to the roughness coefficient, terrain data and outburst lake volume. The explanation of uncertainties is discussed in chapter 6. Roughness value was one of the sensitive parameters in hydrodynamic modelling mentioned in the past studies (Hicks & Peacock, 2005; Parhi et al., 2012; Parhi, 2013; Li et al., 2014). The resistance parameter varies with the water level; decreasing as the water level increases and as the water spills over the floodplain, the resistance increase in the channel again (Chow, 1959). Anacona et al. (2015) argued that the deeper flood depths and larger flood extent were primarily controlled by the input hydrographs having higher volumes and peak discharges and the roughness values had a secondary control. However, the roughness values had dominant control over the flood timing.

Our study area was quite complex due to its topography. Regular mudflows along the valley often affected the channel bed characteristics and deviated the river course. Only the major river, Gunt River was used for the boundary condition. The contributions of several small tributaries to Gunt River were not accounted for in this study. So, the results obtained from the analysis were not suitable for comprehensive flood risk assessment. However, the results could be represented as the first-pass hazard assessment and as a tool to aware the stakeholders about the possible hazards and their mitigation.

6. DISCUSSION

This chapter discusses the uncertainties and limitations of the models used and the challenges of modelling the naturally-dammed lake outburst flood hazard chain. There are four major processes in a lake outburst hazard chain: triggering events such as earthquake, landslides, precipitation etc., impulse wave generation, propagation and run-up, dam breaching or overtopping and downstream flood. Because of the time limitation of this study, only three process models: slope stability (trigger and initiation), impulse wave and flood were considered for this study.

Modelling of the individual processes has its own challenges, let alone modelling the interactions of these processes in a hazard cascade. The complex interaction between the processes also limits the use of models and assumptions are made to ensure the model's performance. Uncertainties are inherent in each process model so understanding their sources and quantifying them is very important. Realization and if possible quantification of the uncertainties will contribute that future studies may incorporate these effects on the results and helps them to quantify them into probabilities. Besides, insights of uncertainties also help to represent the real-world scenarios more accurately and to predict the consequences when the hazard occurs.

6.1. Uncertainties in input parameters

6.1.1. Scoops3D

Identification of the exact location of a mass movement is a crucial factor in modelling the slide volume, which can be done through comprehensive geotechnical surveys. But the lack of infrastructures and accessibility in the mountain environment hinders such surveys making it economically unfeasible. The RBL of Lake Sarez was hardly accessible by foot and was dangerous because of its steep slope so the investigators were only able to execute one seismic profile (Papyrin, 2001). The development of remote sensing techniques and the availability of high-resolution satellite images and topographic data have improved the prediction of the potential landslide areas. However, the sub-surface data relating to a pre-landslide such as the structural geological setting, lithological composition and alteration, slide thickness (deep-seated or shallow-seated), parent material and their formation mechanisms, degree of compactness, cementations, groundwater regimes cannot be understood in detail through remote sensing (Ma, 2018) and separate measurement techniques have to be applied.

Geotechnical parameters vary at different places attributing to their lithological formations, horizontal and vertical variability of soil materials, variations caused by exposure to rainfall, erosion as well as variation due to limitation of measurement techniques. These parameters were assigned from studies at different places other than our study area except for the Usoi rockslide, making the input uncertain. Westoby et al. (2014) argued that even if the geotechnical properties were well-documented, the heterogeneous nature of the material characteristics of the natural environment might not represent the definitive material properties at all.

6.1.2. Heller-Hager model

The analytical equations in Heller-Hager model were derived from the laboratory-based experiment tests. The experimental set-up comprised of sophisticated devices that could initiate the landslide of various dimensions whenever required and measure the wave characteristics in real-time. In short, the parameters were measured in an idealistic situation which was not the case in the real world. Most of the parameters need to be estimated and assumed in the real world hazard scenario. Among the slide characteristics, slide

volume, slide velocity, slide thickness or depth along with lake depth were the most uncertain parameters in our case.

Slide velocity was estimated using Körner (1976) energy equation which depended upon three factors: slide impact angle, friction angle and drop height of the centre of the gravity of the slide. The first two parameters can be estimated from DEM and past studies respectively. However, the drop height of the centre of gravity of slide depends upon the exact location of the mass movement, which is uncertainty by itself.

Lake depth played an important role in wave generation, propagation and run-up. If the lake is not deep enough, the sliding volume of mass movement displaces the water entirely, making the Heller-Hager model inapplicable. Lake depth varies at different locations in the naturally-dammed lakes; often deeper at the dammed side. Generally, glacial-dammed and moraine-dammed lakes are shallower than the landslide-dammed lakes (Ischuk, 2013). Thus, it reflected the importance of lake bathymetric data in modelling.

6.1.3. HEC-RAS

A sufficiently detailed topographic representation of the model domain is the most important factor in producing meaningful, accurate estimates of flood duration, intensity and inundation extent (Westoby et al., 2015). Terrain data was extracted from the freely available SRTM DEM having 30 m resolution for 2D modelling. ALOS PALSAR DEM despite having a higher resolution (12.5 m) than SRTM did not perform well in the mountainous environment attributing to several interferences caused by distortions due to layover, hence attenuating the detection of the features in the study area (de Oliveira Andrades Filho & de Fáltima Rossetti, 2012). Anacona et al. (2015) claimed that despite its coarser resolution, SRTM DEM represented the channel hydraulics better than the ASTEM GDEM2, supported by Guth (2010) and Das et al. (2015). However, for a small scale hydraulic modelling, it is optimum to have a detailed resolution DEM to represent the hydraulic characteristics of rivers in mountainous areas which are mostly narrow and steep and in some parts of the reach, streams may be at a scale below the spatial resolution of coarser DEMs.

Another important source of uncertainty in the modelling was the outburst volume as input due to lack of bathymetric data or gauging stations to restrict our estimates. In this study, the empirical equation derived by Huggel et al. (2002) which related the area and volume of the lakes in Swiss Alps was used. This uncertain estimate of volume would influence the peak discharge since it depends upon the volume of the lake.

The appropriate value for Manning's roughness was another uncertainty in our modelling. A uniform value for the entire computation domain is not appropriate for detailed hydraulic modelling as it influences the effectiveness of flow conveyance (Risley et al., 2006; Westoby et al., 2014). However, roughness coefficients exert little effect on flows with high velocity and flow stage. Besides, HEC-RAS allows the user to input a map with appropriate land use classification with the roughness values. A combination of high-resolution satellite images coupled with field investigations would be needed for a detailed roughness coefficient map.

Table 6.1 lists out the input parameters of all the process models used in this study and summarizes their impacts on the outputs of the modelling with the estimation of uncertainty level. Those input parameters which are impossible and difficult to measure or model will have high uncertainty in the outputs whereas some parameters can be estimated or measured accurately which will have lower level of uncertainty.

Table 6.1: Summary of the impacts of the input parameters on output and the level of uncertainties

Process models	Parameters	Nature of impact/solution	Estimated level of uncertainty
Scoops3D	DEM	Influence the failure volume and location; preference of finer DEM	Medium
	Geotechnical parameters (c,Ψ,ρ)	Influences the FoS and hence failure volume; on site investigations and laboratory tests as well as site specific geotechnical modelling	Medium-High

	Seismic loading	Influences the failure volume; spectral acceleration value more suitable than peak ground acceleration	Medium
	Groundwater	Difficult to estimate in steep areas	High
	Underground soil layers	Vertical heterogeneous composition influences the geotechnical properties	High
	Search resolution	Affect the failure locations and computation time; values used as per recommendation and resolution of DEM	Medium
	Search lattice extent		
	Volume limit	Influences the failure volume and computation time; sensitivity analysis required complemented by field estimation	Medium-High
Heller-Hager model	Slide impact velocity	Empirically determined and sensitive to wave-run up height; physically-based modelling required	Medium-High
	Bulk slide volume	Prediction of slide volume and depth influenced by several parameters and highly sensitive to the wave run-up heights; physically-based modelling required with validation from field investigations	High
	Slide thickness		
	Bulk slide density	Difficult to assign due to heterogeneous composition of the slide; can be updated with lithological maps of finer scale	High
	Bulk slide porosity	Impossible to determine porosity in a moving slide but not sensitive to wave run-up height	Medium
	Still water depth	Determines the impact wave height; requires bathymetric or terrestrial survey	Medium-High
	Slide or reservoir width	Estimated from satellite images and DEM	Low
	Slide impact angle		
	Radial distance		
	Wave propagation angle		
	Streamwise distance		
	Run-up angle		
	Freeboard		
	Crest width		
HEC-RAS 2D	DEM	Channel and floodplain are better represented by high-resolution DEM	Medium-High
	Flow Hydrograph	Affects the peak discharge and flood intensity; requires calibration and validation (highly challenging for a one-time event)	High
	Roughness value	Affects the conveyance at low flows and flooding time; requires in-situ investigations complemented by high-resolution satellite imageries	High
	Computational grid	Slope surface of water is averaged over a long distance; requires a reasonable size of computational grid depending upon study area	Medium
	Time discretization	Courant condition must be satisfied	Medium

6.2. Limitations of the models

The limitations of the models themselves affect the model results as they simplify the real-world phenomenon and make assumptions. This section describes the limitation of all three process models used in this study.

6.2.1. Scoops3D

Scoops3D is unable to model whether the failure occurs as a single event or in several parts. Even with the higher values of geotechnical parameters (Table 4.3), there was not any significant improvement in the stability of the slope and we were not able to obtain the metastable state for the Scenario 1 of Lake Sarez. With such lower FoS values (FoS<1), it is expected that the slope fails irrespective of the triggering factors but it was not shown in Scoops3D. However, the failure volume predicted by the Scoops3D for different

unstable surfaces can be used as an initial condition for a separate landslide runout model to analyse the mass movement.

FoS is calculated in Scoops3D using either the Ordinary (Fellenius) or Bishop's simplified method but both of these methods do not account for the inter-column forces in the soil. The potential failure surface is limited to the rotational slip in Scoops3D. It is inapplicable for shallow, translational slides or complex slip surface geometries. Scoops3D is also unable to estimate the dynamic loading, progressive failure, material deformation and strain (Krahn, 2003; Duncan & Wright, 2005). For inclusive site-specific features, geotechnical programs like CLARA (Hungr et al., 1989), TSLOPE3 (Pyke, 1991), 3D-SLOPE (Lam & Fredlund, 1993) are recommended (Mergili et al., 2014; Reid et al., 2015). However, limit equilibrium methods have been used widely in the slope stability applications and interpretation of the results from Scoops3D requires the insights of its limitations (Reid et al., 2015).

6.2.2. Heller-Hager model

The model is based on laboratory test results which are then used as generally applicable equations to analyse the wave generation, propagation and overtopping of the dam. The laboratory test results exhibit significant scattering, therefore, the results obtained from the equations are considered to be the estimates only. Annex 2 lists the limitations of the parameters at different phases of the model.

One of the major limitations of Heller-Hager model is that it is limited to the slide volumes that are significantly smaller than the volume of the lake. The volumetric displacement of water caused by the mass movement impacting the lake is considered negligible compared to the wave height generation created by the landmass. Likewise, this model assumes the slide as granular and the effect of solid slide has not been tested in detail. Another limitation of the model is regarding the wave propagation angle, which ranges from -90° to +90°. But if the reservoir geometry exceeds or limits within the angle range, then the model application is limited.

Heller-Hager model can be used for estimating the impact wave characteristics at little cost and in a short time but it compromises the results needed for the detailed engineering solutions. Therefore, predictive impact wave generation, propagation and overtopping at present, requires the numerical simulations at a cost of high-resolution data and computational time. Numerical models like BASEMENT solves shallow water equations (SWE) which can be used to model the impact waves and empirical or analytical equations such as in Heller-Hager model can be used for the validation purposes (Somos-Valenzuela et al., 2016; Lala et al., 2018). Another advanced numerical approach to model the impact waves induced by landslides is by applying the Smoothed Particle Hydrodynamics (SPH) method. SPH is a mesh-free numerical method in which flows are discretised into a finite number of elements or particles, possessing specific properties governed by inter-particle physical laws (Dalrymple & Rogers, 2006; Ataie-Ashtiani & Shobeyri, 2008; Westoby et al., 2014; Huan et al., 2018).

6.2.3. HEC-RAS

Lake outburst flood not only comprises of floodwater but also the eroded dam materials, entrained sediments and debris along the routing path. HEC-RAS can only model the outflow as clear water, although it has a module to include sediment entrainment. Nonetheless, it cannot model the debris like flow.

HEC-RAS is also unable to model the short duration overtopping of water over the dam because of its limitation in the output interval. The overtopping duration must be long enough such that a hydrograph can be constructed as an input boundary condition.

6.3. Modelling challenges of naturally-dammed outburst hazards

As mentioned above, the comprehensive modelling of naturally dammed lakes requires an understanding of every process involved in the hazard chain. Despite the catastrophic nature of the outburst flood, few observations or quantitative data are available.

Naturally-dammed lake outburst floods are sudden in nature and characterization of these hazards are challenging yet very essential for modelling. The number of well-documented outburst floods in mountainous terrain is limited in nature and real-time documentation of such events is impossible. As a result, calibration and validation of modelling of such outburst flood hazards are limited. Retrospective modelling or scenario-based (predictive) modelling have been done in most of the lake outburst studies. In retrospective modelling, the input parameters are characterized by similar kind of extreme flow events which are assigned for modelling in the area of interest (Worni et al., 2014). Likewise, in scenario-based modelling, arbitrary scenarios are assumed based on the surrounding and past investigations in the study area. However, compromises have to be made using either type of modelling, as data from similar events may not correspond to the dynamics of the study area or the mechanisms of triggering events may differ completely. Besides, the lack of geomorphological and geotechnical surveys on hazardous lakes also hinder scenario-based modelling.

Characterizing the natural dams and their failure mechanism is another challenging task in modelling the naturally-dammed lake outburst flood. The delineation of the breach initiation and breach formation process due to overtopping of the impact waves or internal erosion (piping) within the dam are very difficult tasks (Wahl, 2004; Westoby et al., 2014). Besides, the natural dams at a higher elevation contain interstitial ice, ice cores, relict crevasses, permafrost, which are difficult to integrate into the models (Worni et al., 2014; Byers et al., 2018; Lala et al., 2018). Several advanced, physically-based models have been developed in recent years to model the dam erosion due to impact waves, which could potentially improve the understanding of dam breach mechanism. However, to identify the hazards related to dam breach and to describe the characteristics of the dam, labour-intensive and logistically challenging geotechnical investigations are required to represent the real-world process, yet their heterogeneous nature could cause a problem. With limited time and lack of data, the dam breach model was not considered in our study, but still very crucial in hazard cascade modelling.

The complex flow hydraulics of the lake outburst flood poses another challenge in the modelling. The hydraulics of the high-magnitude flows and mechanisms of erosion, sediment transport, channel bed dynamics and rheology of the flows are understood in a limited way and remain largely unquantified (Carrivick, 2006; Westoby et al., 2014; Worni et al., 2014). As the lake outbursts, the sudden onset of the flow changes from hyperconcentrated flow to debris flow (Mergili et al., 2011). The rheology of the clear water changes with sediments entrainment along the routing path (Risley et al., 2006; Fan et al., 2012; Anacona et al., 2015; Kougkoulos et al., 2018; Sattar et al., 2019). The debris-laden flow will travel a shorter distance with varying velocities, smaller inundation extent and more devastating effect compared to the clear water flow (Mergili et al., 2011; Worni et al., 2014; Kougkoulos et al., 2018). Nevertheless, HEC-RAS 1D and 2D have been widely used to model clear water flood in past studies (Bajracharya et al., 2007; Osti & Egashira, 2009; Klimeš et al., 2013; Anacona et al., 2015; Kougkoulos et al., 2018; Sattar et al., 2019).

Besides the abovementioned challenges, Westoby et al. (2014) also argued that the hazard dynamics of lake outburst floods in the mountainous regions would be affected by the contemporary and future climate change. These include the fluctuation in the glacier melting, snow and rainfall as well as exposing or melting the ice cores within the dam making it more susceptible to the sudden breach.

Numerous uncertainties exist in the parameterization of models used for lake outburst hazards chain. The lack of historical records and field investigations combined with a reconciliation of the scales to represent a complex environment often leads to simplified parameterization. In such conditions, uncertainties are inherently accepted in the model parameters and the uncertainties are quantified using probabilistic methods rather than finding a set of deterministic and optimal parameters (Beven & Freer, 2001; Westoby et al., 2015). Such models also simulate the outputs in a probabilistic manner, hence incorporating all the possible scenarios for probable flood risk management.

Another common challenge in modelling complex environment such as in our case is the possibility to obtain similar or identical outputs from the different combination of input parameters, model structure or initial conditions (Beven & Binley, 1992; Beven & Freer, 2001). This is known as the equifinality concept. When there are many parameters in the model, it is difficult to obtain an optimal combination of parameters that represent the desired outcomes and there are multiple possibilities of such an optimal combination. Beven & Binley (1992) argued that any combination of parameters that give results within acceptable limits must be included during the modelling of complex systems.

Applying this principle, Westoby et al. (2015) adopted the Monte-Carlo simulation to find the optimal set of parameters from possible ranges. The uncertainties associated with physically-based dam model were quantified for the reconstruction of GLOF in Nepal Himalayas using the weighted, probabilistic Generalized Likelihood Uncertainty Estimation (GLUE) method (Beven & Binley, 1992). Westoby et al. (2015) argued that the probabilistic methods conveyed the effects of uncertainty and equifinality in model input on the resulting output. However, these methods involve a huge number of individual simulations, therefore, high computationally expensive tasks.

Event tree analysis is another simplistic, graphical representation of the sequence of events suitable for estimating the probability of occurrence of the hazard cascade. An event tree fans out like tree branches as the number of the events increase resulting into a particular consequence such as outburst flood (Lacasse et al., 2008). However, the assignment of the probabilities of occurrence requires inputs from experts in the respective fields, especially where there is no historical data. Annex 4 shows the simple event tree analysis of the potential rockslide falling from the RBL into the Lake Sarez and their probability of occurrence.

7. CONCLUSION AND RECOMMENDATIONS

The primary aim of this research was to evaluate the outburst flood hazard chain of naturally-dammed lakes in the mountainous areas by integrated process chain modelling under various scenarios. Among the major processes of outburst hazard cascade, three processes (slope stability, impact wave and flood) were modelled in the study. For this, two case study areas: Lake Sarez and Lake Rivakkul were chosen from the mountainous region of Tajikistan in Central Asia. Lake Sarez has been investigated in detail compared to Lake Rivakkul. Three and two scenarios were developed for Lake Sarez and Lake Rivakkul respectively.

Scoops3D was used in Scenario 1 of Lake Sarez to predict the volume and depth from the potential rockslide in the RBL. These parameters were coupled with the Heller-Hager model for the analysis of wave generation, propagation and run-up. Scenario 2 and Scenario 3 for Lake Sarez used the optimistic and pessimistic set of parameter values from the past studies to model the impact wave characteristics. Simple triangular hydrographs were constructed from the results of Heller-Hager model to check its plausibility to couple with flood model. However, flood modelling was not done for Lake Sarez attributing to its dam stability, validated by many studies.

Scenario 1 of Lake Rivakkul assumed an ideal rotational slip for predicting the failure volume and depth from the potential rockslide due to lack of field data. Heller-Hager model was used to analyse the impact wave characteristics. Since the run-up height was not enough for the wave to overtop the dam, the coupling of the Heller-Hager model was not done with the flood model (HEC-RAS). Scenario 2 was the worst-case scenario for Lake Rivakkul where a complete breach of the dam and emptying of the lake was assumed. HEC-RAS was used to model the consequent downstream flood at two locations: Rivak village and Khorugh, 24 km and 60 km downstream of the Lake Rivakkul. The peak discharge and duration of the breach was estimated from the empirical equations.

The input data and their inherent uncertainties were the most crucial component of this study. The data such as geotechnical parameters, roughness values were assigned from the literature and some were predicted from physically-based models, simple engineering drawings and empirical equations. The application of empirical data and equations derived from one region to other introduces the uncertainties in input parameters attributing to their spatial and temporal heterogeneity. Some uncertainties existed due to the limitations of the model itself. Therefore, the use of the empirical equations and the selection of the models should be done with caution. This study tried to document the uncertainties in all the process models initiating from the mass movement to the flood model. Naturally-dammed lake outburst flood is a sudden and one-time event. The trigger mechanism and characteristics of the dam, dam breaching mechanism and resulting flood vary in different regions. Historical data are archived either from the field and remote investigations or retrospective modelling of the event once it has already happened. Due to these reasons, the calibration and validation of predictive modelling such as in our case are limited.

In general, this study focused on the three major processes of the lake outburst flood and the ways to couple the series of models in a data-scarce mountainous environment. To get a more robust and comprehensive assessment of hazard and risks posed by the outburst flood, advanced models complemented by ample field data are required. It is also important to highlight the quantification of the uncertainties as they influence the final results. Taking these points into considerations, the following recommendations are made to improve the modelling of lake outburst hazard cascade:

- Lake outburst flood is a result of the interaction of several processes. Among the major processes, dam breach was not accounted for in this study which is one of the most important and complex

processes to model. The mechanical strength of the dam needs to be assessed against the impact of the waves generated from the landmass failure into the lake. Even if the dam is stable, the impact waves would influence on the seepage of the lake, hence affecting its internal structure which could lead to internal erosion (Westoby et al., 2014). Besides, erosion of the dam material also influences the flood time and peak discharge, Physically-based modelling of the dam breach is recommended.

- Heller-Hager model is based on simple assumptions and it does not account for the complex bed geometry and has many parametric limitations. So, the simulation of impulse wave dynamics using advanced numerical models is recommended. However, the field data and estimations from Heller-Hager model can be used for calibration and validation.
- The flood results from the HEC-RAS model can be used as the preliminary indicative hazard assessment. To strengthen the results, a high-resolution DEM complemented by the detailed analysis of the land cover with proper values of roughness is required. It would be interesting to model different scenarios of the flood as clear water and debris or mudflows to get insights on the run-out hazards, which was also recommended by Mergili et al. (2011).
- Quantification of uncertainties using probabilistic approaches such as GLUE (Beven & Binley, 1992) is recommended to enhance the credibility of model outcomes. All these recommendations reflect the importance of data collection and availability in the mountainous regions.
- An alternative to the modelling and coupling of the processes in a hazard chain would be using a physically-based multi-hazard model capable of modelling all relevant interacting hazards directly within a single run. These models might not comprehensively analyse each process compared to the individual domain-specific model but the transition between the interacting processes would be smoother and realistic (Worni et al., 2014). BASEMENT has proven as an efficient tool to model GLOFs as it can simulate the impulse wave, dam breach, sediment entrainment and flood in a single run. Promising models that are capable of simulating the hazard cascade due to the mass movement include STEP-TRAMM (Von Ruette et al., 2013; Lehmann et al., 2017; 2018), r.avaflow (Mergili et al., 2017; 2018) and OpenLISEM Hazard (Bout et al., 2018). Future works need to focus on these physically-based multi-hazard models with ample data for calibration and validation.

LIST OF REFERENCES

Aggarwal, A., Jain, S. K., Lohani, A. K., & Jain, N. (2013). Glacial lake outburst flood risk assessment using combined approaches of remote sensing, GIS and dam break modelling. *Geomatics, Natural Hazards and Risk*, *7*(1), 18–36. https://doi.org/10.1080/19475705.2013.862573

Alford, D., Cunha, S. F., & Ives, J. D. (2000). Mountain Hazards and Assistance Development, *20*(1), 20–23.

Alho, P., & Aaltonen, J. (2008). Comparing a 1D hydraulic model with a 2D hydraulic model for the simulation of extreme glacial outburst floods. *Hydrological Processes*, *22*, 1537–1547. https://doi.org/10.1002/hyp

Amirahmadi, A., Pourhashemi, S., Karami, M., & Akbari, E. (2016). Modeling of landslide volume estimation. *Open Geosciences*, *8*(1), 360–370. https://doi.org/10.1515/geo-2016-0032

Anacona, P. I., Mackintosh, A., & Norton, K. (2015). Reconstruction of a glacial lake outburst flood (GLOF) in the Engaño valley, chilean patagonia: Lessons for GLOF risk management. *Science of the Total Environment*, *527–528*, 1–11. https://doi.org/10.1016/j.scitotenv.2015.04.096

Ataie-Ashtiani, B., & Shobeyri, G. (2008). Numerical simulation of landslide impulsive waves by incompressible smoothed particle hydrodynamics. *International Journal for Numerical Methods in Fluids*, *56*, 209–232. https://doi.org/10.1002/fld.1526

Azañón, J. M., Azor, A., Yesares, J., Tsige, M., Mateos, R. M., Nieto, F., … Rodríguez-Fernández, J. (2010). Regional-scale high-plasticity clay-bearing formation as controlling factor on landslides in Southeast Spain. *Geomorphology*, *120*(1–2), 26–37. https://doi.org/10.1016/j.geomorph.2009.09.012

Bajracharya, B., Shrestha, A. B., & Rajbhandari, L. (2007). Glacial Lake Outburst Floods in the Sagarmatha Region. *Mountain Research and Development*, *27*(4), 336–344. https://doi.org/10.1659/mrd.0783

Bell, R., & Glade, T. (2004). Multi-hazard analysis in natural risk assessments. *Management Information Systems*, *9*, 197–206. https://doi.org/10.2495/978-1-84564-650-9/01

Beven, K., & Binley, A. (1992). The future of distributed models: Model calibration and uncertainty prediction. *Hydrological Processes*, *6*(3), 279–298. https://doi.org/10.1002/hyp.3360060305

Beven, K., & Freer, J. (2001). Equifinality, data assimilation, and uncertainty estimation in mechanistic modelling of complex environmental systems using GLUE methodology. *Journal of Hydrology*, *249*, 11–29. https://doi.org/10.1524/anly.2006.26.99.365

Bishop, A. W. (1955). The use of the slip circle in the stability analysis of slopes. *Geotechnique*, *5*(1), 7–17. https://doi.org/10.1680/geot.1955.5.1.7

Blikra, L., Longva, O., Harbitz, C., & Lovholt, F. (2005). Quantification of rock-avalanche and tsunami hazard in Storfjorden , western Norway. *Landslides and Avalanches: ICFL 2005, Norway*, 57–64.

Bosa, S., & Petti, M. (2013). A Numerical Model of the Wave that Overtopped the Vajont Dam in 1963. *Water Resources Management*, *27*(6), 1763–1779. https://doi.org/10.1007/s11269-012-0162-6

Bout, B., Lombardo, L., van Westen, C. J., & Jetten, V. G. (2018). Integration of two-phase solid fluid equations in a catchment model for flashfloods, debris flows and shallow slope failures. *Environmental Modelling and Software*, *105*, 1–16. https://doi.org/10.1016/j.envsoft.2018.03.017

Brunner, G. (2016a). *HEC-RAS River Analysis System 2D Modeling User ' s Manual*.

Brunner, G. (2016b). *HEC-RAS River Analysis System Hydraulic Reference Manual. US Army Corps of Engineers Hydraulic Engineering Center (HEC) Version 5*. Davis,CA. https://doi.org/CPD-68

Butt, M. J., Umar, M., & Qamar, R. (2013). Landslide dam and subsequent dam-break flood estimation using HEC-RAS model in Northern Pakistan. *Natural Hazards*, *65*(1), 241–254. https://doi.org/10.1007/s11069-012-0361-8

Byers, A. C., Rounce, D. R., Shugar, D. H., Lala, J. M., Byers, E. A., & Regmi, D. (2018). A rockfall-induced glacial lake outburst flood, Upper Barun Valley, Nepal. *Landslides*, *16*(3), 533–549. https://doi.org/10.1007/s10346-018-1079-9

Caris, J. P. T., & Van Asch, T. W. J. (1991). Geophysical, geotechnical and hydrological investigations of a small landslide in the French Alps. *Engineering Geology*, *31*(3–4), 249–276. https://doi.org/10.1016/0013-7952(1)90011-9

Carrivick, J. L. (2006). Application of 2D hydrodynamic modelling to high-magnitude outburst floods: An example from Kverkfjöll, Iceland. *Journal of Hydrology*, *321*(1–4), 187–199. https://doi.org/10.1016/j.jhydrol.2005.07.042

Catane, S. G., Cabria, H. B., Zarco, M. A. H., Saturay, R. M., & Mirasol-Robert, A. A. (2008). The 17

February 2006 Guinsaugon rock slide-debris avalanche, Southern Leyte, Philippines: Deposit characteristics and failure mechanism. *Bulletin of Engineering Geology and the Environment*, *67*(3), 305–320. https://doi.org/10.1007/s10064-008-0120-y

Chen, L., van Westen, C. J., Hussin, H., Ciurean, R. L., Turkington, T., Chavarro-Rincon, D., & Shrestha, D. P. (2016). Integrating expert opinion with modelling for quantitative multi-hazard risk assessment in the Eastern Italian Alps. *Geomorphology*, *273*, 150–167. https://doi.org/10.1016/j.geomorph.2016.07.041

Christen, M., Kowalski, J., & Bartelt, P. (2010). RAMMS: Numerical simulation of dense snow avalanches in three-dimensional terrain. *Cold Regions Science and Technology*, *63*(1–2), 1–14. https://doi.org/10.1016/j.coldregions.2010.04.005

Clague, J. J., & O'Connor, J. E. (2015). *Glacier-Related Outburst Floods. Snow and Ice-Related Hazards, Risks, and Disasters*. Elsevier Inc. https://doi.org/10.1016/B978-0-12-394849-6.00014-7

Cook, S. J., & Quincey, D. J. (2015). Estimating the volume of Alpine glacial lakes. *Earth Surface Dynamics*, *3*(4), 559–575. https://doi.org/10.5194/esurf-3-559-2015

Costa, J. E., & Schuster, R. L. (1988). Geological Society of America Bulletin The formation and failure of natural dams. *Geological Society Of America Bulletin*, (July), 1054–1068. https://doi.org/10.1130/0016-7606(1988)100<1054

Crosta, G. B., Imposimato, S., & Roddeman, D. (2016). Landslide spreading, impulse water waves and modelling of the Vajont rockslide. *Rock Mechanics and Rock Engineering*, *49*(6), 2413–2436. https://doi.org/10.1007/s00603-015-0769-z

Dalrymple, R. A., & Rogers, B. D. (2006). Numerical modeling of water waves with the SPH method. *Coastal Engineering*, *53*(2–3), 141–147. https://doi.org/10.1016/j.coastaleng.2005.10.004

Das, A., Agrawal, R., & Mohan, S. (2015). Topographic correction of ALOS-PALSAR images using InSAR-derived DEM. *Geocarto International*, *30*(2), 145–153. https://doi.org/10.1080/10106049.2014.883436

de Oliveira Andrades Filho, C., & de Fáltima Rossetti, D. (2012). Effectiveness of SRTM and ALOS-PALSAR data for identifying morphostructural lineaments in northeastern Brazil. *International Journal of Remote Sensing*, *33*(4), 1058–1077. https://doi.org/10.1080/01431161.2010.549852

De Pippo, T., Donadio, C., Pennetta, M., Petrosino, C., Terlizzi, F., & Valente, A. (2008). Coastal hazard assessment and mapping in Northern Campania, Italy. *Geomorphology*, *97*(3–4), 451–466. https://doi.org/10.1016/j.geomorph.2007.08.015

Delaney, K. B., & Evans, S. G. (2011). Rockslide Dams in the Northwest Himalayas (Pakistan, India) and the Adjacent Pamir Mountains (Afghanistan, Tajikistan), Central Asia. In S. G. Evans, R. L. Hermanns, A. Strom, & G. Scarascia-Mugnozza (Eds.), *Natural and Artificial Rockslide Dams* (Vol. 131). Springer Netherlands.

Dorren, L. K. A., & Seijmonsbergen, A. C. (2003). Comparison of three GIS-based models for predicting rockfall runout zones at a regional scale. *Geomorphology*, *56*(1–2), 49–64. https://doi.org/10.1016/S0169-555X(03)00045-X

Droz, P., Fumagalli, A., Novali, F., & Young, B. (2008). GPS and Insar Technologies: a Joint Approach for the Safety of Lake Sarez. *Proceedings of the 4th Canadian Conference on Geohazards: From Causes to Management*, (Component C), 20–24.

Droz, P., & Spacic-Gril, L. (2002). Lake Sarez risk mitigation project: a global risk analysis. *Symposium IAHR*, (June 2002).

Duncan, J. M., & Wright, S. G. (2005). *Soil Strength and Slope Stability*. John Wiley & Sons, Inc.

Ermini, L., & Casagli, N. (2003). Prediction of the behaviour of landslide dams using a geomorphological dimensionless index. *Earth Surface Processes and Landforms*, *28*(1), 31–47. https://doi.org/10.1002/esp.424

Fan, X. (2013). Understanding the causes and effects of earthquake-induced landslide dams. *Vasa*. Retrieved from http://medcontent.metapress.com/index/A65RM03P4874243N.pdf%5Cnhttp://doc.utwente.nl/90363/

Fan, X., Tang, C. X., Van Westen, C. J., & Alkema, D. (2012). Simulating dam-breach flood scenarios of the Tangjiashan landslide dam induced by the Wenchuan Earthquake. *Natural Hazards and Earth System Science*, *12*(10), 3031–3044. https://doi.org/10.5194/nhess-12-3031-2012

Fell, R., Hungr, O., Leroueil, S., & Riemer, W. (2000). Keynote lecture - Geotechnical engineering of the stability of natural slopes, and cuts and fills in soil. *ISRM International Symposium 2000, IS 2000*,

(January).
Fread, D. L. (1991). BREACH: AN EROSION MODEL FOR EARTHEN DAM FAILURES by D.L. Fread 1 July 1988 (Revision 1, August 1991). *Noaa*, *1988*(July 1988).
Fritz, H. M. (2002). *Initial phase of landslide generated impulse waves*. *Experiments in Fluids*. https://doi.org/10.1007/s00348-003-0659-0
Froehlich, D. C. (1995). Peak Outflow from Breached Embankment Dam. *Journal of Water Resources Planning and Management*, *121*(5766), 90–97.
Froehlich, D. C. (2008). Embankment Dam Breach Parameters and Their Uncertainties. *Journal of Hydraulic Engineering*, *134*(12), 1708–1721. https://doi.org/10.1061/(ASCE)0733-9429(2008)134
Gallina, V., Torresan, S., Critto, A., Sperotto, A., Glade, T., & Marcomini, A. (2016, March 1). A review of multi-risk methodologies for natural hazards: Consequences and challenges for a climate change impact assessment. *Journal of Environmental Management*. Academic Press. https://doi.org/10.1016/j.jenvman.2015.11.011
Genevois, R., & Tecca, P. (2013). The Vajont Landslide: State-of-the-Art. *Italian Journal of Engineering Geology and Environment*, (6), 15–40. https://doi.org/10.4408/IJEGE.2013-06.B-02
Gill, J. C., & Malamud, B. D. (2014). Reviewing and visualizing the interactions of natural hazards. *Reviews of Geophysics*, *52*(4), 680–722. https://doi.org/10.1002/2013RG000445.Received
Glastonbury, J., & Fell, R. (2008). A decision analysis framework for the assessment of likely post-failure velocity of translational and compound natural rock slope landslides. *Canadian Geotechnical Journal*, *45*(3), 329–350. https://doi.org/10.1139/T07-082
Guth, P. L. (2010). Geomorphometric Comparison of Aster Gdem and Srtm. *A Special Joint Symposium of ISPRS Technical Commission IV & AutoCarto - ASPRS/CaGIS 2010 Fall Specialty Conference*, 10.
Guzzetti, F., Ardizzone, F., Cardinali, M., Rossi, M., & Valigi, D. (2009). Landslide volumes and landslide mobilization rates in Umbria, central Italy. *Earth and Planetary Science Letters*, *279*(3–4), 222–229. https://doi.org/10.1016/j.epsl.2009.01.005
Hack, R. (2000). Geophysics for slope stability. *Surveys in Geophysics*, *21*, 423–448. https://doi.org/10.1023/A
Hanisch, J., & Söder, C.-O. (2000). Geotechnical assessment of the Usoi landslide dam and the right bank of Lake Sarez. In D. Alford & R. L. Schuster (Eds.), *Usoi Landslide Dam and Lake Sarez: An assessment of hazard and risk in the Pamir Mountains, Tajikistan* (pp. 59–62). Geneva: United Nations Secretariat for International Strategy for Disaster Reduction.
Harbitz, C. B., Glimsdal, S., Løvholt, F., Kveldsvik, V., Pedersen, G. K., & Jensen, A. (2014). Rockslide tsunamis in complex fjords: From an unstable rock slope at Åkerneset to tsunami risk in western Norway. *Coastal Engineering*, *88*, 101–122. https://doi.org/10.1016/j.coastaleng.2014.02.003
Harrison, S., Kargel, J. S., Huggel, C., Reynolds, J. M., Shugar, D. H., Betts, R., … Vilímek, V. (2017). Climate change and global pattern of moraine-dammed glcaila lake outburst floods. *The Cryosophere*, (October), 1–39.
Heller, V. (2011). Scale effects in physical hydraulic engineering models. *Journal of Hydraulic Research*, *49*(3), 293–306. https://doi.org/10.1080/00221686.2011.578914
Heller, V., & Hager, W. H. (2009). Impulse product parameter in landslide generated impulse waves. *Journal of Waterway, Port, Coastal and Ocean Engineering*, *136*(3), 145–155. https://doi.org/10.1061/(ASCE)WW.1943-5460.0000037
Heller, V., & Hager, W. H. (2011). Wave types of landslide generated impulse waves. *Ocean Engineering*, *38*(4), 630–640. https://doi.org/10.1016/j.oceaneng.2010.12.010
Heller, V, Hager, W. H., & Minor, H. (2009). Landslide generated impulse waves in reservoirs: basics and computation. *Laboratory of Hydraulics, Hydrology, and Glaciology, ETH Zürich*, 172.
Heller, V. (2007). *Landslide generated impulse waves: Prediction of near field characteristics*. ETH Zurich.
Heller, V., Bruggemann, M., Spinneken, J., & Rogers, B. D. (2016). Composite modelling of subaerial landslide-tsunamis in different water body geometries and novel insight into slide and wave kinematics. *Coastal Engineering*, *109*, 20–41. https://doi.org/10.1016/j.coastaleng.2015.12.004
Hendron, A. J., & Patton, F. D. (1987). The Vaoint Slide- A Geotechnical Analysis Based on New Geologic Observation of the Failure Surface. *Science*, *1*.
Hermanns, R. L., Dahle, H., Bjerke, P. L., Crosta, G. B., Anda, E., Blikra, L. H., … Longva, O. (2013). Rockslide dams in Møre og Romsdal County, Norway. *Landslide Science and Practice: Risk Assessment, Management and Mitigation*, *6*, 3–12. https://doi.org/10.1007/978-3-642-31319-6-1
Hicks, F. E., & Peacock, T. (2005). Suitability of HEC-RAS for Flood Forecasting. *Canadian Water Resources*

Journal, *30*(2), 159–174. https://doi.org/10.4296/cwrj3002159
Huan, V. N. P., Harahap, I. S. H., & Alaloul, W. S. (2018). Modelling of Tsunami Due to Submarine Landslide by Smoothed Particle Hydrodynamics Method. *MATEC Web of Conferences*, *203*, 1–6. https://doi.org/10.1051/matecconf/201820301001
Huber, A., Hager, W.H. (1997). Forecasting impulse waves in reservoirs. Proc. 19th Congrès des Grands Barrages, Florence C.31:993-1,005. ICOLD, Paris.
Huggel, C., Haeberli, W., Kääb, A., Bieri, D., & Richardson, S. (2004). An assessment procedure for glacial hazards in the Swiss Alps. *Canadian Geotechnical Journal*, *41*(6), 1068–1083. https://doi.org/10.1139/T04-053
Huggel, C., Kääb, A., Haeberli, W., Teysseire, P., & Paul, F. (2002). Remote sensing based assessment of hazards from glacier lake outbursts: A case study in the Swiss Alps. *Canadian Geotechnical Journal*, *39*(2), 316–330. https://doi.org/10.1139/t01-099
Hungr, O., Salgado, F. M., & Byrne, P. M. (1989). Evaluation of a three-dimensional method of slope stability analysis. *Canadian Geotechnical Journal*, *26*(4), 679–686. https://doi.org/10.1139/t89-079
Ischuk, A. R. (2006). Usoy Natural Dam : Problem of Security (Lake Sarez , Pamir Mountains , Tadjikistan). *Italian Journal of Engineering Geology and Environment*, *1*(1), 189–192. https://doi.org/10.4408/IJEGE.2006-01.S-26
Ischuk, A. R. (2011). Natural and Artificial Rockslide Dams, *133*, 423–440. https://doi.org/10.1007/978-3-642-04764-0
Ischuk, N, & Saidov, M. (2016). *Natural Hazards and Climate Change Vulnerability Mapping in Pyanj and Syr-Darya river basins of Tajikistan. Organization for Security and Co-operation in Europe Office in Tajikistan Office in Tajikistan.*
Ischuk, N. (2013). The origin of the mountain river dams in Tajikistan. *Landslide Science and Practice*, *6*, 13–17. https://doi.org/10.1007/978-3-642-31319-6
Jongmans, D., & Garambois, S. (2007). Geophysical investigation of landslides: A review. *Bulletin de La Societe Geologique de France*, *178*(2), 101–112. https://doi.org/10.2113/gssgfbull.178.2.101
Kappes, M. S., Keiler, M., & Glade, T. (2010). From Single- to Multi-Hazard Risk Analyses: a concept addressing emerging challenges. *Mountain Risks: Bringing Science to Society*, (November), 351–356.
Kappes, M. S., Keiler, M., von Elverfeldt, K., & Glade, T. (2012). Challenges of analyzing multi-hazard risk: A review. *Natural Hazards*, *64*(2), 1925–1958. https://doi.org/10.1007/s11069-012-0294-2
Kattelmann, R. (2003). Glacial Lake Outburst Floods in the Nepal Himalaya. *Natural Hazards*, *28*, 145–154. Retrieved from http://www.ce.utexas.edu/prof/maidment/giswr2016/Papers/lala.pdf
Kidyaeva, V., Chernomorets, S., Krylenko, I., Wei, F., Petrakov, D., Su, P., … Xiong, J. (2017). Modeling potential scenarios of the Tangjiashan Lake outburst and risk assessment in the downstream valley. *Frontiers of Earth Science*, *11*(3), 579–591. https://doi.org/10.1007/s11707-017-0640-5
Klimeš, J., Benešová, M., Vilímek, V., Bouška, P., & Cochachin Rapre, A. (2013). The reconstruction of a glacial lake outburst flood using HEC-RAS and its significance for future hazard assessments: An example from Lake 513 in the Cordillera Blanca, Peru. *Natural Hazards*, *71*(3), 1617–1638. https://doi.org/10.1007/s11069-013-0968-4
Körner, H. J. (1976). Reichweite und Geschwindigkeit yon Bergstfirzen und Flief ~ schneelawinen. *Rock Mechanics*, *8*(4), 225–256.
Korup, O. (2002). Recent research on landslide dams -a literature review with special attention to New Zealand. *Progress in Physical Geography*, *26*(2), 206–235.
Korup, O. (2005). Distribution of landslides in southwest New Zealand. *Landslides*, *2*(1), 43–51. https://doi.org/10.1007/s10346-004-0042-0
Korup, O., Clague, J. J., Hermanns, R. L., Hewitt, K., Strom, A. L., & Weidinger, J. T. (2007). Giant landslides, topography, and erosion. *Earth and Planetary Science Letters*, *261*(3–4), 578–589. https://doi.org/10.1016/j.epsl.2007.07.025
Kougkoulos, I., Cook, S. J., Edwards, L. A., Clarke, L. J., Symeonakis, E., Dortch, J. M., & Nesbitt, K. (2018). Modelling glacial lake outburst flood impacts in the Bolivian Andes. *Natural Hazards*, *94*(3), 1415–1438. https://doi.org/10.1007/s11069-018-3486-6
Krahn, J. (2003). The 2001 R . M . Hardy Lecture : The limits of limit. https://doi.org/10.1139/T03-024
Lacasse, S., Nadim, F., Eidsvig, U., & Blikra, L. H. (2008). Event tree analysis of Aknes rock slide hazard. *4th Canadian Conference on Geohazards : From Causes to Management*, *2*(2), 551–558.

Lala, J. M., Rounce, D. R., & McKinney, D. C. (2018). Modeling the glacial lake outburst flood process chain in the Nepal Himalaya: Reassessing Imja Tsho's hazard. *Hydrology and Earth System Sciences*, *22*(7), 3721–3737. https://doi.org/10.5194/hess-22-3721-2018

Lam, L., & Fredlund, D. G. (1993). A general limit equilibrium model for three-dimensional slope stability analysis: Reply. *Canadian Geotechnical Journal*, *31*(5), 795–796. https://doi.org/10.1139/t94-094

Lehmann, P., von Ruette, J., & Or, D. (2017). STEP-TRAMM – Soil and Terrestrial Environmental Physics | ETH Zurich. Retrieved June 17, 2020, from https://step.ethz.ch/step-tramm.html

Lehmann, P., von Ruette, J., & Or, D. (2018). How Landslides Become Disasters. *Eos*, *99*. https://doi.org/10.1029/2018eo104549

Li, S., Zhang, J. M., Xu, W. L., Wang, Y. R., Peng, Y., Li, J. N., … Li, P. (2014). Sensitivity analysis of parameters in HEC-RAS software. *Applied Mechanics and Materials*, *641–642*(September 2014), 201–204. https://doi.org/10.4028/www.scientific.net/AMM.641-642.201

Ma, C. (2018). *Comparing and Evaluating Two Physically-Based Models : Openlisem and Scoops3D , for Landslide Volume Prediction*. University of Twente.

Marzocchi, W., Garcia-Aristizabal, A., Gasparini, P., Mastellone, M. L., & Ruocco, A. Di. (2012). Basic principles of multi-risk assessment: A case study in Italy. *Natural Hazards*, *62*(2), 551–573. https://doi.org/10.1007/s11069-012-0092-x

McKinnon, M., Hungr, O., & McDougall, S. (2008). Dynamic analyses of Canadian landslides. *Proceedings of the Fourth Canadian Conference on GeoHazards: From Causes to Management.*, 594–602. Retrieved from http://www.saguenay.ggl.ulaval.ca/geohazard/technologies/mckinnon.pdf

Mergili, M., Marchesini, I., Alvioli, M., Metz, M., Schneider-Muntau, B., Rossi, M., & Guzzetti, F. (2014). A strategy for GIS-based 3-D slope stability modelling over large areas. *Geoscientific Model Development*, *7*(6), 2969–2982. https://doi.org/10.5194/gmd-7-2969-2014

Mergili, M., & Schneider, J. F. (2011). Regional-scale analysis of lake outburst hazards in the southwestern Pamir, Tajikistan, based on remote sensing and GIS. *Natural Hazards and Earth System Science*, *11*(5), 1447–1462. https://doi.org/10.5194/nhess-11-1447-2011

Mergili, M., Emmer, A., Juřicová, A., Cochachin, A., Fischer, J. T., Huggel, C., & Pudasaini, S. P. (2018). How well can we simulate complex hydro-geomorphic process chains? The 2012 multi-lake outburst flood in the Santa Cruz Valley (Cordillera Blanca, Perú). *Earth Surface Processes and Landforms*, *43*(7), 1373–1389. https://doi.org/10.1002/esp.4318

Mergili, M., Fischer, J. T., Krenn, J., & Pudasaini, S. P. (2017). R.avaflow v1, an advanced open-source computational framework for the propagation and interaction of two-phase mass flows. *Geoscientific Model Development*, *10*(2), 553–569. https://doi.org/10.5194/gmd-10-553-2017

Mergili, M., Marchesini, I., Rossi, M., Guzzetti, F., & Fellin, W. (2014). Spatially distributed three-dimensional slope stability modelling in a raster GIS. *Geomorphology*, *206*, 178–195. https://doi.org/10.1016/j.geomorph.2013.10.008

Mergili, M., Müller, J. P., & Schneider, J. F. (2013). Spatio-temporal development of high-mountain lakes in the headwaters of the Amu Darya River (Central Asia). *Global and Planetary Change*, *107*, 13–24. https://doi.org/10.1016/j.gloplacha.2013.04.001

Mergili, M., Schneider, D., Worni, R., & Schneider, J. F. (2011). Glacial Lake Outburst Floods in the Pamir of Tajikistan: Challenges in Prediction and Modelling. *Italian Journal of Engineering Geology and Environment - Book*, 973–982. https://doi.org/10.4408/IJEGE.2011-03.B-106

Mergili, M., Schneider, D., Worni, R., Schneider, J. F., & Schneider, F. (2011). Glacial Lake Outburst Floods in the Pamir of Tajikistan : *Italian Journal of Engineering Geology and Environment*, 973–982. https://doi.org/10.4408/IJEGE.2011-03.B-106

Müller, D. R. (1995). *Mitteilungen*.

O'Connor, J. E., Hardison, J. H., & Costa, J. E. (2001). *Debris flows from failures of neoglacial-age moraine dams in the Three Sisters and Mount Jefferson wilderness areas, Oregon*. *US Geological Survey Professional Paper*.

Osti, R., & Egashira, S. (2009). Hydrodynamic characteristics of the Tam Pokhari Glacial Lake outburst flood in the Mt. Everest region, Nepal. *Hydrological Processes*, (August), 2943–2955. https://doi.org/10.1002/hyp.7405

Papyrin, L. P. (2001). Sarez catatrophe: geophysical forecast. Retrieved May 20, 2020, from http://sarez.ferghana.ru/papyrin.html

Parhi, P. K. (2013). HEC-RAS Model for Mannnig's Roughness: A Case Study. *Open Journal of Modern Hydrology*, *03*(03), 97–101. https://doi.org/10.4236/ojmh.2013.33013

Parhi, P. K., Sankhua, R. N., & Roy, G. P. (2012). Calibration of Channel Roughness for Mahanadi River, (India) Using HEC-RAS Model. *Journal of Water Resource and Protection*, *04*(10), 847–850. https://doi.org/10.4236/jwarp.2012.410098

Pazzi, V., Tanteri, L., Bicocchi, G., D'Ambrosio, M., Caselli, A., & Fanti, R. (2017). H/V measurements as an effective tool for the reliable detection of landslide slip surfaces: Case studies of Castagnola (La Spezia, Italy) and Roccalbegna (Grosseto, Italy). *Physics and Chemistry of the Earth*, *98*, 136–153. https://doi.org/10.1016/j.pce.2016.10.014

Peel, M. C., Finalayson, B. L., & McMahon, T. A. (2007). Updated world map of the Koppen-Geiger climate classification. *Hydrology and Earth System Sciences*, *11*, 1633–1644. https://doi.org/10.1002/ppp.421

Peng, M., & Zhang, L. M. (2012). Breaching parameters of landslide dams. *Landslides*, *9*(1), 13–31. https://doi.org/10.1007/s10346-011-0271-y

Pohl, E., Knoche, M., Gloaguen, R., Andermann, C., & Krause, P. (2015). Sensitivity analysis and implications for surface processes from a hydrological modelling approach in the Gunt catchment, high Pamir Mountains. *Earth Surface Dynamics*, *3*(3), 333–362. https://doi.org/10.5194/esurf-3-333-2015

Preobrajensky, J. (1920) The Usoi Landslide, Geological Committee Papers on Applied Geology 14, 21 p.

Pyke, R., 1991. TSLOPE3: User Guide. Taga Engineering System and Software, Lafayette.

Qiao, B., Zhu, L., & Yang, R. (2019). Temporal-spatial differences in lake water storage changes and their links to climate change throughout the Tibetan Plateau. *Remote Sensing of Environment*, *222*(October 2017), 232–243. https://doi.org/10.1016/j.rse.2018.12.037

Quincey, D., & Carrivick, J. L. (2015). Glacier floods. In C. Huggel, J. J. Clague, & A. Kääb (Eds.), *The High-Mountain Cryosphere* (pp. 204–226). Cambridge University Press.

Raetzo, H. (2006). Hazard Assessment of Lake Sarez Rockslides and Usoy Dam in Pamir Mountains (Tadjikistan). *Italian Journal of Engineering Geology and Environment*, *1*(1), 193–196. https://doi.org/10.4408/IJEGE.2006-01.S-27

Ramsden, J. D. (1996). Forces on a vertical wall due to long waves, bores, and dry-bed surges., *122*, 134–141.

Reid, M. E., Christian, S. B., Brien, D. L., & Henderson, S. . (2015). Scoops3D — Software to Analyse Three-Dimensional Slope Stability Throughout a Digital Landscape. *U.S. Geological Survey Techniques and Methods, Book 14*, 218. https://doi.org/10.3133/tm14A1

Risley, J. C., Walder, J. S., & Denlinger, R. P. (2006). Usoi dam wave overtopping and flood routing in the Bartang and Panj Rivers, Tajikistan. *Natural Hazards*, *38*(3), 375–390. https://doi.org/10.1007/s11069-005-1923-9

Sainflou, G. (1928). Essai sur les digues maritimes verticales. Annales des Ponts et Chaussées 128.

Sattar, A., Goswami, A., & Kulkarni, A. V. (2019). Hydrodynamic moraine-breach modeling and outburst flood routing - A hazard assessment of the South Lhonak lake, Sikkim. *Science of the Total Environment*, *668*, 362–378. https://doi.org/10.1016/j.scitotenv.2019.02.388

Schneider, D., Huggel, C., Cochachin, A., Guillén, S., & García, J. (2014). Mapping hazards from glacier lake outburst floods based on modelling of process cascades at Lake 513, Carhuaz, Peru. *Advances in Geosciences*, *35*, 145–155. https://doi.org/10.5194/adgeo-35-145-2014

Schuster, R. L., & Alford, D. (2004). Usoi Landslide Dam and Lake Sarez, Pamir Mountains, Tajikistan. *Environmental and Engineering Geoscience*, *10*(2), 151–168. https://doi.org/10.2113/10.2.151

Somos-Valenzuela, M. A., Chisolm, R. E., Rivas, D. S., Portocarrero, C., & McKinney, D. C. (2016). Modeling a glacial lake outburst flood process chain: The case of Lake Palcacocha and Huaraz, Peru. *Hydrology and Earth System Sciences*, *20*(6), 2519–2543. https://doi.org/10.5194/hess-20-2519-2016

Statistics Agency Tajikistan. (2019). *The population of the Republic of Tajikistan (in Tajik).*

Strom, A. (2006). Morphology and Internal Structure of Rockslides and Rock Avalanches: Grounds and Constraints for their Modelling. In S. G. Evans, G. Mugnozza, A. Strom, & R. L. Hermanns (Eds.), *Landslides from Massive Rock Slope Failure* (Vol. 49, pp. 285–304). Springer Netherlands.

Strom, A. (2010). Landslide dams in Central Asia region. *Journal of Japan Landslide Society*, *47*(6), 309–324.

Strom, A. (2013). Geological prerequites for landslide dam's disaster assessment and mitigation in Central Asia. In F. Wang, M. Miyajima, L. Tonglu, S. Wei, & T. Faisal Fathani (Eds.), *Progress of Geo-Disaster Mitigation Technology in Asia*. Springer Berlin Heidelberg. https://doi.org/10.1139/l91-019

Strom, A. (2014). Sarez Lake problem:ensuring long-term safety. In *Proceedings of World Landslide Forum 3*. Beijing. https://doi.org/10.1007/978-3-319-04996-0

Strom, A. L., & Korup, O. (2006). Extremely large rockslides and rock avalanches in the Tien Shan Mountains, Kyrgyzstan. *Landslides*, *3*(2), 125–136. https://doi.org/10.1007/s10346-005-0027-7

Strozzi, T., Wiesmann, A., Kääb, A., Joshi, S., & Mool, P. (2012). Glacial lake mapping with very high resolution satellite SAR data. *Natural Hazards and Earth System Science*, *12*(8), 2487–2498. https://doi.org/10.5194/nhess-12-2487-2012

Synolakis, C. E. (1987). The runup of solitary waves. *Journal of Fluid Mechanics*, *185*, 523–545. https://doi.org/10.1017/S002211208700329X

Tarvainen, T., Jarva, J., & Greiving, S. (2006). Spatial patterns of hazards nad hazard interactions in Europe. In P. Schmidt-thom (Ed.), *Development of Natural Hazard maps for European Regions Natural and Technological Hazards and Risks Affecting the Spatial Development of European Regions Edited by Philipp Schmidt-Thomé Geological Survey of Finland*.

Stucky Consulting Engineers (2001) Lake Sarez Mitigation Project, Design Report, 149 p.

Tenzer, R., Sirguey, P., Rattenbury, M., & Nicolson, J. (2011). A digital rock density map of New Zealand. *Computers and Geosciences*, *37*(8), 1181–1191. https://doi.org/10.1016/j.cageo.2010.07.010

Tseng, C. M., Lin, C. W., Stark, C. P., Liu, J. K., Fei, L. Y., & Hsieh, Y. C. (2013). Application of a multi-temporal, LiDAR-derived, digital terrain model in a landslide-volume estimation. *Earth Surface Processes and Landforms*, *38*(13), 1587–1601. https://doi.org/10.1002/esp.3454

Van Westen, C. J., & Greiving, S. (2017). Multi-hazard risk assessment and decision making. In N. Dalezios (Ed.), *Environmental Hazards Methodologies for Risk Assessment and Management* (pp. 31–94). London: IWA Publishing. https://doi.org/10.2166/9781780407135_0031

Von Ruette, J., Lehmann, P., & Or, D. (2013). Rainfall-triggered shallow landslides at catchment scale: Threshold mechanics-based modeling for abruptness and localization. *Water Resources Research*, *49*(10), 6266–6285. https://doi.org/10.1002/wrcr.20418

Wahl, T. L. (2004). Uncertainty of predictions of embankment dam breach parameters. *Journal of Hydraulic Engineering*, *130*(5), 389–397. https://doi.org/10.1061/(ASCE)0733-9429(2004)130:5(389)

Walder, J. S., Watts, P., Sorensen, O. E., & Janssen, K. (2003). Tsunamis generated by subaerial mass flows. *Journal of Geophysical Research: Solid Earth*, *108*(B5). https://doi.org/10.1029/2001jb000707

Wang, F., Zhang, Y., Huo, Z., Peng, X., Wang, S., & Yamasaki, S. (2008). Mechanism for the rapid motion of the Qianjiangping landslide during reactivation by the first impoundment of the Three Gorges dam reservoir, China. *Landslides*, *5*(4), 379–386. https://doi.org/10.1007/s10346-008-0130-7

Wang, W., Chen, G., Yin, K., Zhou, S., Jing, P., & Chen, L. (2015). Modeling of landslide generated waves in Three Gorges Reservoir, China using SPH method. *15th Asian Regional Conference on Soil Mechanics and Geotechnical Engineering, ARC 2015: New Innovations and Sustainability*, 1183–1188. https://doi.org/10.3208/jgssp.ATC1-3-07

Ward, S. N., & Day, S. (2010). The 1958 Lituya Bay landslide and tsunami a tsunami ball approach. *Journal of Earthquake and Tsunami*, *4*(4), 285–319. https://doi.org/10.1142/S1793431110000893

Westoby, M. J., Brasington, J., Glasser, N. F., Hambrey, M. J., Reynolds, J. M., Hassan, M. A. A. M., & Lowe, A. (2015). Numerical modelling of glacial lake outburst floods using physically based dam-breach models. *Earth Surface Dynamics*, *3*(1), 171–199. https://doi.org/10.5194/esurf-3-171-2015

Westoby, M. J., Glasser, N. F., Brasington, J., Hambrey, M. J., Quincey, D. J., & Reynolds, J. M. (2014). Modelling outburst floods from moraine-dammed glacial lakes. *Earth-Science Reviews*, *134*, 137–159. https://doi.org/10.1016/j.earscirev.2014.03.009

Worni, R., Huggel, C., Clague, J. J., Schaub, Y., & Stoffel, M. (2014). Coupling glacial lake impact, dam breach, and flood processes: A modeling perspective. *Geomorphology*, *224*(November), 161–176. https://doi.org/10.1016/j.geomorph.2014.06.031

Worni, R., Huggel, C., & Stoffel, M. (2012). Glacial lakes in the Indian Himalayas - From an area-wide glacial lake inventory to on-site and modeling based risk assessment of critical glacial lakes. *Science of the Total Environment*, *468–469*, S71–S84. https://doi.org/10.1016/j.scitotenv.2012.11.043

Yin, Y., Huang, B., Wang, W., Wei, Y., Ma, X., Ma, F., & Zhao, C. (2016). Reservoir-induced landslides and risk control in Three Gorges Project on Yangtze River, China. *Journal of Rock Mechanics and Geotechnical Engineering*, *8*(5), 577–595. https://doi.org/10.1016/j.jrmge.2016.08.001

Zweifel, A. (2004). *Impuls wellen : Effekte der Rutschdichteund der Wassertiefe*.

ANNEXES

Annex 1: Description of internal parameters and triggers in Scoops3D

Scoops3D uses several internal parameters during search method which influence the final volume. Users are given the choice to adjust the volume limit and search strategy according to the objective of the study. Model internal parameters include search lattice extent, search resolution and volume limit.

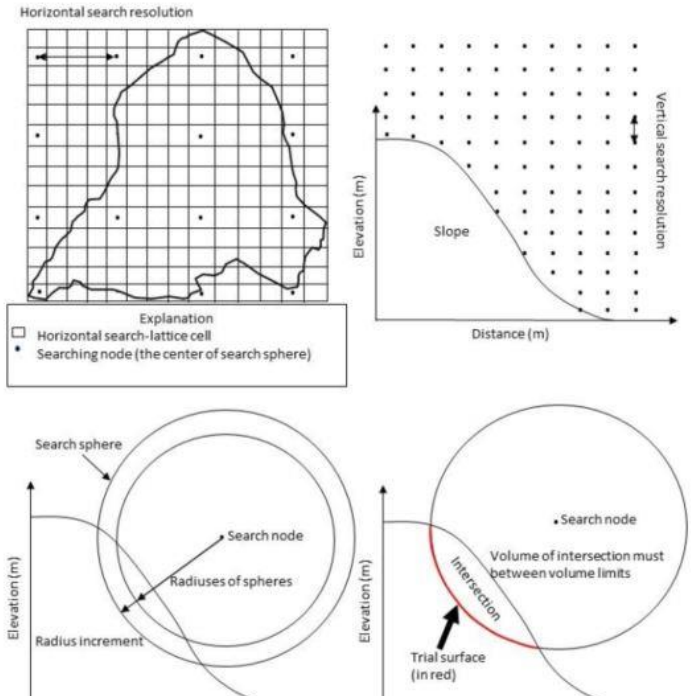

Plate 1: Different internal model parameters in search method of Scoops3D [Ma (2018])

Search lattice extent is of two types: horizontal extent and vertical extent as shown in Plate 1. Horizontal extent is defined as index counters relative to the centre of the lower-left cell of the DEM which corresponds to i =1, j =1. Horizontal extent of search lattice is recommended to be equal to the size of DEM. Vertical extent defines the minimum and maximum vertical extent of the search box in length units of the DEM. The minimum value of vertical extent is recommended to be slightly greater than the lowest elevation of the DEM and appropriate value is obtained by trial and error method until minimum FoS can be determined for all parts of DEM. The maximum vertical limit is recommended to twice the relief above the highest point in the topography.

Search resolution refers to the density of the search nodes horizontally and vertically which equals to the size of DEM. Depending upon the memory and runtime in computation, the resolution can be decreased into coarser size up to four times the DEM size.

The maximum and minimum volume assigned limits the volume search in the model. If the intersected volume between sphere and terrain is less than the minimum volume limit, the nodes will continue searching the volume. Radius increment defines the radius length increment for the set of spheres analysed at a given lattice node, which should produce the failure within the selected volume limit (Plate 1).

Two landslide triggers can be assigned in Scoops3D: pore water pressure due to groundwater and seismic loading. Pore water pressure can be introduced in three ways: 1) Dry underground with no groundwater pressure, 2) Pore pressure ratio defined as a ratio of pore pressure to vertical stress at a point and 3) Piezometric surface representing water table with vertically hydrostatic pressure heads beneath the surface. Seismic loading is applied as a uniform horizontal force representing the influence of ground accelerations due to earthquake. The user defines the dimensionless and scaled fraction of gravity (g) as a horizontal pseudo-acceleration coefficient.

Annex 2: Description of governing parameters, equations and limitations of the Heller-Hager model

The governing parameters for the impact wave generation in channel form (2D) and basin form (3D) reservoir are shown in Plate 2.

Slide impact velocity (V_s)

Bulk slide volume (V'_s)

Slide thickness (s)

Slide width or reservoir width (b)

Bulk slide density (ϱ_s)

Bulk slide porosity (n)

Slide impact angle (α)

Still water depth at the point of impact (h)

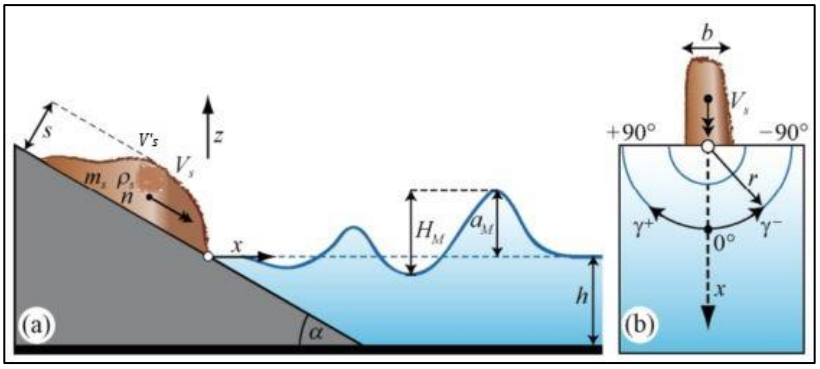

Plate 2: Illustrations of the governing parameters on impact wave generation in (a) 2D and (b) 3D [Heller et al. (2009)]

The slide impact velocity is derived from the Körner (1976) energy equation (B-1) that relates the inclination slope and bed friction with the centre of gravity of the slide mass impacting the lake.

$$\mathbf{V_s = (2g\Delta z_{sc}(1- \tan\delta\cot\alpha))^{0.5}} \qquad \mathbf{[B\text{-}1]}$$

where, V_s is slide impact velocity, g (m/s^2) is the acceleration due to gravity (9.81 m/s^2), Δz_{sc} (m) is drop height of the centre of gravity of slide, δ (°) is the dynamic bed friction angle, α (°) is the slide impact angle. The slide impact angle is the angle measured from the horizontal bed.

The origin (x,z) coordinates are the intersection between the slide slope and still water level (Plate 2). The bulk slide volume V'_s and bulk slide density ϱ_s comprises of bulk slide porosity n related by a formula $\varrho_s = \varrho_g(1\text{-}n)$ and $V'_s = V'_g/(1\text{-}n)$, so it is not introduced as an independent parameter in the calculation. ϱ_g and V'_g are grain density and grain volume respectively. The slide thickness s is measured perpendicular to the slide slope at the moment of impact. The slide width b is the average slide width at the moment of impact and if the slide width is larger than the reservoir width, then only the reservoir width would be considered for b. The still water depth h is the average depth of the water in the impact zone.

In this study, only the extreme case with 3D equations was used for the computation process, attributing to the environment of the study areas that resemble the 3D basin form. The wave celerity c of a landslide induced impact wave is calculated using equation B-2, which is required to calculate the wavelength of the wave. Wave celerity is the speed by which the wave travels in surface water.

$$\mathbf{c = [g(h+a)]^{0.5}} \qquad \mathbf{[B\text{-}2]}$$

where, c (m/s) is wave celerity, g (m/s^2) is the acceleration due to gravity (9.81 m/s^2), h (m) is still water depth, a (m) is wave amplitude. The amplitude is computed from the wave height indirectly using equation B-3.

$$\mathbf{a = (4/5)H} \qquad \mathbf{[B\text{-}3]}$$

where, a (m) is wave amplitude, H (m) is wave height.

The Heller-Hager model introduces a dimensionless quantity known as Impulse Product Parameter P (Heller & Hager, 2009), which refers to the slide momentum flux component. This quantity combines most of the wave parameters required to generate and propagate the wave towards the dam and therefore, can be estimated prior to any event, represented by equation B-4.

$$\mathbf{P = FS^{0.5}M^{0.25}\{\cos[(6/7)\alpha]\}^{0.5}} \quad \textbf{[B-4]}$$

where, P (-) is the impulse product parameter, F (-) is slide Froude number [$F = V_s/(gh)^{0.5}$], S (-) is relative slide thickness [$S = s/h$], M (-) is relative slide mass [$M = \varrho_s V'_s/(\varrho_w bh^2)$], α (°) is slide impact angle, V_s is slide impact velocity, h (m) is still water depth, s (m) is slide thickness, ϱ_s (kg/m^3) is bulk slide density, V'_s (m^3) is bulk slide volume, ϱ_w (kg/m^3) is water density, and b (m) is slide width. During the computation of impact wave generation, limitations shown in Table B 1 must be respected. Exceedance of the limitations will question the model's validity.

Table B 1: Limitation of the computation of impact wave propagation

Parameter	Description	Range
Slide Froude number	$F=V_s/(gh)^{0.5}$	$0.86 \le F \le 6.85$
Relative slide thickness	$S=s/h$	$0.09 \le S \le 1.64$
Relative slide mass	$M=\rho_s V'_s/(\rho_w bh^2)$	$0.11 \le M \le 10.02$
Relative slide density	$D=\rho_s/\rho_w$	$0.59 \le D \le 1.72$
Relative granulate density	ρ_g/ρ_w	$0.96 \le \rho_g/\rho_w \le 2.75$
Relative slide volume	$V=V'_s/(bh^2)$	$0.05 \le V \le 5.94$
Bulk slide porosity	n	$30.7\% \le n \le 43.3\%$
Slide impact angle	α	$30° \le \alpha \le 90°$
Relative slide width	$B=b/h$	$0.74 \le B \le 3.33$
Relative radial distance	r/h	$5 \le r/h \le 30$
Wave propagation angle	γ	$-90° \le \gamma \le +90°$
Relative streamwise distance	$X=x/h$	$2.7 \le X \le 59.2$
Impulse product parameter	$P=FS^{0.5}M^{0.25}\{\cos[(6/7)\alpha]\}^{0.5}$	$0.17 \le P \le 8.13$

The 3D equations were developed by Heller (2007) based on Huber & Hager (1997) for analyzing the impact waves propagating freely and radially in a reservoir. Therefore, the wave height in the slide impact zone, the time and wavelength are estimated using the equations B-5, B-6, and B-7 respectively and illustrated in Plate 3.

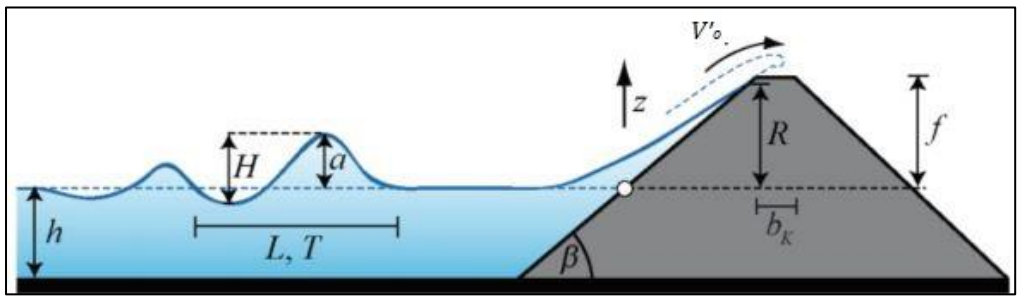

Plate 3: Illustration of governing parameters for wave run-up and overtopping [Heller et al. (2009)]

$$\mathbf{H(r,\gamma) = (3/2)P^{0.8}\cos^2(2\gamma/3)(r/h)^{-0.66}h \quad for\ r/h>X_M} \quad \textbf{[B-5]}$$

where, H (m) is wave height, r (m) is radial distance from impact point to the basin, γ (°) is wave propagation angle, P (-) is impulse product parameter, h (m) is still water depth (at the slide impact zone γ=0°), X_M (m)

is relative streamwise distance of the maximum wave amplitude from the impact location [$X_M=x_M/h$], and x_M (m) is streamwise distance of the maximum wave amplitude from the impact location.

$$T(r,\gamma) = 15(H/h)^{0.25}(h/g)^{0.5} \quad \text{for } r/h>X_M \qquad \textbf{[B-6]}$$

where, T (s) is wave period, r (m) is radial distance from impact point to the basin, γ (°) is wave propagation angle, H (m) is wave height, h (m) is still water depth (at a given position), g (m/s^2) is acceleration due to gravity (9.81 m/s^2), X_M (m) is relative streamwise distance of the maximum wave amplitude from the impact location [$X_M=x_M/h$], and x_M (m) is streamwise distance of the maximum wave amplitude from the impact location.

$$L(r,\gamma) = T(r,\gamma)c(r,\gamma) \qquad \textbf{[B-7]}$$

where, L (m) is wave length, T (s) is wave period, and c (m/s) is wave celerity.

The equations for the wave run-up and overtopping are based on only 2D investigations, devised by Müller (1995) and run-up height is determined by equation B-8.

$$R = 1.25(H/h)^{1.25}(H/L)^{-0.15}(90°/\beta)^{0.2}h \qquad \textbf{[B-8]}$$

where, R (m) is run-up height, H (m) is wave height (in front of the dam), h (m) is still water depth (in front of the dam), L (m) is the wavelength (in front of the dam), and β (°) is run-up angle equal to dam face slope. The limitations for the calculation of wave run-up height are shown in Table B 2.

Table B 2: Limitations for the computation of wave run-up height

Parameter	Range
Relative wave height	0.011 ≤ H/h ≤ 0.521
Wave steepness	0.001 ≤ H/L ≤ 0.013
Relative angle	1.0 ≤ 90°/β ≤ 4.9

Likewise, the overtopping volume per unit dam crest from a wave run-up is estimated assuming no freeboard (f = 0) by the equation B-9, as an intermediate step to find out the actual overtopping volume from the dam with certain freeboard. The volume of overtopping for f > 0 will be lower compared to f = 0, so the result from equation B-9 sets an upper limit for overtopping volume.

$$V_o = 1.45K(H/h)^{1.33}\{T/(h/g)^{0.5}\}^{0.44}h^2 \qquad \textbf{[B-9]}$$

where, V_o (m^3/m) is overtopping volume per unit length dam crest for f = 0, f (m) is freeboard, K (-) is the overfall coefficient for overtopping [$K=K_qK_bK_w^{0.15}$], K_q (-) is the overfall coefficient for the crest width, K_b(-) is the overfall coefficient for the steady case, K_w (-) is the overfall coefficient for the increased flow energy compared with the steady case, H (m) is wave height (in front of the dam), h (m) is still water depth (in front of the dam), T (s) is wave period (in front of the dam), g (m/s^2) is acceleration due to gravity (9.81 m/s^2).

Therefore, the equation B-10 is used to compute the overtopping volume per unit dam crest for f > 0.

$$V_o' = (1-f/R)^{2.2}V_o \qquad \textbf{[B-10]}$$

where, V_o' (m^3/m) is overtopping volume per unit length dam crest, f (m) is freeboard, R (m) is run-up height, and V_o (m^3/m) is overtopping volume per unit length dam crest for f = 0. The limitations for the calculation of overtopping volume are shown in Table B 3.

Table B 3: Limitations for the computation of overtopping volume

Parameter	Range
Relative wave height	0.019 ≤ H/h ≤ 0.488

Non-linearity	$0.59 \le a/H \le 0.95$
Wave steepness	$0.001 \le H/L \le 0.023$
Relative period	$9.0 \le T(g/h)^{0.5} \le 21.0$
Relative wave celerity	$0.83 \le c^2/(gh) \le 1.40$
Relative wavelength	$6.0 \le L/h \le 24.0$
Relative angle	$1.0 \le 90°/\beta \le 4.9$

Müller (1995) also estimated the average discharge per unit dam crest, for which duration of overtopping for f = 0 is estimated using equation B-11.

$$\mathbf{t_o = 4\{T(g/h)^{0.5}\}^{0.44}(h/g)^{0.5}} \qquad \textbf{[B-11]}$$

where, t_o (s) is duration of overtopping for f = 0, T (s) is wave period (in front of the dam), g (m/s^2) is acceleration due to gravity (9.81 m/s^2), and h (m) is still water depth (in front of the dam). Thus, the average discharge per unit length dam crest for f =0 is determined by equation B-12.

$$\mathbf{q = V_o/t_o} \qquad \textbf{[B-12]}$$

where, q (m^2/s) is average discharge per unit length dam crest for f = 0, V_o (m^3/m) is overtopping volume per unit length dam crest for f = 0, t_o (s) is duration of overtopping for f = 0. The maximum discharge per unit length dam crest for f =0 is determined by equation B-13.

$$\mathbf{q_M = 2q} \qquad \textbf{[B-13]}$$

where, q_M (m^2/s) is maximum discharge per unit length dam crest for f = 0, and q (m^2/s) is average discharge per unit length dam crest for f =0. The values of q and q_M comprise of the upper limiting values for the unknown values with f > 0 since no empirical equation is available on discharge for f > 0. The limitations for the computation of duration of overtopping are shown in Table B 4.

Table B 4: Limitation for computation of overtopping duration

Parameter	Range
Relative period	$14 \le T(g/h)^{0.5} \le 22$
Relative duration of overtopping	$10.5 \le t_o(g/h)^{0.5} \le 13.5$

The second phase of Heller-Hager model deals with the force exerted by the impact waves on dams and their computation based on the wave profile and internal water movement. However, this study does not compute the wave forces so these are not discussed in detail. Likewise, the model assumes the mass movement to be a granular slide but in the real world, the mass movement could be of different types. Zweifel (2004) argues that at low velocity if the mass moves as a solid body, the wave height is significantly higher than that caused by a granular slide. Water displacement is higher for the solid body of porosity (n = 0) whereas, for the granular slide, water enters the pore volume hence, attenuating the displacement.

According to equation B-8, the sensitivity analysis of wave run-up height (R) indicated that it was primarily sensitive to slide impact velocity as it varies approximately in 1:1 ratio (Heller et al., 2009). Besides, the wave run-up height also varied significantly with change in still water depth at the impact site and slide thickness approximately in 2:1 ratio each. Run-up height positively varied with the change in slide volume and slide density but not significantly. However, the importance of slide volume could be argued with its dependency to slide thickness. Run-up height varied significantly with wave propagation angle in a negative trend. Likewise, the variation in still water depth at the dam site, slide or reservoir width, impact angle and run-up angle did not affect the run-up notably.

Landslide generated impulse waves in reservoirs - Basics and computation Spread sheets			
Project name	Lake Rivakkul	Operator	Anish
Computational point	Scenario 1	Date	13/05/2020

Governing parameters			
Wave generation (Subsection 3.2.2)			
Slide impact velocity V_s [m/s]	58	Bulk slide density ρ_s [kg/m^3]	1575
Bulk slide volume $\mathcal{V}_s$ [m^3]	18,000,000	Bulk slide porosity n [%]	37
Slide thickness s [m]	43	Slide impact angle α [°]	33
Slide or reservoir width b [m]	655	Still water depth h [m]	36
Wave propagation (3D or 2D) (Subsection 3.2.2)			
Wave basin (3D)		Wave channel (2D)	
Radial distance r [m]	1675	Streamwise distance x [m]	-
Wave propagation angle γ [°]	-85		
Wave run-up and overtopping (Subsection 3.3.2)			
Still water depth h [m]	36	Freeboard f [m]	43
Run-up angle β [°]	12	Crest width b_K [m]	255

Main results	
Wave heigth H (H_M) [m]	6.3
Wave amplitude a (a_M) [m]	5.1
Wave period T (T_M) [s]	18.6
Wave length L (L_M) [m]	373.8
Run-up height R [m]	14.2
Overtopping volume $\mathcal{V}_0$ per unit length dam crest for f = 0 [m^3/m]	No value
Duration of overtopping t_0 for f = 0 [s]	No value
Average discharge q_{0m} per unit length dam crest for f = 0 [m^2/s]	No value
Maximum discharge q_{0M} per unit length dam crest for f = 0 [m^2/s]	No value
Overtopping volume per unit length dam crest $\mathcal{V}$ [m^3/m]	No value
Hor. force comp. p.u.l. dam crest resulting only from hydrostatic pressure K_{RWsh} [N/m]	6,356,880
Ver. force comp. p.u.l. dam crest resulting only from hydrostatic pressure K_{RWsv} [N/m]	29,906,769
Wave type (Stokes-like wave 3.4.3 or remaining wave types 3.4.4)	Remaining
Remaining: total horizontal force component per unit length dam crest resulting from an impulse wave and hydrostatic pressure K_{totsh} [N/m]	10,043,505
Remaining: reduced total horizontal force component per unit length dam crest resulting from an impulse wave and hydrostatic pressure $K_{totshsubg}$ [N/m]	No value
Remaining: elevation $z_{Ktotshsubg}$ of the resultant of $K_{totshsubg}$ [m]	No value
S/r: additional hor. force comp. p.u.l. dam crest resulting from impulse wave ΔK_h [N/m]	No value
Stokes: elevation $z_{\Delta Ksh}$ of the resultant of ΔK_h [m]	No value
S/r: ad. vertical force component p.u.l. dam crest resulting from impulse wave ΔK_v [N/m]	No value

Limitations	
Number of not satisfied limitations out of 23 (2D) or 24 (3D), respectively	6

Plate 4: Interface of Heller-Hager model constructed in MS-Excel using Macros [Heller et al. (2009)]

Annex 3: General steps to perform 2D modelling in HEC-RAS

1) RAS Mapper, a GIS-based module embedded in HEC-RAS, is used for starting a new project for which an ESRI horizontal coordinate projection of the study area is added.
2) It is followed by the addition of terrain data of different data formats such as floating-point grid format (*.flt), GeoTIFF (*.tif), ESRI grid files, USGS DEM file etc. Terrain data is also used for making inundation maps.
3) Land classification map can be prepared to assign the Manning's roughness value for the terrain.
4) Any additional information such as aerial photography, image layers etc. can also be added to support the project.
5) Next, the 2D flow areas are delineated using a boundary polygon from Geometric editor. The 2D flow areas represent the model domain.
6) The break lines can be drawn within the 2-D flow area to represent any significant hydraulic barriers to the flow such as levees, weirs etc.
7) An appropriate computational mesh or cells are assigned using a 2D flow area editor. Here, the Manning's roughness for the model domain can be adjusted either as single uniform value or from

the land classification map. The computational mesh can be refined by editing, deleting, changing cell density as per required.

8) Then, the 2D geometric pre-processor is run from RAS-Mapper to assign the geometric and hydraulic properties for cell centre and cell faces from the terrain data.
9) The boundary conditions are drawn in the 2D flow area through Geometric data editor.
10) The initial conditions and boundary conditions are assigned for 2D flow areas in Unsteady Flow data editor.
11) In the Unsteady Flow Simulation window, necessary computational time intervals and simulation period are added. User can also select either Full momentum or Diffusive wave equations for the simulation in the settings.
12) Finally, unsteady flow simulation is executed and outputs are reviewed in the RAS Mapper.

Annex 4: Event tree analysis of potential rockslide scenarios from the Right Bank Landslide into Lake Sarez

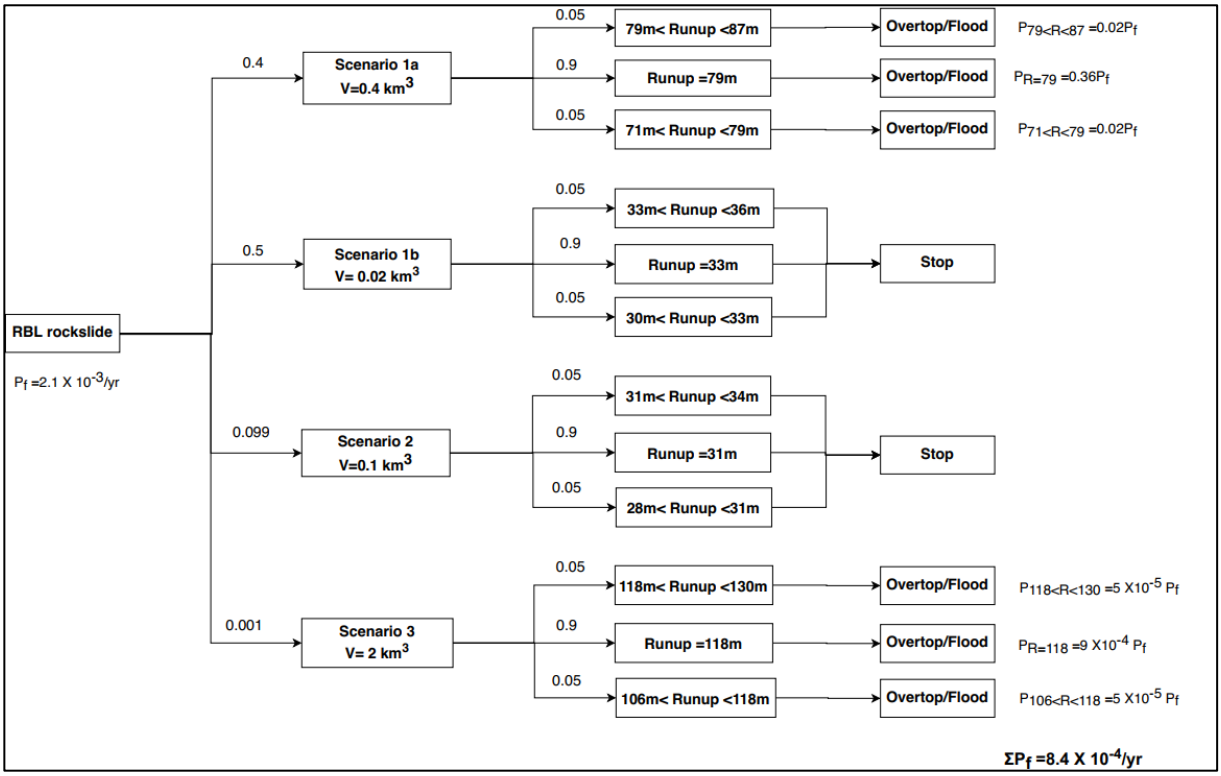

Plate 5: Event tree of potential rockslide scenarios for Lake Sarez

In this analysis, a co-seismic rockslide was assumed to occur. The failure probability of slide corresponded to the earthquake return period of 475 years as mentioned in Section 4.2.1. Among the scenarios designed for Lake Sarez, the volume estimated from the physically-based models were assigned higher probabilities. Scenario 3 was given the lowest because it was the most unlikely scenario among others supported by past literature. Different failure volumes into the lake generated different run-up heights. Run-up heights estimated from the Heller-Hager model were given higher probabilities than the values of run-up heights with ±10% deviation. Scenario 1b and Scenario 2 did not generate enough run-up to overtop the Usoi dam having freeboard of 50 m, so their event branch gets terminated. For rest of the Scenarios, the overtopping and subsequent flood prevailed because of their higher run-up heights. The final probability of occurrence of the flood due to overtopping was the summation of the product of individual probabilities, which corresponded to $8.4 \cdot 10^{-4}$/yr. The convention of probability values can be found in Lacasse et al. (2008).